UCL ENVIRONMENTAL CHANGE RESEARCH CENTRE

UCL

Research Report # 132

Palaeolimnological Study of Selected Lakes in the Wood Buffalo Region

C J Curtis, R J Flower, S Pla, N Rose, J Shilland,
G L Simpson, S Turner, H Yang

May 2009

PALAEOLIMNOLOGICAL STUDY OF SELECTED LAKES IN THE WOOD BUFFALO REGION BY UNIVERSITY COLLEGE LONDON

FINAL

Prepared for:

NO_xSO_2 Management Working Group

Prepared by:

UNIVERSITY COLLEGE LONDON
C.J. Curtis, R.J. Flower, S. Pla*, N. Rose, J. Shilland, G.L. Simpson, S. Turner, H. Yang

*Present address: CEAB-CSIC, Blanes, Spain

MAY 2009

CONTENTS Page

List of figures

List of Tables

EXECUTIVE SUMMARY

Background

Palaeolimnology is the reconstruction of past environments using information recorded in lake sediments, including preserved biological organisms and chemical indicators. A key assumption of palaeolimnology is that undisturbed lake sediments may provide a faithful, continuous record of change over long time periods, ranging from years to millennia. Using proven methods available for dating lake sediments, both the continuity of the record and the dates of recorded changes may be established. Palaeolimnology has been widely employed across the world, for example in reconstructing past climate over thousands of years and for the study of pollutant impacts over the last 200 years following the Industrial Revolution. It is particularly well suited to the study of pollution arising from fossil fuel combustion because several indicators of pollutant inputs and biological changes may be recorded. The main purpose of this study was to employ various palaeolimnological techniques to establish whether there have been chemical or biological changes in lakes in Northern Alberta as a result of the industrial activities associated with exploitation of the Athabasca Oil Sands.

Aims and approach

The key aims of this study were to obtain and analyse lake sediment cores from a number of lakes across spatial and environmental gradients in the Wood Buffalo region of Northern Alberta to:

1. provide historical records of natural and/or anthropogenic changes in lake water quality, in particular any possible changes associated with industrial activity in the Oil Sands region; and
2. assist in the verification of a time-to-effects model, MAGIC, being developed for the implementation of the CEMA Acid Deposition Management Framework.

The major potential change in lakes arising from acid deposition in the region is lake water acidification. Diatoms, a group of algae ubiquitously found in lakes, are particularly good indicators of lake water acidity (pH), with a large number of species occurring over different ranges of pH. Statistical models called transfer functions may be used to determine the optimum pH (or other chemical parameter) for a given diatom species, so that the diatom assemblage found in a lake may be used to model lake water chemistry. Furthermore, diatom remains are often well preserved in lake sediments so they provide an ideal tool for reconstructing changes in pH over time. Intact lake sediment cores are extruded and sliced up into consecutive intervals each representing a given time period which may be assessed by radiometric dating. The slicing interval may be selected to give an appropriate temporal resolution but is often 5 mm or 10 mm intervals which can represent time periods of years to decades or more, depending on site specific sediment accumulation rates.

An earlier CEMA funded project used lake surface sediment samples and contemporary water chemistry previously collected from 47 lakes across the region to develop a diatom-pH transfer function, i.e. to establish the current relationships between diatom assemblages and lake water pH in the region. The second phase described here applied this transfer function to diatom data obtained from 12 lake

sediment cores to assess regional changes through time in lake water acidity. Diatom analysis was combined with radiometric dating, isotopic analyses and other physical and geochemical methods to assess several strands of evidence for contaminants linked to fossil fuel combustion and acid deposition.

Methods

The suite of analyses performed on each of the 12 cores included:

1. lithostratigraphy - dry weight and loss on ignition (LOI) – provides a standard check for disturbance of the accumulated sediment record;
2. spheroidal carbonaceous particle (SCP) analysis – provides an unambiguous indicator of contamination by the products of coal or oil combustion;
3. radiometric dating (^{210}Pb) – provides dating profiles for each core;
4. sediment isotopic analysis (δ^{15}N and δ^{13}C) - provides evidence of changes in N and C sources, lake biogeochemical cycles and potentially N deposition inputs;
5. X-ray fluorescence spectrometry (XRF) – measures concentrations of metals and other elements in lake sediments; and
6. diatom analysis – provides a diatom-inferred pH for each dated slice of the sediment core.

Results

1. Dry weight and LOI analysis
Standard lithostratigraphic analyses indicate little evidence of discontinuous sediment records or major disturbances to sedimentation regimes so the 12 sediment cores are deemed appropriate for other palaeolimnological analyses.

2. SCP analysis
SCP contamination is low but detectable in all cored lakes. Low concentrations, the small size of most SCPs found and a lack of spatial patterns probably indicate that the main sources are high temperature coal and/or oil combustion plants remote from the Oil Sands region.

3. Radiometric dating
Dating of sediment cores using ^{210}Pb and ^{137}Cs reveals a large range of sediment accumulation rates, but all 12 cores encompass at least 100 years of accumulated sediment. Most cores showed straightforward dating profiles, although three showed possible evidence of missing surface sediments (lakes SM8, WF3 and S3) introducing uncertainty into the interpretation of very recent changes.

4. Stable isotope analysis of sediments
All lakes show a trend of declining δ^{13}C towards the present although the magnitude of change is small. Several sites show a faster rate of change since the 1930s-40s. Such changes are generally indicative of increased availability of dissolved inorganic carbon. There are no consistent patterns in lake sediment δ^{15}N which suggest biogeochemical changes induced by increased nitrogen deposition in the region. C/N ratios suggest a progressively greater contribution from aquatic algae to sediment organic matter which may indicate increasing algal productivity, as also suggested by the diatom analyses at several sites (see below).

5. XRF analysis

There are few strong trends in the XRF data indicating recent contamination from fossil fuel combustion products. Two sites in the Stony Mountains (SM6, SM8) show minor increases in several elements in recent decades, including P, Si, Pb, V, Al. More widespread increases in P and Fe could be indicative of nutrient enrichment in many sites, as indicated by diatom analysis and possibly by C/N ratios, but diagenetic effects (in-situ transformations and movement within sediments) cannot be ruled out. Additional, unfunded analyses of mercury (Hg) in surface sediments found the highest concentration in lake NE7 (see below). Down-core analyses at this site reveal a pattern of long term increase in Hg concentrations since the 19th century and calculation of fluxes in sediments show a steep increase since the 1980s which are comparable with values for a contaminated site in the UK.

6. Diatom analysis

Diatom analysis of the 12 cores provides clear evidence of environmental change trends in the majority of lakes, but only one lake (NE7) shows recent acidification which could be associated with acid deposition from the industrial activities associated with exploitation of the Oil Sands. This site is small and acidic but other chemically comparable sites (e.g. SM6 and SM8 in the Stony Mountains; WF3 west of Fort McMurray) do not show acidification. Instead, many sites show increasing abundances of planktonic diatoms associated with more nutrient rich conditions and some show increases in diatom-inferred pH (alkalinisation). While some of these changes indicative of eutrophication have occurred over periods of more than 100 years, suggesting e.g. climatic drivers are responsible, some sites show more recent enrichment which could be associated with enhanced nitrogen deposition from fossil fuel combustion, forest fires or other industrial sources.

The widespread increases in alkalinity and nutrient status confirm the results of an earlier study in the region (Hazewinkel *et al.*, 2008) that nutrient enrichment in the lakes of Northern Alberta is at present much more common than lake acidification due to industrial activities. However, the relative importance of climatic change and anthropogenic pollution in causing eutrophication is not yet known.

Conclusions and potential future work

The strongest evidence of industrial contamination of lakes in Northern Alberta from the present study comes mainly from one site north-east of Fort McMurray (NE7), which shows both recent acidification since about 1970 and increasing fluxes of mercury to lake sediments since the 1980s. Of the other 11 cored lakes, most do show strong evidence of environmental change, but rather than acidification, nutrient enrichment appears to be the cause of changes in diatom communities. This apparent eutrophication occurs over various timescales from the last 20-30 years to over 100 years, suggesting several potential drivers including climatic change, forest fires and possibly increased nitrogen deposition in the region.

Several areas for future research are strongly suggested by the data from this study.

1. Further palaeolimnological investigations and/or chemical monitoring of lakes in the vicinity of the acidified site NE7, and typologically similar lakes

elsewhere in the region, to determine whether acidification could be more widespread;

2. A more detailed study of Hg contamination in lake sediment cores, in particular comparison of longer cores with new short cores, would indicate the relative importance of longer-term global drivers versus local, industrial sources of Hg. An extension of this approach also measuring polycyclic aromatic hydrocarbons (PAHs) could take in the delta and surrounding lakes of Lake Athabasca to determine whether currently observed levels there are a product of longer term natural seepage from the Oil Sands (hydrologically transported) or due to recently enhanced levels caused by industrial activities (hydrological and/or atmospheric).
3. Most lakes in the region are undergoing rapid ecological change, generally due to nutrient enrichment rather than acidification at present. Palaeolimnology does not provide information on recent changes (within the last decade) so there is the need for establishment of a diatom monitoring programme to augment ongoing water quality monitoring to track changes into the future. This could be combined with phytoplankton bioassays to determine the nutrient limitation status of phytoplankton production, i.e. whether lakes are nitrogen limited (see below).
4. Given relatively high natural levels of phosphorus in the region's lakes, it remains a distinct possibility that nitrogen deposition could be contributing to nutrient enrichment. More detailed palaeolimnological work could help to separate longer term (climatic) drivers from recent industrial pollution impacts, using a) longer sediment cores to better establish longer-term natural variability; b) other proxies such as chrysophyte remains in sediments which may give better indications of nutrient related changes, and c) improvement of the diatom-pH transfer function and potentially development of a diatom – phosphorus and/or chrysophyte – nitrogen transfer function using a broader (new or existing) lake surface sediment / water chemistry dataset.

Any of these studies would add greatly to our understanding of current and potential impacts of industrial activities in the Oil Sands region on the boreal lake ecosystems which are such an important natural resource, both nationally and internationally.

1. BACKGROUND

The NO_xSOx Management Working Group (NSMWG) of the Cumulative Environmental Management Association (CEMA) had a contract with the University of Alberta (U of A) for palaeolimnological work. This work involved preparing six detailed palaeolimnological records from a transect of lakes spanning a gradient of acid neutralization capacity (ANC) in the Firebag River-Johnson Lake-Marguerite River area of northeastern Alberta. The preliminary results from this work were presented to the NSMWG on September 14, 2005, while a presentation on the finalized work and write-up was presented to the NSMWG on March 10, 2006. The study did find evidence of temporal changes in lake quality but these do not appear to be related to acid inputs. Factors such as climate change, nutrient status and/or natural chemical oxidation/reduction processes appeared to be the more likely explanations of the changes measured.

As part of this U of A research project, surface and bottom sediment samples were collected from the 50 acid sensitive lakes in the region that are part of the acid sensitive lake monitoring program. Time constraints did not allow for their analysis. Sediment core samples comprised approximately 1 cm thick sections from the top and from the bottom of 7.5 to 10 cm diameter sediment cores.

As part of NSMWG's modelling research program, which is developing a time-to-effect acid deposition model (called MAGIC) for the Athabasca Oil Sands Region, Dr. Chris Curtis of University College London was asked to submit a proposal to do further palaeolimnological work in the region. The proposal submitted involved two phases. The overall aim was to provide independent palaeolimnological validation/cross comparison with MAGIC modelled reconstructions of past chemical change in the region's lakes, and also to provide essential information on baseline chemical conditions and variability against which recovery targets could be established in impacted lakes. The two phases were:

1. Phase 1 (2005) – collection of lake sediment core tops from 50 lakes and generation of diatom – water chemistry transfer function (calibration or training set); plus trial analysis of a small number of full sediment cores to assess the quality of the palaeo record, given the shallowness of many lakes and possible sediment disturbance.
2. Phase 2 (2006) – collection of sediment cores from the most acid sensitive sites for detailed palaeolimnological analysis

Phase 1 was modified by the NSMWG in the fall of 2005. The core top samples collected by the U of A were sent to Dr. Curtis in the fall of 2005 for analysis. The purpose of this work was to:

1. Determine if there is enough variability in diatom assemblages in the 50 acid sensitive lakes to give a "training set" for the palaeolimnology model used to relate diatom speciation to lake pH, and
2. Calibration of the diatom–pH model using the "training set" provided it is adequate.

This work was completed and a "training set" obtained.

In 2006, the NSMWG agreed to fund analysis of the core bottoms and to collect core samples of 20 lakes in the region. The lakes to be sampled were selected based on differences measured between core bottoms vs. core tops as well as priorities

established by the modelling research group. Alberta Environment (a member of the NSMWG) made the final decision on the lakes to be sampled and the cores to be analyzed.

2. INTRODUCTION

This project report covers work undertaken under two separate, consecutive CEMA contracts 2007-0006 and 2008-004, to determine the acidification status of lakes in the Wood Buffalo region of Northern Alberta (spanning the Regional Municipality of Wood Buffalo and Caribou Mountains adjacent to Wood Buffalo National Park) through a suite of comprehensive palaeolimnological analyses of lake sediment cores.

The work conducted under the current study as stated in the contract document was:

1. The collection and diatom assemblage analysis of surface, bottom and full core sediment samples from selected acid sensitive lakes in the Wood Buffalo region to:
    a) provide an historical record of natural and/or anthropogenic related water quality changes for parameters such as pH and/or nutrients; and
    b) assist in the verification of the MAGIC model being developed for the implementation of the CEMA Acid Deposition Management Framework;
2. Interpretive report describing diatom change and likely drivers of change through time in all cored lakes; and
3. Assistance in linking diatom modelled change to MAGIC outputs – this would be contingent on the availability of MAGIC data.

The project follows on from a previous CEMA contract which utilized existing sediment core material collected by Rod Hazewinkel at the University of Alberta and from a "pilot study" conducted by University College London to obtain a training set of contemporary lake diatom and water chemistry data for building a transfer function which allows the reconstruction of lakewater pH from subfossil diatom remains preserved in lake sediment cores. This pilot study ("Lake Sediment Core Top Analysis" – CEMA Contract Number 2005-0038) was completed in January 2006 and provided diatom-pH transfer functions using 47 lake surface sediment samples (core tops) and corresponding water chemistry data. With the successful derivation of the diatom-pH transfer function, CEMA funded a subsequent contract (2006-0020) with the following aims:

1. analysis of corresponding core bottom sediment samples collected by the University of Alberta;
2. comparison of the data from the core bottom sediment analysis to the previous core top (surface) sediment samples and identification of lakes that have undergone chemical change over time (specifically in pH);
3. recommend lakes for full core sampling and analysis; and
4. carry out sediment coring of 20 selected sites and identify a priority shortlist of 12 sites for full palaeolimnoligical analysis under a subsequent contract from CEMA.

Core bottom samples were received from CEMA on April 24, 2006 and analysis commenced immediately. Of the 47 core top sites used in the Phase 1 study, core bottoms were available for only 33 sites and three were unsuitable for diatom analysis. Analysis of the remaining 30 samples was completed in June 2006 and a Project Report detailing changes in diatom-inferred pH in these lakes was provided to CEMA in July 2006 (Lake Sediment Core Bottom Sample Analysis and Assessment of Diatom Change: Report prepared for the CEMA NO_xSO_x Management Working Group under Contract Number 2006-0020; Sergi Pla, Chris Curtis and Gavin Simpson). This report classified 44 of the original study lakes (three of the 47 samples initially provided were duplicates) according to measured water chemistry and, where available, diatom-inferred acidification status. This classification formed the basis of the subsequent phase of work - site selection and lake coring for full palaeolimnological analysis, to be undertaken in August 2006.

3. METHODS, RESULTS AND DISCUSSION

3.1 Site selection and sediment coring

Site selection was based on a matrix to include the following gradients:

- acid sensitivity
- diatom-inferred pH change
- magnitude of overall diatom change
- regional coverage

The list of sites for coring was agreed with CEMA and Alberta Environment prior to the field trip in August 2006. Four staff from University College London (Chris Curtis, Gavin Simpson, James Shilland and Roger Flower) carried out the fieldwork in conjunction with Alberta Environment staff working on the routine Regional Aquatics Monitoring Program (RAMP) survey between August 21 - 31, 2006. It was decided during the field trip that two additional sites would be cored at no extra cost to CEMA to maximise the chances of obtaining high quality, undisturbed sediment cores with good stratigraphy and to maximise the environmental gradients covered (Table 1). The cored lakes covered all the sub-regions of the RAMP survey with three sites in the Birch Mountains (code prefix BM), four in the Stony Mountains (code prefix SM), four in the Caribou Mountains (code prefix CM), six in the region north-east of Fort McMurray (code prefix NE), two in the region west of Fort McMurray (code prefix WF) and three remote Shield lakes north of Lake Athabasca (code prefix S).

Each lake site was cored twice to provide a back-up core in case the primary core (judged by visual assessment of the least disturbed and/or longest core) was lost or provided insufficient material for the suite of analyses proposed. Accidental loss or disturbance of intact cores may sometimes occur during transport or extrusion. Cores were numbered consecutively in the order in which they were taken (Table 1). With 22 lakes cored in duplicate, a total of 44 sediment cores were obtained and successfully extruded (sliced) at the field station. Cores were extruded at 0.5 cm intervals to the bottom of the core depth obtained.

Extruded sediments were freighted back to University College London in September 2006. Discussions were then initiated with CEMA, Alberta Environment and a postgraduate student (Colin Whitfield) from Trent University involved in the CEMA MAGIC modelling contract to which this work is linked. The purpose of these discussions was to identify the most appropriate shortlist of 12 lakes for full palaeolimnological analysis in the next phase of the study. The final list of 12 sites covers all the environmental gradients and regions listed above, takes into account the quality of the cores obtained in the field and the likelihood of undisturbed stratigraphies assessed by expert judgement (Table 2). A key factor was the requirement to work at sites where MAGIC modelling applications by Trent University would be focused, in particular sites NE7 and SM8. This list was approved by CEMA in November 2006 (Table 2) and sample preparation at University College London (UCL) commenced in December 2006. Selected water chemistry from the RAMP surveys is shown for the 12 sites in Fig.1, while the distribution of the shortlisted lake core sites is shown in Fig. 2.

The suite of analyses to be performed on each core includes the following:

1. lithostratigraphy - dry weight and loss on ignition (LOI)
2. spheroidal carbonaceous particle (SCP) analysis
3. radiometric dating (^{210}Pb)
4. sediment isotopic analysis (δ^{15}N and δ^{13}C)
5. X-ray fluorescence spectrometry (XRF)
6. diatom analysis

The sequence of sample preparation and analysis entailed the following steps for each sediment sample (0.5cm intervals in each core):

1. sample wet density every 5 cm (used in ^{210}Pb method) and subsequent drying of all intervals;
2. dry weight and LOI determinations of every second subsampled interval;
3. Concurrent subsample analysis for –
   a) ^{210}Pb dating of subsample following a period of sample equilibration;
   b) slide preparation of subsample and diatom analysis;
   c) sediment isotopic analysis of subsample (δ^{15}N and δ^{13}C)
4. selective SCP and XRF analyses on the basis of LOI and ^{210}Pb results.

Note that to ensure sufficient material for analyses in each core, ^{210}Pb analyses were performed on every second interval alternating with the dry weight/LOI, diatom and isotopic analysis samples. Analysis was performed down to 25 cm depth or the core bottom if <25 cm, since only 20 levels were budgeted for. However, deeper samples were archived in case of future requirement for analysis.

The final results for each of these analyses are described in sequence below.

Table 1: Lakes selected for coring and core details

Consecutive Coring ID	Code	Alternative code / name	Cored by	Coring date	LAT	LONG	Coring depth (m)	Corecode #1	Core Length (cm)	Corecode #2	Core Length (cm)
ALB01	BM1	L25 (Legend)	GLS	21-Aug-06	57.41574	112.91676	8.5	ALB01A	0-34.0	ALB01B	0-15.5
ALB02	BM3	L60	GLS	21-Aug-06	57.65232	112.61289	3.1	ALB02A	0-25.5	ALB02B	0-27.5
ALB03	SM8	287	JS	22-Aug-06	56.21567	111.20536	1.4	ALB03A	0-18.5	ALB03B	0-18.5
ALB04	SM6	A26	JS	22-Aug-06	56.22227	111.17004	1.6	ALB04A	0-19.0	ALB04B	0-23.0
ALB05	SM3	289	JS	22-Aug-06	56.20155	111.36388	3.1	ALB05A	0-26.0	ALB05B	0-25.5
ALB06	SM5	A29	JS	22-Aug-06	56.16694	111.54568	1.4	ALB06A	0-29.5	ALB06B	0-27.0
ALB07	NE11	Kearl Lake	RF	23-Aug-06	57.29327	111.23430	1.8	ALB07A	0-19.5	ALB07B	0-22
ALB08	NE3	L8	RF	23-Aug-06	57.04481	110.59026	1.7	ALB08A	0-23.0	ALB08B	0-22.0
ALB09	NE2	L7	RF	23-Aug-06	57.09281	110.75042	1.65	ALB09A	0-24.5	ALB09B	0-28.5
ALB10	NE1	L4	RF	23-Aug-06	57.15172	110.84687	1.6	ALB10A	0-23.0	ALB10B	0-19.5
ALB11	WF3	A59	GLS	24-Aug-06	55.90871	112.86468	1.2	ALB11A	0-25.0	ALB11B	0-23.5
ALB12	WF2	A47	GLS	24-Aug-06	56.24551	113.14144	1.6	ALB12A	0-38.0	ALB12B	0-42.0
ALB13	CM3	E68 (Whitesand)	RF/CC	25-Aug-06	59.19388	115.45974	1.55	ALB13A	0-26.0	ALB13B	0-27.5
ALB14	CM4	E67	CC/RF	25-Aug-06	59.30997	115.32947	A 7.7, B 9.7	ALB14A	0-17.5	ALB14B	0-22.5
ALB15	CM2	E59 (Rocky Island)	CC/RF	25-Aug-06	59.11909	115.12837	A 5.4, B 5.5	ALB15A	0-35.0	ALB15B	0-34.5
ALB16	CM5	O1 (Unnamed #6)(E55)	CC/RF	25-Aug-06	59.23804	114.52351	1.3	ALB16A	0-18.0	ALB16B	0-24.0
ALB17	S4	A301	CC	26-Aug-06	59.16801	110.56855	9.5	ALB17A	0-32.0	ALB17B	0-33.5
ALB18	S3	R1	CC	26-Aug-06	59.19059	110.67251	10.5	ALB18A	0-33.5	ALB18B	0-31.5
ALB19	S5	O10	CC	26-Aug-06	59.12409	110.69410	1.8	ALB19A	0-38.0	ALB19B	0-39.5
ALB20	NE5	E15 (268)	GLS	27-Aug-06	56.89557	110.90451	1.5	ALB20A	0-22.0	ALB20B	0-39.5
ALB21	NE7	185	JS	30-Aug-06	57.14667	110.86483	1.5	ALB21A	0-25.0	ALB21B	0-24.0
ALB22	BM11	199	CC	31-Aug-06	57.69367	111.90820	A 1.9, B 1.7	ALB22A	0-32.0	ALB22B	0-31.5

Cored by: GLS = Gavin Simpson; JS = James Shilland; RF = Roger Flower; CC = Chris Curtis

Table 2: Selection of 12 lake sites for full sediment core analysis on several criteria

CORE CODE	Region	Code	Alternative code / name	Lake area	Max depth	LAT	LONG	Lake elevation	Diatom change? (chord dist)	Acid chemistry	Acidified?
ALB01	Birch Mountains	BM1	L25 (Legend)	16.80	10.2	57.412	112.934		minor	Sensitive	No
ALB02	Birch Mountains	BM3	L60	0.91	2.7	57.662	112.613		large	Non sensitive	Slightly
ALB15	Caribou Mountains	CM2	E59 (Rocky Island)	0.52		59.000	114.983	895	large	Sensitive	Yes
ALB16	Caribou Mountains	CM5	O1 (Unnamed #6)(E55)	0.80	1.8	59.238	114.525	856	large	Very sensitive	Yes
ALB09	NE of Ft McMurray	NE2	L7	3.71	1.7	57.458	111.650	467	large	Very sensitive	No
ALB21	**NE of Ft McMurray**	**NE7**	**185**	**0.09**	**2.5**	**57.147**	**110.863**	**600**	**No bottom sample**	**Acidic**	
ALB18	Shield lakes	S3	R1	0.55	13.1	59.199	110.687	297	No bottom sample	Non sensitive	
ALB17	Shield lakes	S4	A301		8.2				large	Non sensitive	No
ALB05	Stony Mountains	SM3	289	1.83		56.200	111.367			Very sensitive	
ALB04	Stony Mountains	SM6	A26	2.78	1.5	56.223	111.169	725		Acidic	
ALB03	**Stony Mountains**	**SM8**	**287**	**2.18**		**56.208**	**111.200**			**Acidic**	
ALB12	W of Ft McMurray	WF2	A47	431.00	1.7	56.245	113.141	628	large	Sensitive	Yes
ALB11	W of Ft McMurray	WF3	A59	108.00	2.0	55.911	112.864	564	large	Acidic	Yes

NB Core ALB01 (from lake BM1 / L25 “Legend”) is an additional site for SCP analysis only; all other analyses done previously by Rod Hazewinkel. Bold text indicates cores from the sites to be used for direct comparison of diatom-inferred change and MAGIC reconstructions being done by Trent University (NE7 and SM8).

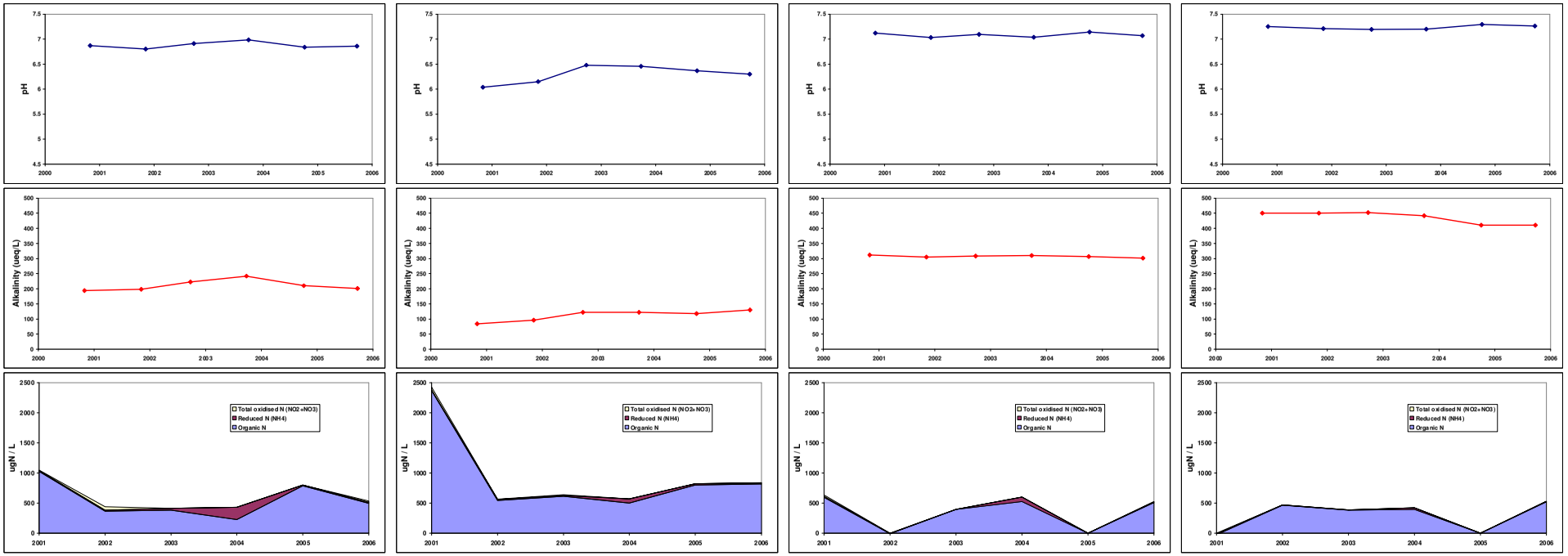

Figure 1a: Selected water chemistry data from lake sites selected for full core analysis; Caribou Mountains and Canadian Shield lakes

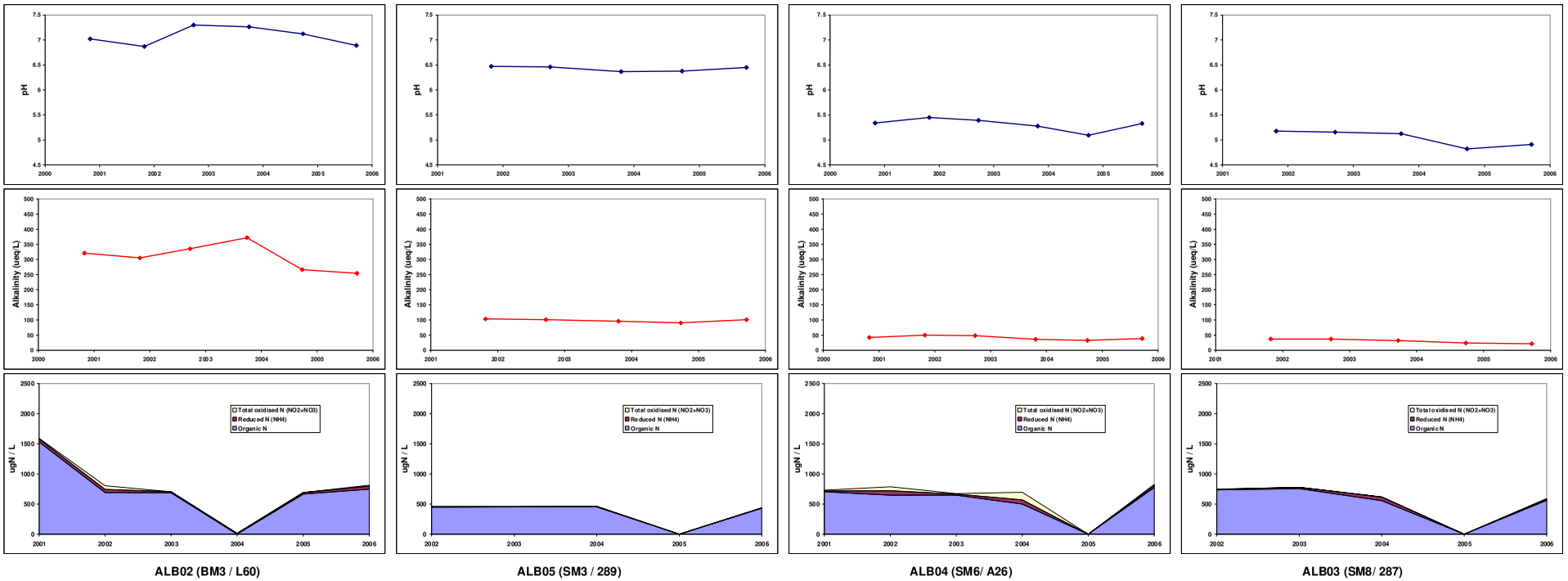

Figure 1b: Selected water chemistry data from lake sites selected for full core analysis; Birch Mountains and Stony Mountains

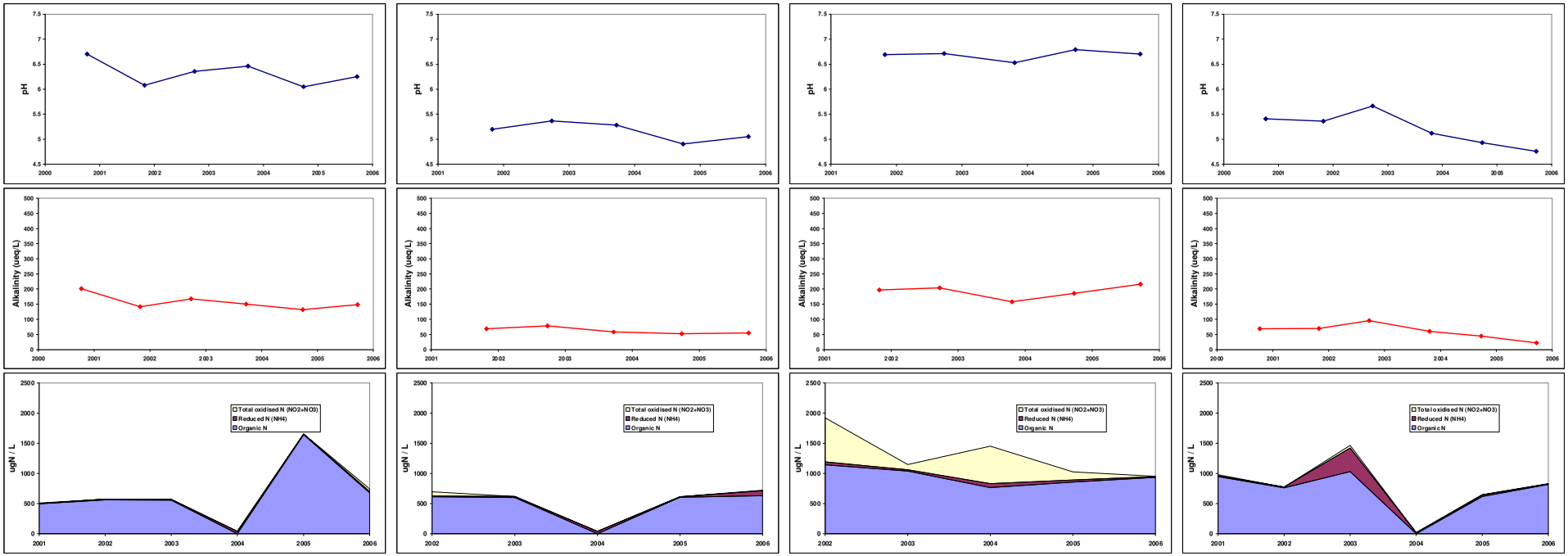

Figure 1c: Selected water chemistry data from lake sites selected for full core analysis; lakes NE and W of Fort McMurray

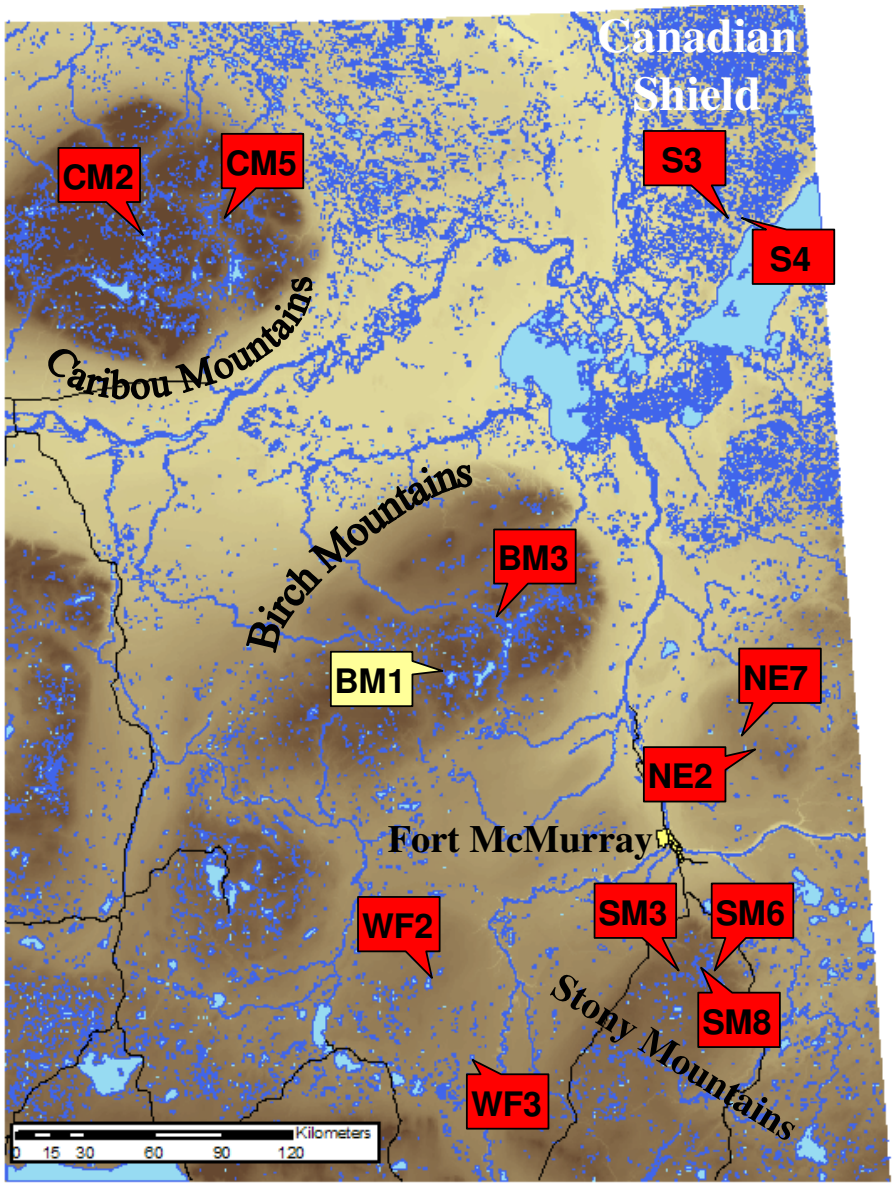

Figure 2: Distribution of study sites for lake sediment core analysis

3.2 Dry weight and loss-on-ignition (LOI) analysis

Sediment dry weight and LOI determinations were made gravimetrically following heating of sediment sub-samples to 105 and 550°C respectively. These analyses are routinely carried out during stratigraphic studies to provide a check for major changes in organic matter content of sediment cores which might indicate changes in sedimentation regimes or sediment inwash events. The cores show a wide range in organic matter content as shown by LOI values (Fig. 3), ranging from <20% at S3 to >80% at WF2. The presence of dramatic short-term fluctuations in dry weight or LOI can indicate that stratigraphic integrity has been compromised e.g. through discontinuities in the record. While there are few such indications in the present core records, there are small shifts in LOI in the bottom of core ALB04A (SM6) and at 5cm depth in both ALB02A (BM3) and ALB05A (SM3).

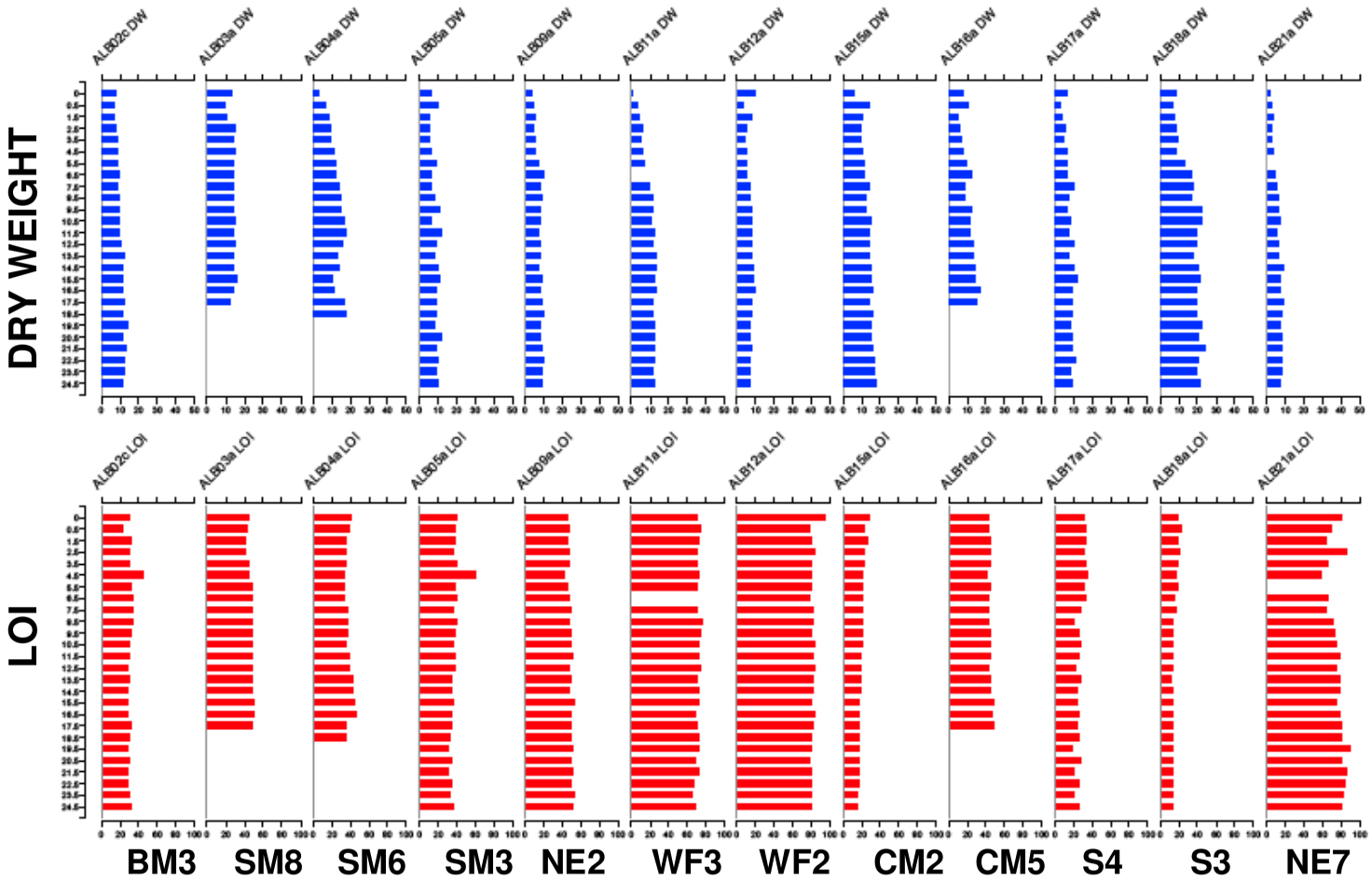

Figure 3: Dry weight (%) and loss on ignition at 550°C (LOI) profiles

3.3 SCP analysis

Rationale and Methods

Spheroidal carbonaceous particles (SCPs) provide an unambiguous indicator of contamination from fossil fuel combustion because they are not produced from wood, biomass or charcoal combustion (e.g. forest fires) and hence have no natural sources (Rose, 2001).

SCP analyses were undertaken on 13 cores (12 cores + Legend) following the method described in Rose (1994). Dried sediment was subjected to sequential chemical attack by mineral acids to remove unwanted fractions leaving a suspension of mainly carbonaceous material and a few persistent minerals in water. SCPs are composed mostly of elemental carbon and are chemically robust. The use of concentrated nitric acid (to remove organic material), hydrofluoric acid (siliceous material) and hydrochloric acid (carbonates and bicarbonates) therefore does them no damage. A known fraction of the resulting suspension was evaporated onto a cover slip and mounted onto a microscope slide. The number of SCPs on the cover slip was counted using a light microscope at x400 magnification and the sediment concentration calculated in units of 'number of particles per gram dry mass of sediment' (gDM^{-1}). The criteria for SCP identification under the light microscope followed Rose (2008). Analytical blanks and SCP reference material (Rose, 2008) were included in each batch of sample digestions. Reference concentrations agreed with the expected values while no SCPs were observed in the blanks. The detection limit for the technique is c. 100 gDM^{-1} and concentrations have an accuracy of c. ± 45 gDM^{-1}.

Results and Discussion

SCPs were found at low but detectable concentrations in all cores. The highest recorded concentration exceeded 1000 gDM^{-1} only in ALB09A (see Fig. 4). No SCPs were detected below 5 cm in any core suggesting any contamination is recent. This is confirmed by the radiometric dating which shows that the earliest presence of SCP contamination was found in ALB04A (SM6) in the late-1950s and in ALB15A (CM2) in the 1960s (Fig. 4). Temporal profiles are highly irregular and, given the low concentrations, the SCP temporal records are likely to be linked to detection limits of the analytical technique. As a consequence, the first presence of SCPs in the cores is not synchronous across the region and the profiles show no consistent temporal trends.

Full SCP inventories were calculated for each core. These provide a measure of the full record of contamination at each lake. These have also been normalised to the ^{210}Pb inventories for each core in order to allow for both sediment focussing effects in each lake and enhanced catchment inputs from, for example, bare rock areas. Both SCP inventories and SCP/^{210}Pb inventory ratios confirm the low contamination status of all the lakes. Highest values for both parameters are found at ALB15A (CM2), followed by ALB03A (SM8), ALB04A (SM6) and ALB09A (NE2) (Fig. 5). For SCP/^{210}Pb inventory ratios ALB16A (CM5) also shows an elevated value. While ALB03A (SM8), ALB04A (SM6) and ALB09A (NE2) are reasonably close to the centre of Oil Sands processing activities, the elevated levels in ALB15A (CM2) and ALB16A (CM5) are among the most remote, suggesting a possible local source near the Caribou Mountains. This source is currently unidentified. Analysis of the full dataset shows no relationship of any SCP parameter (surface and peak concentrations;

surface fluxes; inventories and inventory ratios) with distance from the centre of the Oil Sands processing activities. This indicates that these activities are not a major source of these particulate contaminants. The SCP data also show no agreement with the Hg surface sediment concentrations (see below).

SCP size has also been considered. Only very small SCPs (c. 5 μm) were observed in ALB15A (CM2), ALB16A (CM5) and mostly in ALB01A (Legend) whereas other SCPs were larger (10 – 20 μm) (Fig. 6). While smaller particles are generally indicative of longer transport distances the small number of particles observed do not allow a particle size distribution to be considered and the presence of larger particles in cores closer to the Oil Sands processing may be coincidental.

Summary

SCP contamination is low but detectable in all sites. There are no good relationships between any SCP parameter with distance from the Oil Sands processing area and no relationship between any SCP parameter and the Hg surface sediment data (Section 5).

From these data it appears likely that the Oil Sands processing activities either do not produce SCPs or, if they do, then only in small numbers. The very low concentrations of SCPs in all sites and lack of any spatial patterns within the region are probably more indicative of contamination as a result of long-range transport from high temperature industrial coal and/or oil combustion in an area remote from the Fort McMurray region.

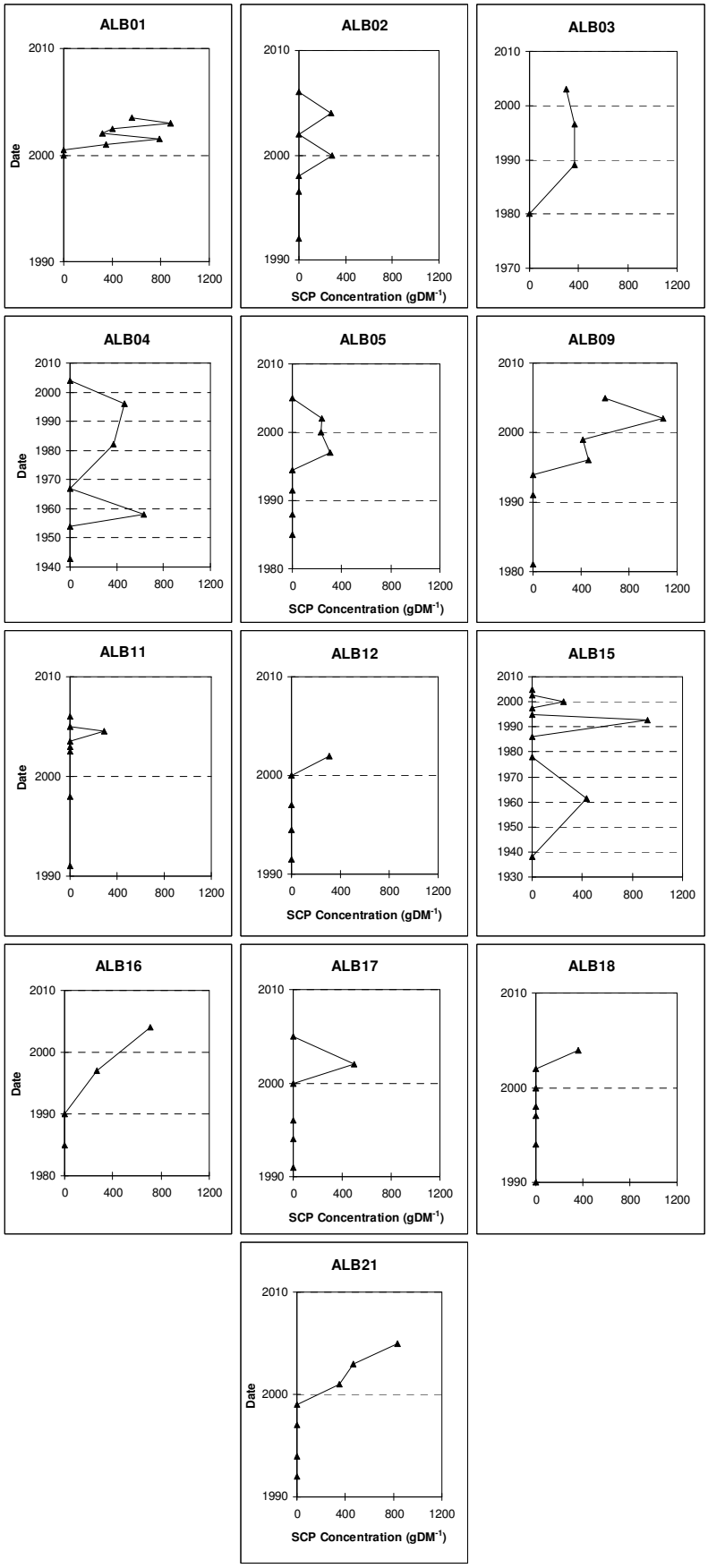

Figure 4: SCP concentration profiles for the 13 cores plotted on radiometric date axes

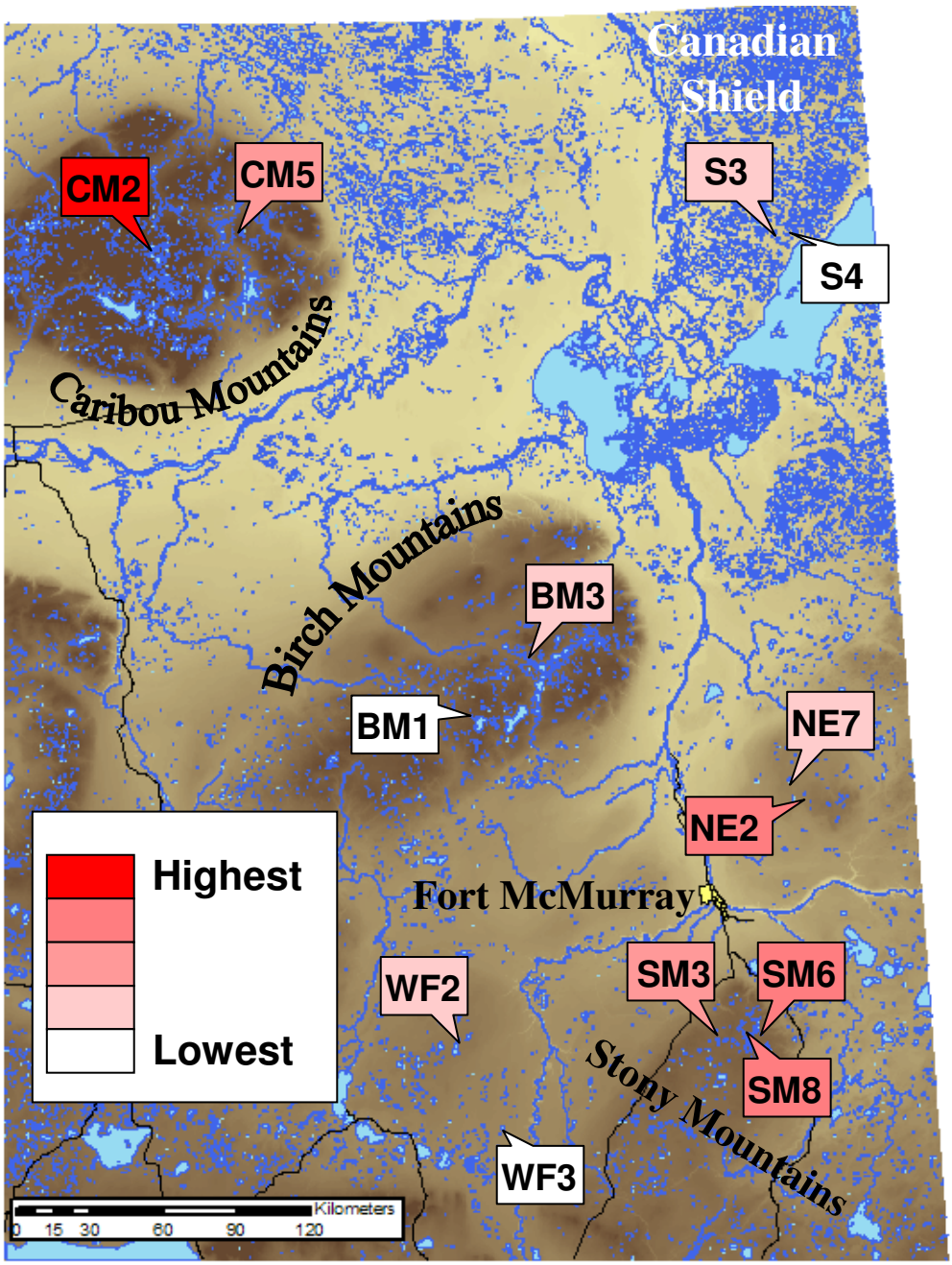

Consecutive Coring ID	CEMA Code	Alternative code / name	SCP Presence
ALB01	BM1	L25 (Legend)	2000
ALB02	BM3	L60	1999
ALB03	SM8	287	1985
ALB04	SM6	A26	1956
ALB05	SM3	289	2002
ALB09	NE2	L7	1993
ALB21	NE7	185	1998
ALB11	WF3	A59	2004
ALB12	WF2	A47	2001
ALB15	CM2	E59 (Rocky Island)	1991
ALB16	CM5	O1 (Unnamed #6)(E55)	1995
ALB17	S4	A301	2001
ALB18	S3	R1	2003

Figure 5: SCP inventory data

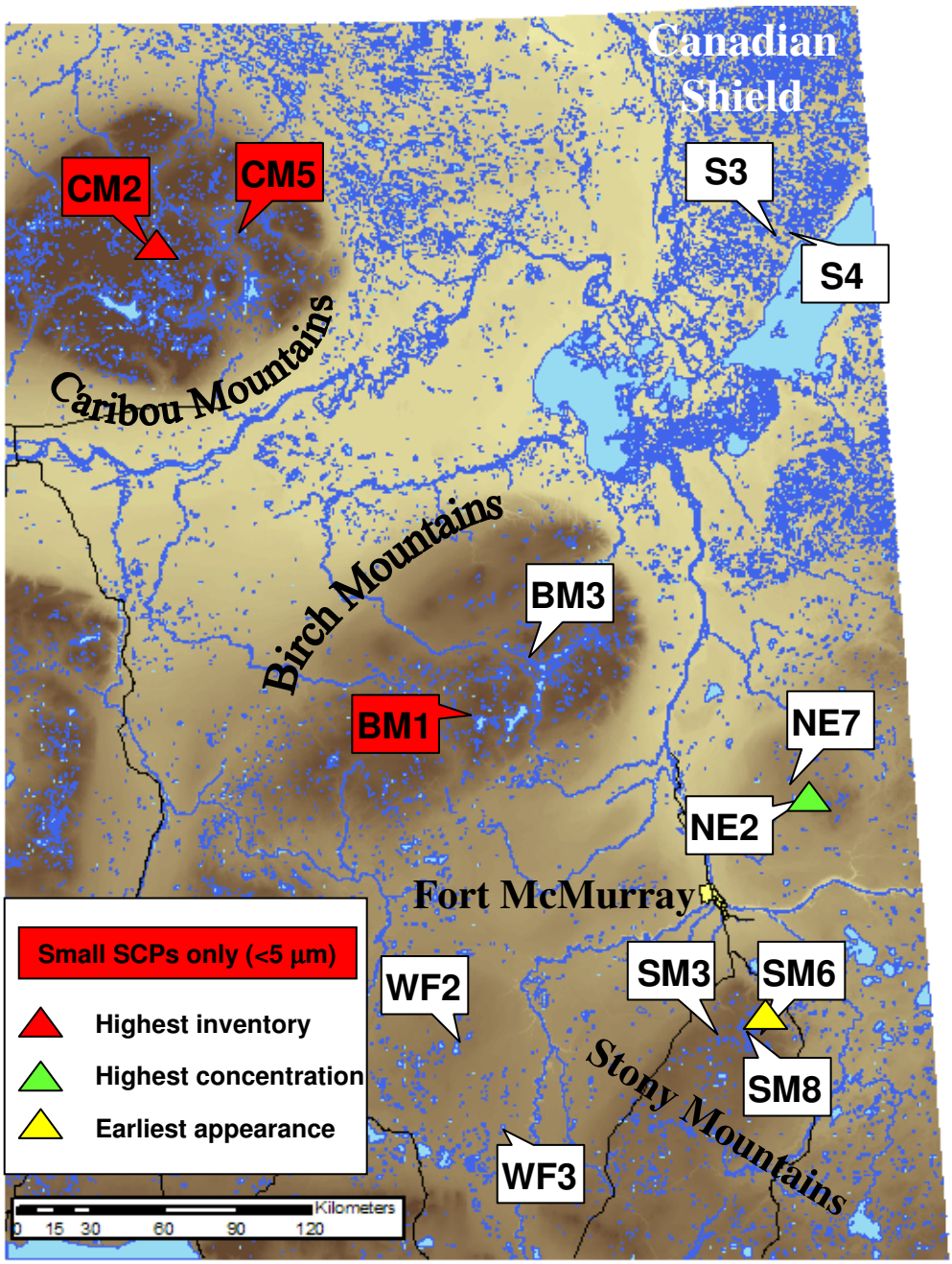

Consecutive Coring ID	CEMA Code	Alternative code / name	SCP Presence
ALB01	BM1	L25 (Legend)	2000
ALB02	BM3	L60	1999
ALB03	SM8	287	1985
ALB04	SM6	A26	1956
ALB05	SM3	289	2002
ALB09	NE2	L7	1993
ALB21	NE7	185	1998
ALB11	WF3	A59	2004
ALB12	WF2	A47	2001
ALB15	CM2	E59 (Rocky Island)	1991
ALB16	CM5	O1 (Unnamed #6)(E55)	1995
ALB17	S4	A301	2001
ALB18	S3	R1	2003

Figure 6: SCP size distribution data

3.4 Radiometric dating (^{210}Pb, ^{137}Cs and ^{241}Am)

Rationale and methodology

^{210}Pb is a naturally produced radionuclide which is a product of the ^{238}U decay series including ^{226}Ra and ^{222}Rn. ^{226}Ra levels in soils and bedrock effectively remain constant because it is produced from the decay of ^{238}U at the same rate at which it decays itself (half-life is 1600 years), a situation called secular equilibrium. Further down the decay series, ^{222}Rn gas is produced, which decays to ^{210}Pb through several rapid steps with an overall half-life of 3.82 days. Since ^{222}Rn gas diffuses from surface soils to the atmosphere and quickly decays to ^{210}Pb, there is a relative excess of ^{210}Pb in the atmosphere, some of which is redeposited to aquatic ecosystems. ^{210}Pb itself decays further with a half-life of 22.3 years.

The proportion of ^{210}Pb in a sample derived from in-situ decay of the parent radionuclide ^{226}Ra may be calculated by measurement of ^{226}Ra activity since the half-lives of the decay series are known. This in-situ ^{210}Pb production is termed "supported" ^{210}Pb. Any excess ^{210}Pb activity above the supported level is termed "unsupported" and is assumed to derive from atmospheric deposition. As surface sediments are buried by material accumulating above, the input flux from the atmosphere ceases and the decay of the trapped ^{210}Pb continues. The decline in unsupported ^{210}Pb is therefore related to the time period for which it has been buried.

Various models are available to determine sediment age from unsupported ^{210}Pb activity which make differing assumptions about the fluxes of ^{210}Pb to the sediment surface. The Constant Initial Concentration (CIC) model assumes that throughout the core the sediment had a constant initial unsupported ^{210}Pb concentration, but lake sediments rarely meet this condition. The Constant Rate of Supply (CRS) model assumes a constant ^{210}Pb flux from the atmosphere but allows sediment accumulation rate to vary. The choice of model may be guided by stratigraphic markers such as peaks in ^{137}Cs (half-life is 30 years) and ^{241}Am, which are artificially produced radionuclides, introduced to the study area by atmospheric fallout from nuclear weapons testing and nuclear reactor accidents which occurred at known dates. The CRS model is generally deemed to be more appropriate where unsupported ^{210}Pb profiles are irregular rather than declining exponentially with depth. The decay of unsupported ^{210}Pb within buried sediments means that detection limits of the method (i.e. ability to distinguish supported and unsupported ^{210}Pb) typically allow its use for sediments aged up to about 150 years.

It is generally assumed that atmospheric fluxes of unsupported ^{210}Pb are relatively constant for a region, so that annual fallout to a lake surface occurs at a constant rate (allowing for year to year variations in precipitation). The total amount or inventory of ^{210}Pb in a sediment core may be calculated to provide an estimate of ^{210}Pb fluxes to

the sediment relative to the (known) atmospheric flux. If the ^{210}Pb flux to the sediment is greater than the atmospheric deposition flux, the implication is that sediment focussing has occurred, whereby the sediment accumulation is concentrated at the coring location by lateral movement and is not constant throughout the lake. Conversely, if the sediment flux is lower than the deposition flux, sediment focussing elsewhere in the lake may have occurred, such that sediment moves away from the coring location.

Sediment samples from 12 cores were analysed for ^{210}Pb, ^{226}Ra, ^{137}Cs and ^{241}Am by direct gamma assay in the Bloomsbury Environmental Isotope Facility (BEIF) at University College London, using an ORTEC HPGe GWL series well-type coaxial low background intrinsic germanium detector. ^{210}Pb was determined via its gamma emissions at 46.5keV, and ^{226}Ra by the 295keV and 352keV gamma rays emitted by its daughter isotope ^{214}Pb following three weeks storage in sealed containers to allow radioactive equilibration. Cesium-137 and ^{241}Am were measured by their emissions at 662keV and 59.5keV. The absolute efficiencies of the detector were determined using calibrated sources and sediment samples of known activity. Corrections were made for the effect of self absorption of low energy gamma rays within the sample.

Results

Core ALB02A (lake BM3 / L60)

^{210}Pb Activity

Total ^{210}Pb activity is in excess of the supporting ^{226}Ra in all of the sections analysed (Table 3a; Fig. 7a). The trends of unsupported ^{210}Pb activities, calculated by subtracting ^{226}Ra activity from total ^{210}Pb activity, decline with depth, with a significant non-monotonic feature from 8.5 – 9.5cm. The relatively low unsupported ^{210}Pb activities in this part of the core suggest a period of rapid sedimentation.

Artificial Fallout Radionuclides

The ^{137}Cs activity versus depth shows a relatively well-resolved peak at 8.75 cm (sample 8.5 – 9 cm) (Table 3a; Fig. 7a) that records the 1963/4 fallout maximum from the atmospheric testing of nuclear weapons.

Core Chronology

Core chronologies were calculated using the CRS and CIC dating models (Appleby, 2001). The CRS model puts the 1963/4 layer at 9 cm whilst the CIC model puts the 1963/4 layer at 11.5 cm. The 1963/4 layer worked out from the CRS model is in a good agreement with the 1963/4 layer suggested by the ^{137}Cs record. Chronology of the core calculated by the CRS model is shown in Table 3b and Fig. 7b. Sedimentation rates in this core have increased from c. 1890s to the present day (from 0.0067 to 0.025 g cm^{-2} yr^{-1}), but the sedimentation rate in the 1960s is relatively high.

Table 3a: ^{210}Pb concentrations in core ALB02A

Depth	Dry Mass	Pb-210						Cs-137	
		Total		Unsupported		supported			
cm	g cm^{-2}	Bq Kg^{-1}	±	Bq Kg^{-1}	±	Bq Kg^{-1}	±	Bq Kg^{-1}	±
0.25	0.0204	568.57	59.37	546.43	61.09	22.14	14.39	76.21	9.61
3.25	0.2709	464.77	34.05	438.51	34.47	26.26	5.35	173.62	7.71
6.25	0.5542	419.38	31.64	397.31	31.98	22.07	4.68	224.22	7.63
8.25	0.7671	281	29.85	260.61	30.18	20.39	4.46	258.2	7.63
8.75	0.8204	271.26	67.96	198.57	70.65	72.69	19.32	266.84	4.38
9.25	0.8736	226.36	23.16	202.04	23.61	24.32	4.61	241.69	6.61
9.75	0.931	274.26	45.25	241.59	45.94	32.67	7.92	199.23	9.75
12.25	1.2181	170.84	17.71	148.55	17.93	22.29	2.78	119.73	4.15
15.25	1.5726	105.18	14.86	73.38	15.1	31.8	2.67	68.89	3.1
18.25	1.9369	102.88	12.46	77.65	12.67	25.23	2.32	30.28	2.04
21.25	2.3398	64.52	11.36	33.28	11.55	31.24	2.08	15.41	1.62
24.25	2.7547	48.71	10.85	20.1	11.03	28.61	1.98	5.02	1.4

Table 3b: ^{210}Pb chronology of core ALB02A

Depth	Dry mass	Chronology			Sedimentation Rate		
		Date	Age				
cm	g cm^{-2}	AD	yr	±	g cm^{-2} yr^{-1}	cm yr^{-1}	± %
0	0	2006	0				
1	0.083	2003	3	2	0.0252	0.298	12
2	0.1665	1999	7	2	0.0244	0.283	11.4
3	0.25	1996	10	2	0.0237	0.268	10.7
4	0.3417	1991	15	2	0.0217	0.24	11.1
5	0.4362	1987	19	2	0.0195	0.208	11.9
6	0.5306	1982	24	2	0.0172	0.175	12.6
7	0.634	1976	30	3	0.0168	0.165	14.9
8	0.7405	1970	36	4	0.017	0.161	17.7
9	0.847	1964	42	4	0.0195	0.18	29.6
10	0.9597	1957	49	6	0.0136	0.118	28.1
11	1.0745	1948	58	9	0.0124	0.108	35
12	1.1894	1938	68	12	0.0113	0.097	41.8
13	1.3067	1926	80	15	0.0098	0.084	46.6
14	1.4249	1912	94	17	0.0083	0.07	50.6
15	1.5431	1899	107	20	0.0067	0.056	54.6

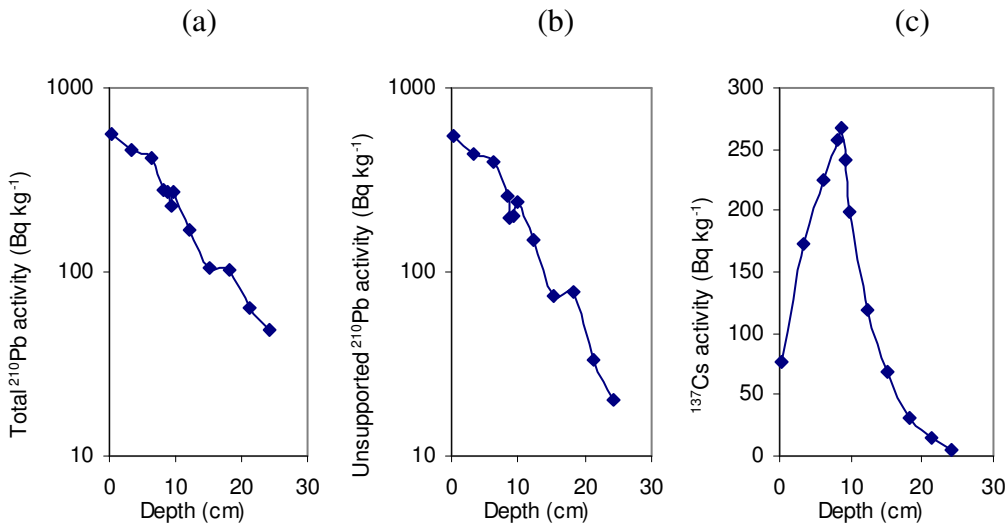

Figure 7a: Fallout radionuclide concentrations in core ALB02A showing (a) total ^{210}Pb, (b) unsupported ^{210}Pb, (c) ^{137}Cs concentrations versus depth.

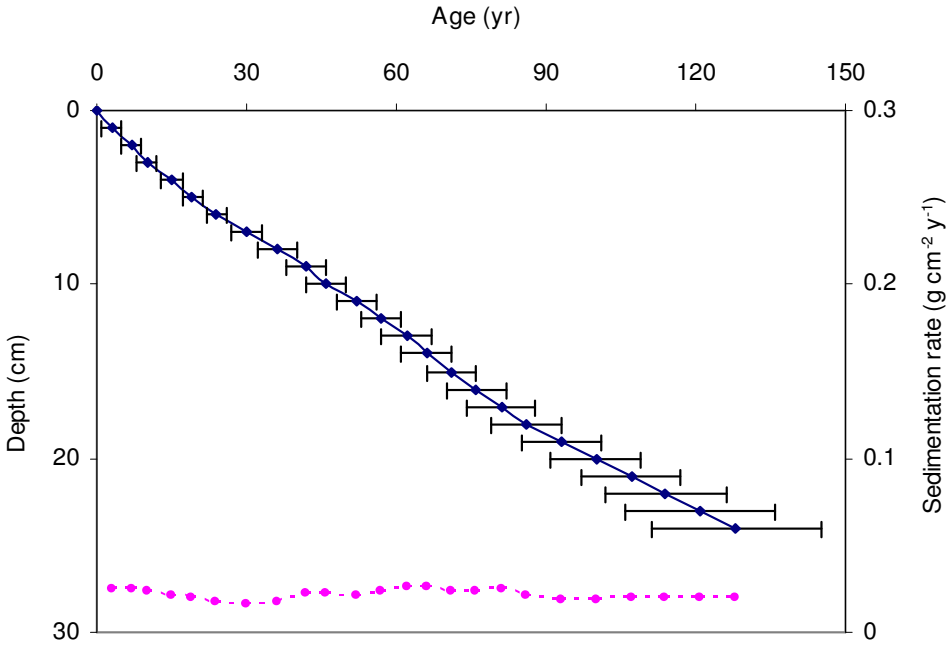

Figure 7b: Radiometric chronology of core ALB02A
(♦ - age ± years; ● – sedimentation rate)

Core ALB03A (lake SM8 / 287)

^{210}Pb Activity

Equilibrium between total ^{210}Pb activity and the supporting ^{226}Ra occurs at a depth of c.7 cm (Table 4a). The trends of unsupported ^{210}Pb activities, calculated by subtracting ^{226}Ra activity from total ^{210}Pb activity, decline with depth (Fig. 8a). The

decline is small in the top 1.5 cm, but more or less exponential below 1.5 cm down to 7 cm (Fig. 8a), suggesting that sedimentation rates are relatively stable.

Artificial Fallout Radionuclides

The ^{137}Cs activities decline with depth showing that there is little use of the ^{137}Cs record for dating (Table 4a; Fig. 8a).

Table 4a: Fallout radionuclide concentrations in core ALB03A

Depth	Dry Mass	Pb-210						Cs-137	
		Total		Unsupported		Supported			
cm	g cm^{-2}	Bq Kg^{-1}	±	Bq Kg^{-1}	±	Bq Kg^{-1}	±	Bq Kg^{-1}	±
0.25	0.0361	529.37	35.52	486.68	36.35	42.69	7.71	168.89	7.53
1.25	0.1577	521.35	31.56	478.97	32.04	42.38	5.5	165.97	6.31
2.25	0.2879	413.19	27.99	373.62	28.49	39.57	5.29	143.07	5.76
3.25	0.433	191.29	21.11	146.31	21.58	44.98	4.5	98.92	4.29
4.25	0.6	137.88	19.51	97.46	19.9	40.42	3.94	61.27	3.44
5.25	0.767	56.25	12.3	13.27	12.59	42.98	2.68	32.12	1.94
6.25	0.934	37.81	13.49	6.86	13.79	30.95	2.85	18.29	1.88
7.25	1.097	49.72	15.22	-9.87	16.63	59.59	6.71	18.12	2.08
9.25	1.423	41.49	8.86	6.95	9.09	34.54	2.03	4.61	1.03
12.25	1.915	27.64	10.41	-8.99	10.7	36.63	2.47	0	0
18.25	2.8765	13.36	9.97	-23.79	10.27	37.15	2.48	0	0

Table 4b: ^{210}Pb chronology of core ALB03A

Depth	Dry mass	Chronology			Sedimentation Rate		
		Date	Age				
cm	g cm^{-2}	AD	yr	±	g cm^{-2} yr^{-1}	cm yr^{-1}	± %
0	0	2006	0				
0.5	0.0665	2000	6	2	0.0105	0.083	9.1
1	0.1273	1993	13	2	0.0087	0.069	9.3
1.5	0.1903	1985	21	2	0.0071	0.056	10.1
2	0.2554	1975	31	3	0.0059	0.044	11.6
2.5	0.3242	1964	42	3	0.0055	0.039	14.8
3	0.3967	1951	55	5	0.0059	0.039	19.8
3.5	0.4748	1935	71	7	0.0053	0.034	27.6
4	0.5583	1916	90	11	0.0036	0.022	38.4
4.5	0.6418	1893	113	14	0.0031	0.019	47
5	0.7253	1867	139	16	0.0037	0.022	53.6

Core Chronology

There is a 1963/4 peak recording the fallout maximum from the atmospheric testing of nuclear weapons and the 1986 peak recording the 1986 Chernobyl accident in the ^{137}Cs profiles in cores taken from the same area (e.g. ALB05A and ALB12A), but the ^{137}Cs profile of this core does not have those peaks. The decline of ^{137}Cs activity

starting from the surface of the core suggests that the surface of the core may be missing. Therefore, the core can only be dated using the ^{210}Pb activities. As the other cores show that sedimentation rates have significantly increased in the surface sediments, the core chronology is calculated using the CRS dating model (Table 4b; Appleby, 2001). Sedimentation rates in this core increased from the 1860s to the 1970s (from 0.0037 to 0.0059 g cm^{-2} yr^{-1}), followed by a relatively rapid increase to the surface at c. 0.0105 g cm^{-2} yr^{-1} (Fig. 8b).

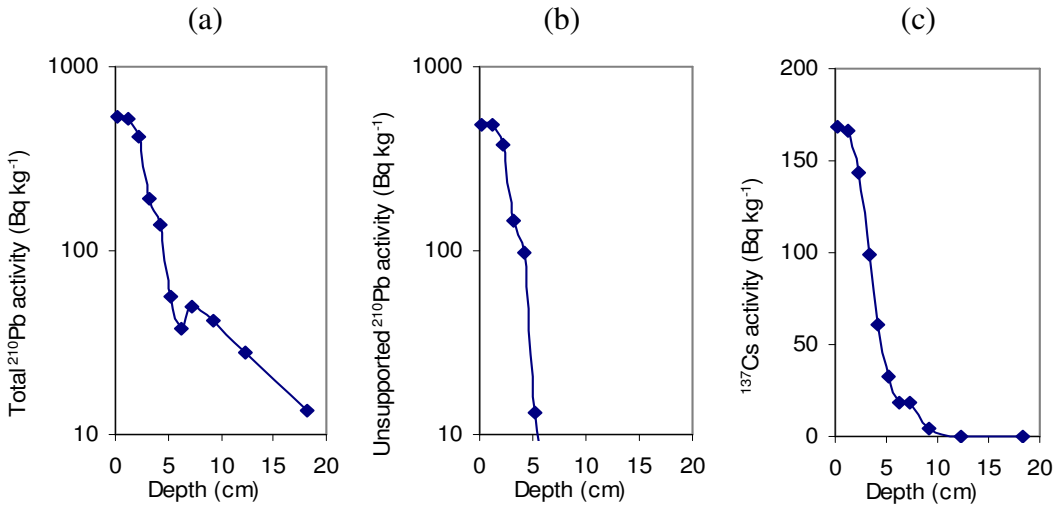

Figure 8a: Fallout radionuclide concentrations in core ALB03A showing (a) total ^{210}Pb, (b) unsupported ^{210}Pb, (c) ^{137}Cs concentrations versus depth.

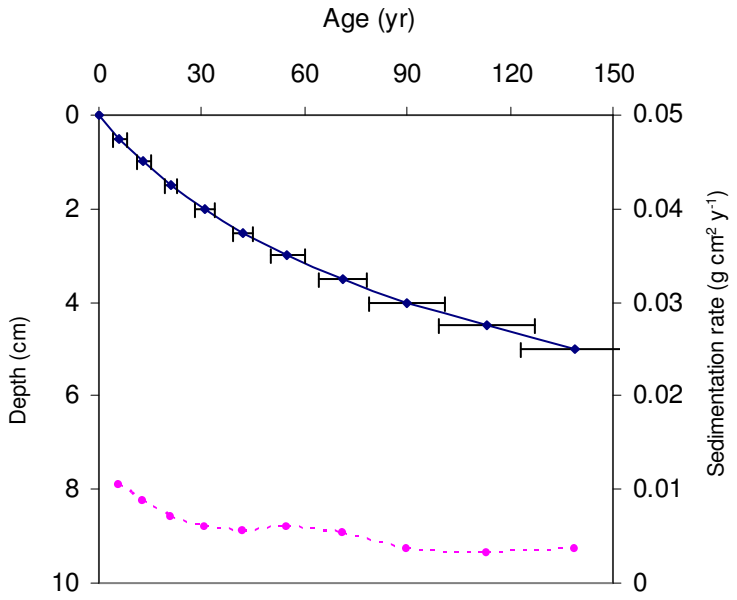

Figure 8b: Radiometric chronology of core ALB03A
(♦ - age ± years; ● – sedimentation rate)

Core ALB04A (lake SM6 / A26)

^{210}Pb Activity

Total ^{210}Pb activity reaches equilibrium with the supporting ^{226}Ra at c. 8 cm (Table 5a). Unsupported ^{210}Pb activities, calculated by subtracting ^{226}Ra activity from total ^{210}Pb activity, show that the maximum value is at 0.75 cm (Fig. 9a), suggesting an increase in sedimentation at the surface. There is a decline more or less exponentially with depth for unsupported ^{210}Pb in sections from 0.75-4 cm, suggesting a relatively uniform sedimentation; but there is a non-monotonic decline from 4 cm downwards, suggesting an increase in sedimentation rate upwards.

Artificial Fallout Radionuclides

The ^{137}Cs activities versus depths show a well-resolved peak at 1.75 cm (sample 1.5 – 2 cm; Table 5a; Fig. 9a). This peak is derived from the 1963/4 fallout maximum from the atmospheric testing of nuclear weapons.

Core Chronology

The non-monotonic decline in unsupported ^{210}Pb has precluded use of the CIC model. Core chronologies were calculated using the CRS dating model. The raw CRS model places the 1963 depth at 4 cm, which is below the depth suggested by the ^{137}Cs record. Using the 1963/4 depth suggested by the ^{137}Cs record as a reference point, corrected results of chronology for the core are shown in Table 5b. Sedimentation in the core gradually increased from the 1890s to the 1950s followed by a relatively uniform rate in the last 50 years (Fig. 9b).

Table 5a: Fallout radionuclide concentrations in core ALB04A

Depth	Dry Mass	Pb-210						Cs-137	
		Total		Unsupported		Supported			
cm	g cm^{-2}	Bq Kg^{-1}	±	Bq Kg^{-1}	±	Bq Kg^{-1}	±	Bq Kg^{-1}	±
0.25	0.0088	500.46	57.18	465.99	58.88	34.47	14.03	216.73	12.38
0.75	0.0358	608.03	75.9	538.13	78.57	69.9	20.29	238.04	14.55
1.25	0.0808	458	32.16	434.17	33.06	23.83	7.64	254.01	7.52
1.75	0.1257	371.32	51.2	318.93	51.73	52.39	7.36	266.58	11.66
2.25	0.1707	277.49	37.85	226.86	39.05	50.63	9.59	231.08	9.42
2.75	0.2157	236.16	19.68	203.37	19.93	32.79	3.13	210.54	5.06
3.75	0.3056	165.65	31.4	118.83	31.92	46.82	5.72	150.03	7.04
4.25	0.3679	162.31	26.44	120.64	26.85	41.67	4.7	131.71	5.9
4.75	0.4302	149.17	25.19	105	25.6	44.17	4.54	88.97	5
5.25	0.4924	121.23	19.23	85.38	19.57	35.85	3.62	65.75	3.83
6.25	0.617	98.66	21.58	66.51	21.86	32.15	3.46	41.1	3.66
6.75	0.6953	76.62	15.33	41.52	15.56	35.1	2.69	34.21	2.49
7.75	0.8518	59.76	18.33	29.12	18.6	30.64	3.16	20.86	2.79
8.75	1.0083	46.75	12.43	2.01	12.67	44.74	2.48	12.93	1.83
9.75	1.1765	34.52	18.87	1.1	19.12	33.42	3.07	10.32	2.64
12.25	1.6262	33.55	8.59	5.25	8.73	28.3	1.55	0	0
18.25	2.561	27.52	8.25	-4.04	8.39	31.56	1.5	0	0

Table 5b: ^{210}Pb chronology of core ALB04A

Depth	Dry mass	Chronology			Sedimentation Rate		
		Date	Age				
cm	g cm^{-2}	AD	yr	±	g cm^{-2} yr^{-1}	cm yr^{-1}	± %
0	0	2006	0				
0.5	0.0223	2001	5	2	0.0042	0.075	17.6
1	0.0583	1990	16	3	0.0031	0.039	19.3
1.5	0.1032	1973	33	6	0.0031	0.035	27.7
2	0.1482	1961	45	6	0.0053	0.059	39
2.5	0.1932	1956	50	7	0.0085	0.095	17.7
3	0.2382	1951	55	7	0.0088	0.095	19.2
3.5	0.2831	1946	60	8	0.0099	0.1	26.8
4	0.3368	1940	66	9	0.0094	0.085	29.4
4.5	0.3991	1933	73	10	0.008	0.064	30.3
5	0.4613	1925	81	11	0.0073	0.059	33.6
5.5	0.5235	1915	91	14	0.0065	0.052	40.2
6	0.5859	1905	101	17	0.0054	0.041	50.7
6.5	0.6561	1891	115	23	0.0050	0.036	68.4

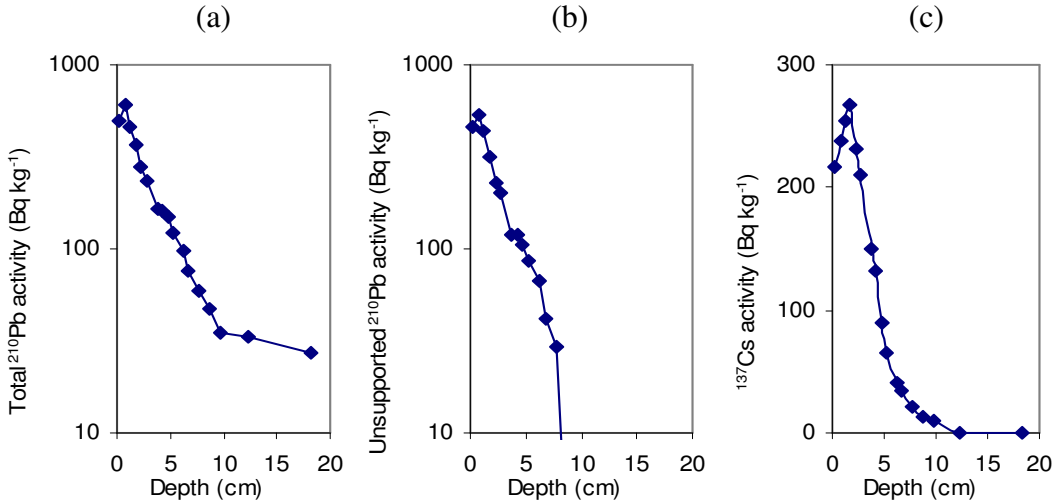

Figure 9a: Fallout radionuclide concentrations in core ALB04A showing (a) total ^{210}Pb, (b) unsupported ^{210}Pb, (c) ^{137}Cs concentrations versus depth.

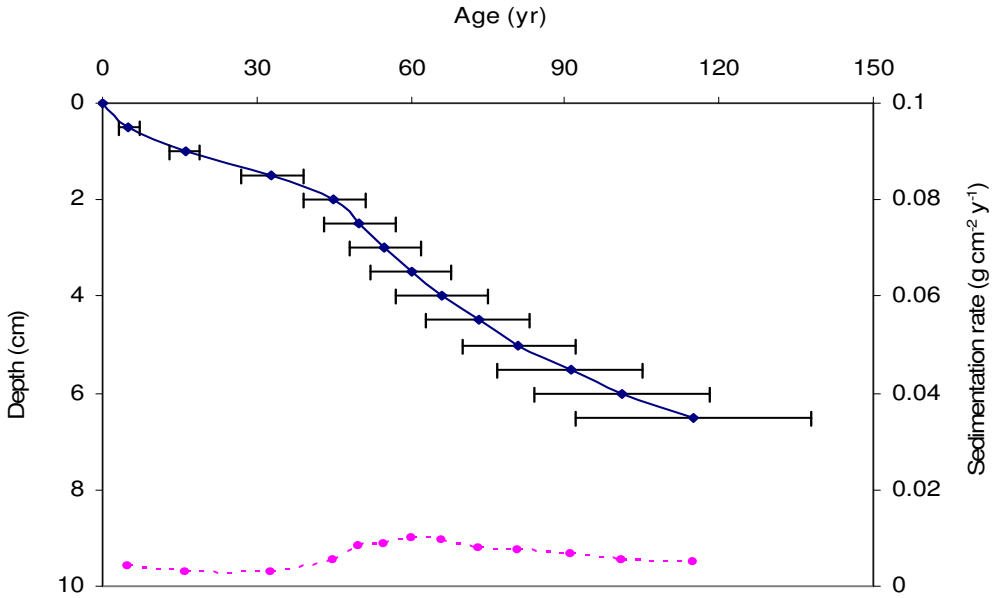

Figure 9b: Radiometric chronology of core ALB04A
(♦ - age ± years; ● – sedimentation rate)

Core ALB05A (lake SM3 / 289)

^{210}Pb Activity

Total ^{210}Pb activity reaches equilibrium with the supporting ^{226}Ra at a depth of c.23 cm (Table 6a). The unsupported ^{210}Pb profile of the core can be divided into two distinct zones. In the top 12.5 cm, there is little net decline in ^{210}Pb concentrations with depth with the highest value at 3.25 cm. The distinct flattening of the gradient of the profile above 12.5 cm suggests sedimentation rates have significantly increased in this section (Fig. 10a). From 12.5 cm down to the equilibrium depth, ^{210}Pb concentrations decline more or less exponentially with depth, suggesting that sedimentation rates are relatively stable.

Artificial Fallout Radionuclides

The ^{137}Cs activities versus depth profile (Fig. 10a) has two well-resolved peaks. These two peaks record fallout from the 1986 Chernobyl accident at 8 – 9 cm and the 1963 fallout maximum from the atmospheric testing of nuclear weapons at 12 – 13 cm.

Core Chronology

Use of the CIC model was precluded by the non-monotonic variation in unsupported ^{210}Pb activities in the core. The CRS model places the 1963 layer and 1986 layer at c. 12.5 cm and c. 8 cm in the core respectively. These are in a good agreement with the dates provided by the ^{137}Cs profile, suggesting the CRS model is valid for the core. The CRS model calculated sedimentation rates are shown in Table 6b. Sedimentation

rates in this core increased in the second half of the 19th century from 0.0032 g cm^{-2} yr^{-1}, followed by a relatively stable period to the 1960s (Fig. 10b). In the last three decades or so, sedimentation rates have been increasing rapidly to the surface at c. 0.04 g cm^{-2} yr^{-1}.

Table 6a: Fallout radionuclide concentrations in core ALB05A

Depth	Dry Mass	Pb-210						Cs-137	
		Total		Unsupported		Supported			
cm	g cm^{-2}	Bq Kg^{-1}	±	Bq Kg^{-1}	±	Bq Kg^{-1}	±	Bq Kg^{-1}	±
0.25	0.0187	355.33	28.14	304.39	29.08	50.94	7.34	175.66	7.04
3.25	0.2242	346.83	23.41	312.61	23.96	34.22	5.11	170.16	6.24
6.25	0.4702	305.13	21.41	259.77	22.07	45.36	5.37	167.78	5.5
8.25	0.6766	293.18	19.99	245.41	20.54	47.77	4.73	172.13	5.53
9.25	0.7798	325.25	21.33	290.24	21.76	35.01	4.32	185.79	5.55
10.25	0.8862	322.86	20.32	283.77	20.81	39.09	4.5	165.79	5.35
11.25	0.9925	294.64	21.22	253.68	21.68	40.96	4.45	170.71	5.58
12.25	1.0989	313.48	19.37	278.86	19.78	34.62	4.01	181.32	5.24
12.75	1.1544	257.8	19.49	217.2	19.96	40.6	4.31	187.89	5.54
15.25	1.4319	175.43	16.78	133.15	17.29	42.28	4.16	144.2	4.82
18.25	1.7658	100.81	11.17	61.07	11.65	39.74	3.3	55.24	2.42
21.25	2.1018	69.18	8.31	32.28	8.62	36.9	2.29	24.73	1.51
24.25	2.4438	24.74	7.51	-17.26	7.87	42	2.36	6.21	1.06

Table 6b: ^{210}Pb chronology of core ALB05A

Depth	Dry mass	Chronology			Sedimentation Rate		
		Date	Age				
cm	g cm^{-2}	AD	yr	±	g cm^{-2} yr^{-1}	cm yr^{-1}	± %
0	0	2006	0				
1	0.0701	2004	2	2	0.0402	0.572	9.7
2	0.1386	2002	4	2	0.0377	0.522	9.1
3	0.2071	2001	5	2	0.0352	0.472	8.6
4	0.2857	1998	8	2	0.0343	0.437	8.7
5	0.3677	1996	10	2	0.0338	0.406	9
6	0.4497	1994	12	2	0.0333	0.375	9.3
7	0.5476	1990	16	2	0.0315	0.333	9.4
8	0.6508	1987	19	2	0.0291	0.288	9.5
9	0.754	1983	23	2	0.023	0.221	9.1
10	0.8596	1978	28	2	0.019	0.18	9.2
11	0.9659	1972	34	2	0.0173	0.163	10.4
12	1.0723	1965	41	2	0.0135	0.125	10.7
13	1.1821	1957	49	3	0.0136	0.122	13.2
14	1.2931	1948	58	4	0.0126	0.114	15.3
15	1.4041	1939	67	4	0.0117	0.105	17.5
16	1.5154	1929	77	5	0.0109	0.098	21.1
17	1.6267	1918	88	6	0.0101	0.091	25.1
18	1.738	1908	98	8	0.0093	0.084	29.1
19	1.8498	1890	116	14	0.0075	0.067	32.4
20	1.9618	1870	136	21	0.0054	0.048	35.6
21	2.0738	1850	156	29	0.0032	0.029	38.8

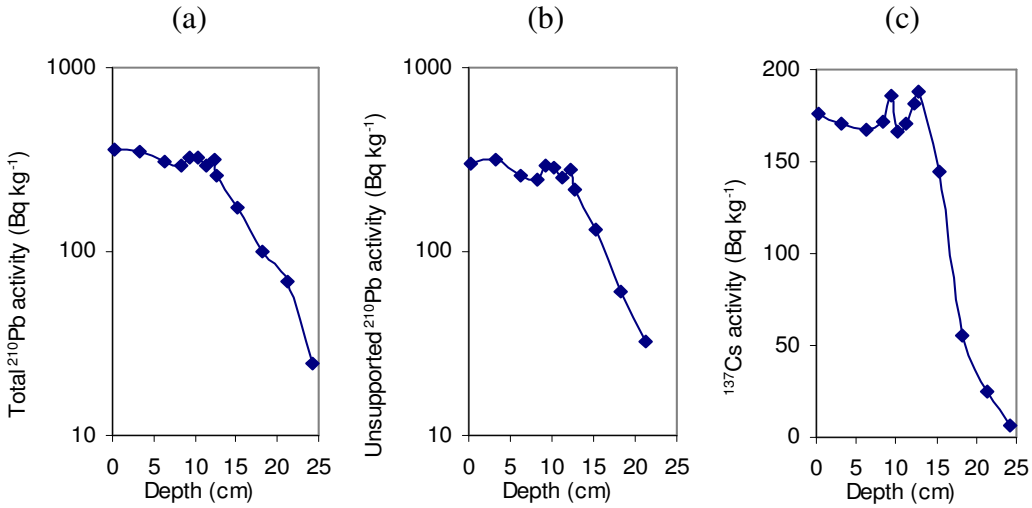

Figure 10a: Fallout radionuclide concentrations in core ALB05A showing (a) total ^{210}Pb, (b) unsupported ^{210}Pb, (c) ^{137}Cs concentrations versus depth.

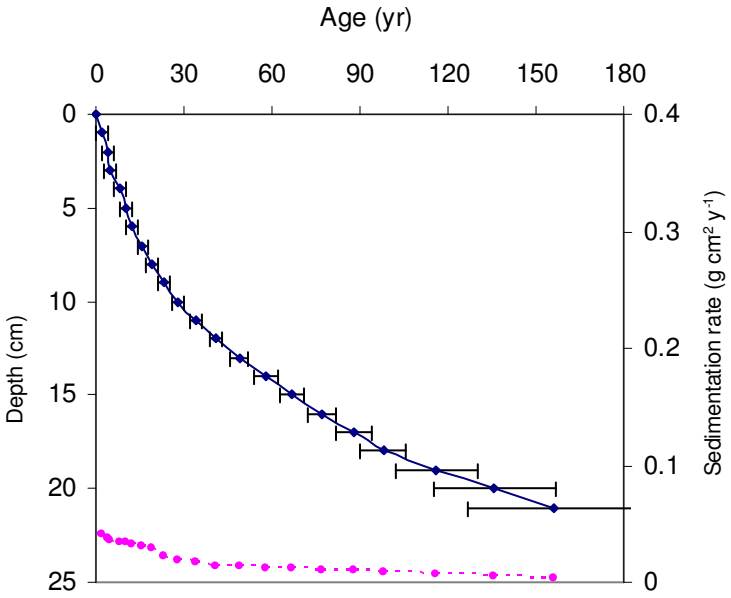

Figure 10b: Radiometric chronology of core ALB05A (♦ - age ± years; ● – sedimentation rate)

Core ALB09A (lake NE2 / L7)

^{210}Pb Activity

Equilibrium of total ^{210}Pb activity with the supporting ^{226}Ra activity appears to occur at c. 15 cm (Table 7a). Trends in unsupported ^{210}Pb activities show a decline more or less exponentially with depth, but with small non-monotonic features. This suggests some changes in sediment accumulation, but sedimentation rates are relatively stable.

Artificial Fallout Radionuclides

The ^{137}Cs activity versus depth profile shows two peaks at 3.25 and 6.25 cm (sample 6 – 6.5 cm; Fig. 11a). The peak at 6.25 cm may indicate the 1963/4 fallout maximum from the atmospheric testing of nuclear weapons.

Core Chronology

Chronology of the core was calculated using the CRS dating model (Table 7b). The raw CRS model places the 1963 depth at 6.5 cm, which is in good agreement with the peak at 6.25 cm in the ^{137}Cs record. Sedimentation rates in the core for the last hundred years were relatively stable with a mean at 0.011 g cm $^{-2}$ y^{-1} (Fig. 11b).

Table 7a: ^{210}Pb concentrations in core ALB09A

Depth	Dry Mass	Pb-210						Cs-137	
		Total		Unsupported		Supported			
cm	g cm^{-2}	Bq Kg^{-1}	±	Bq Kg^{-1}	±	Bq Kg^{-1}	±	Bq Kg^{-1}	±
0.25	0.0113	676.91	53.12	634.49	63.33	42.42	34.49	159.51	9.48
2.25	0.1196	338.52	36.22	322.04	37	16.48	7.57	154.12	7.34
3.25	0.1737	368.21	33.1	322.75	41.38	45.46	24.83	223.89	7.47
3.75	0.2158	245.92	38.43	199.54	39.4	46.38	8.68	159.03	8.2
6.25	0.4262	190.6	25.45	177.48	57.64	13.12	5.172	204.47	6.44
7.25	0.5236	135.98	20.86	115.86	22.08	20.12	7.23	102.04	3.89
8.25	0.6211	95.43	21.97	62.05	22.61	33.38	5.36	89.59	4.33
9.25	0.7185	125.53	23.31	116.93	24.97	8.6	8.95	94.13	4.46
10.25	0.8122	85.93	20.06	55.21	20.62	30.72	4.77	46	3.35
11.25	0.9058	63.14	14.03	29.79	14.37	33.35	3.12	40.99	2.14
12.25	0.9995	78.05	20.8	39.68	47.41	38.37	42.6	54.79	3.73
13.25	1.1006	59.85	19.21	33.77	19.64	26.08	4.11	29.12	2.59
14.25	1.2018	59.73	16.79	29.11	17.23	30.62	3.89	29.87	2.51
15.25	1.3029	12.53	22.1	-1.1	26.53	13.63	4.68	35	3.78
18.25	1.6226	30.27	19.59	0.27	19.59	30	10	24.71	3.23

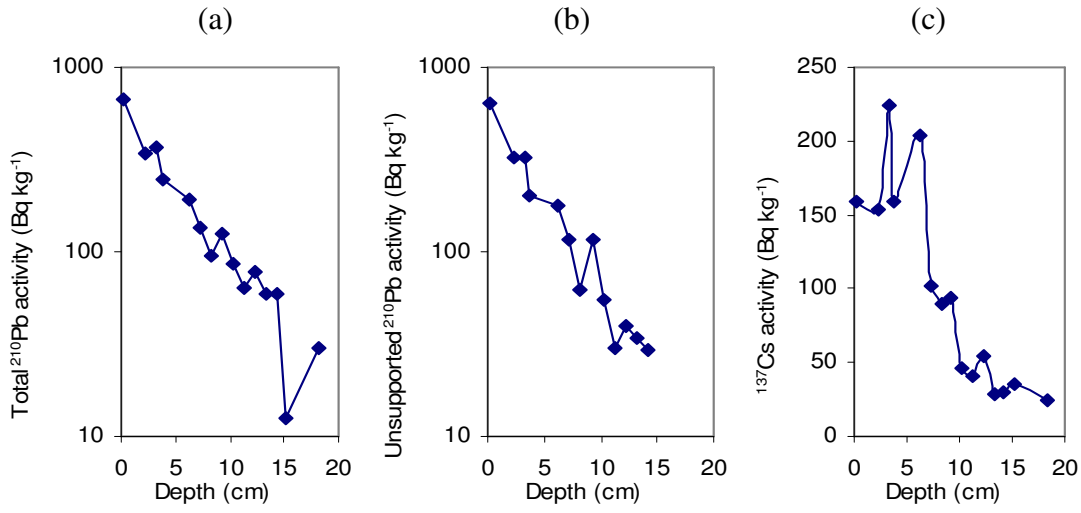

Figure 11a: Fallout radionuclide concentrations in core ALB09A showing (a) total ^{210}Pb, (b) unsupported ^{210}Pb, (c) ^{137}Cs concentrations versus depth.

Table 7b: ^{210}Pb chronology of core ALB09A

Depth	Dry mass	Chronology			Sedimentation Rate		
		Date	Age				
cm	g cm^{-2}	AD	yr	±	g cm^{-2} yr^{-1}	cm yr^{-1}	± %
0	0	2006	0				
1	0.0519	2001	5	2	0.0097	0.181	14.1
2	0.1061	1995	11	2	0.0113	0.21	15.7
3	0.1602	1990	16	2	0.0105	0.172	17.7
4	0.2368	1983	23	3	0.0141	0.167	25.2
5	0.321	1976	30	4	0.012	0.14	30.1
6	0.4052	1969	37	4	0.01	0.114	35
7	0.4993	1960	46	6	0.0104	0.109	30.4
8	0.5967	1952	54	7	0.0145	0.149	40.5
9	0.6942	1943	63	10	0.0085	0.088	41.2
10	0.7888	1930	76	14	0.008	0.085	56.3
11	0.8824	1920	86	19	0.011	0.118	76
12	0.9761	1908	98	23	0.0088	0.091	90.3
13	1.0753	1892	114	27	0.005	0.05	108.1

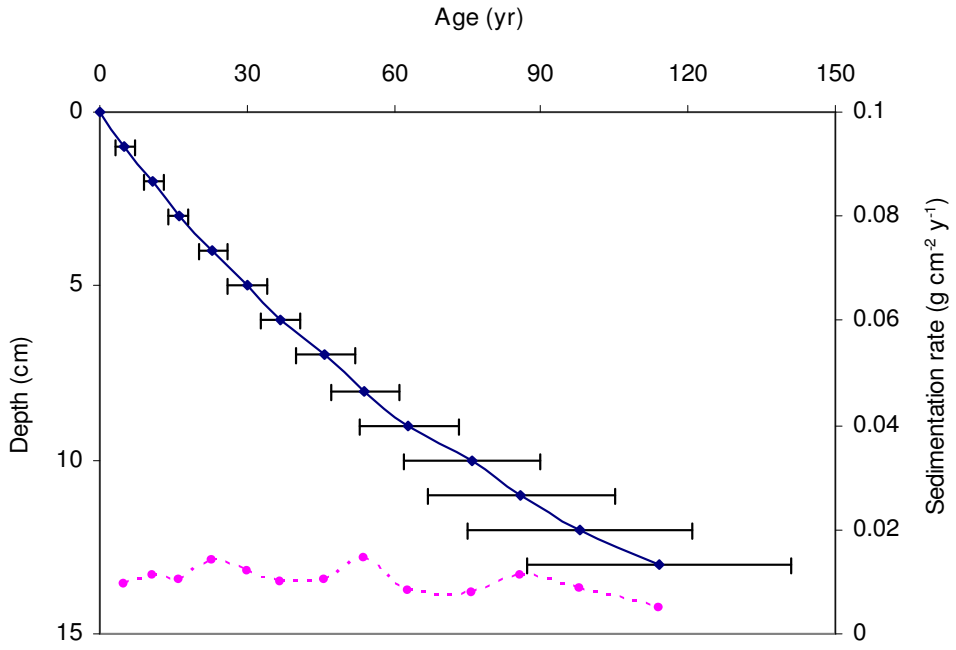

Figure 11b: Radiometric chronology of core ALB09A
(♦ - age ± years; ● – sedimentation rate)

Core ALB11A (lake WF3)

^{210}Pb Activity

The equilibrium depth for total ^{210}Pb and supporting ^{226}Ra activities is about 13 cm (Table 8a). Unsupported ^{210}Pb activity declines irregularly with depth in the top 6 cm, with significant non-monotonic feature at 5.25 cm (Fig. 12a). Below 6 cm, unsupported ^{210}Pb activity declines more or less exponentially with depth, implying a relatively uniform sedimentation rate (Fig. 12b).

Artificial Fallout Radionuclides

The ^{137}Cs activity versus depth profile again shows a well-resolved peak at 5.25 cm (sample 5–5.5 cm) which indicates the 1963/4 fallout maximum from the atmospheric testing of nuclear weapons (Fig. 12a).

Core chronology

Due to the non- monotonic decline in unsupported ^{210}Pb, use of the CIC model has been precluded. Core chronologies were calculated using the CRS dating model. The raw CRS model places the 1963 depth at 6.5 cm, which is below 5.25 cm suggested by the ^{137}Cs record for 1963/4. Using the 1963/4 depth suggested by the ^{137}Cs record as a reference point, the chronology for the core was re-calculated and is shown in Table 8b. Sedimentation rates in the last c. 140 years have doubled. The mean post-1963 unsupported ^{210}Pb flux is 128 Bq m^{-2} y^{-1}, compared to 173 Bq m^{-2} y^{-1} before 1963. Reduced ^{210}Pb flux after 1963 may imply missing surface sediment.

Table 8a: ^{210}Pb concentrations in core ALB11A

Depth	Dry Mass	Pb-210						Cs-137	
		Total		Unsupported		Supported			
cm	g cm^{-2}	Bq Kg^{-1}	±	Bq Kg^{-1}	±	Bq Kg^{-1}	±	Bq Kg^{-1}	±
0.25	0.0011	472.41	54.11	452.78	55.53	19.63	12.46	171.7	11.12
3.25	0.1366	430.43	34.17	404.74	34.91	25.69	7.13	205.51	7.72
5.25	0.9993	248.82	47.04	192.71	48.17	56.11	10.36	225.24	10.61
6.25	1.4306	237.67	30.08	213.38	30.76	24.29	6.43	214.09	7.68
7.25	1.8953	176.36	32.21	135.39	33.02	40.97	7.29	183.92	7.17
9.25	2.8246	68	19.21	43.42	19.71	24.58	4.4	76.43	3.71
12.25	3.2078	34.14	16.59	10.52	17.07	23.62	4	31.95	2.63
13.25	3.3401	46.51	17.01	-9.06	17.49	55.57	4.08	20	2
15.25	3.6046	43.39	12.01	5.41	12.38	37.98	3.02	17.08	1.66
17.25	3.8786	31.57	19.8	-3.36	20.34	34.93	4.67	5.75	2.42
18.25	4.0156	28.08	12.27	8.95	12.58	19.13	2.79	6.25	1.51
20.25	4.2865	25.35	20.92	1.35	20.92	24	5	0	0

Table 8b: ^{210}Pb chronology of core ALB11A

Depth	Dry mass	Chronology			Sedimentation Rate		
		Date	Age				
cm	g cm^{-2}	AD	yr	±	g cm^{-2} yr^{-1}	cm yr^{-1}	± %
0	0	2006	0				
1	0.035	2005	1	2	0.0281	0.541	14.2
2	0.0801	2003	3	2	0.0278	0.361	13.4
3	0.1253	2002	4	2	0.0274	0.182	12.6
4	0.4601	1987	19	3	0.0236	0.0588	18.4
5	0.8915	1968	38	4	0.027	0.0625	26.5
6	1.3228	1955	51	6	0.0277	0.0625	25.1
7	1.7791	1936	70	9	0.0181	0.0392	34.4
8	2.2438	1904	102	12	0.0137	0.023	42.2
9	2.7084	1869	137	13	0.0132	0.029	48

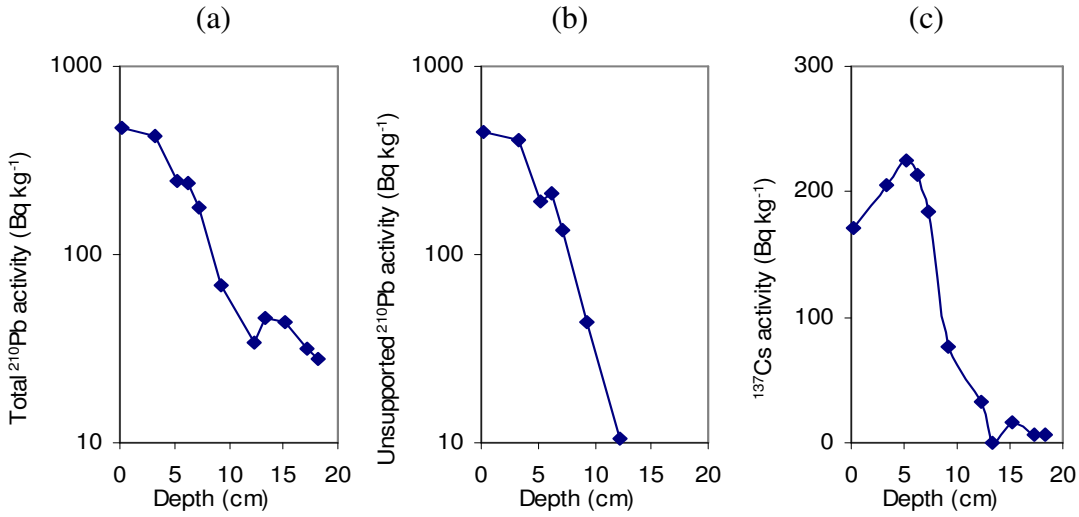

Figure 12a: Fallout radionuclide concentrations in core ALB11A showing (a) total ^{210}Pb, (b) unsupported ^{210}Pb, (c) ^{137}Cs concentrations versus depth.

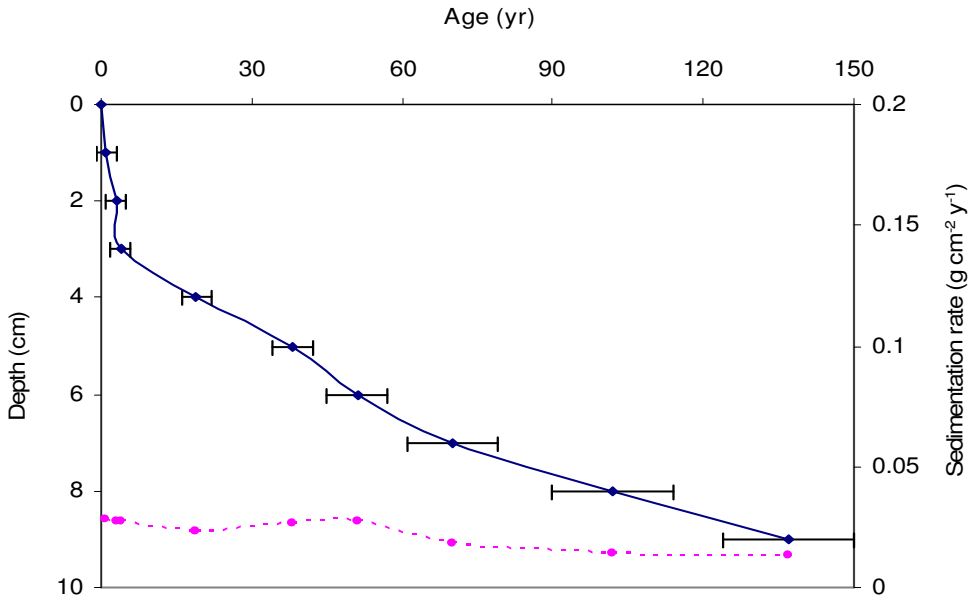

Figure 12b: Radiometric chronology of core ALB11A
(♦ - age ± years; ● – sedimentation rate)

Core ALB12A (lake WF2 / A47)

^{210}Pb Activity

In this core, total ^{210}Pb activity reaches equilibrium with the supporting ^{226}Ra at a depth of c.20 cm (Table 9a). The unsupported ^{210}Pb profile of the core shows that the maximum value of unsupported ^{210}Pb concentration is below the surface sediments showing an increase in sedimentation rate in recent years (Fig. 13a). From 4 cm down to the equilibrium depth, ^{210}Pb concentrations decline more or less exponentially with depth, suggesting that sedimentation rates are relatively stable.

Artificial Fallout Radionuclides

The ^{137}Cs activities versus depth profile (Fig. 13a) has two well-resolved peaks. The peak at 7.25 cm (sample 7 – 7.5 cm) records the 1963 fallout maximum from the atmospheric testing of nuclear weapons. The 1986 Chernobyl accident may be recorded at 2.25 cm as there is a peak in the ^{137}Cs profile, but if compared with the values of unsupported ^{210}Pb and ^{137}Cs activities at 2 - 4 cm depth, the relatively low ^{137}Cs activity at 3.25 cm may be diluted by high sedimentation rates or caused by errors, and the 1986 layer could therefore be located at 3.25 cm.

Table 9a: Fallout radionuclide concentrations in core ALB12A

Depth	Dry Mass	Pb-210						Cs-137	
		Total		Unsupported		Supported			
cm	g cm^{-2}	Bq Kg^{-1}	±	Bq Kg^{-1}	±	Bq Kg^{-1}	±	Bq Kg^{-1}	±
0.25	0.0282	350.56	37.88	318.9	38.67	31.66	7.76	134.28	8.04
2.25	0.1645	447.83	34.88	420.7	35.46	27.13	6.4	148.67	6.95
3.25	0.2273	368.84	28.98	346.81	29.57	22.03	5.89	141.55	5.85
4.25	0.284	382.77	29.21	354.68	29.65	28.09	5.09	129.43	5.48
6.25	0.3973	247.67	24.34	223	24.89	24.67	5.18	122.52	5.13
7.25	0.4639	210.39	26.51	187.22	27.22	23.17	6.17	139.48	5.71
9.25	0.597	120.69	14.1	92.56	14.5	28.13	3.4	100.31	3.1
10.25	0.6748	106.55	13.54	78.72	13.99	27.83	3.5	94.97	2.85
12.25	0.8304	82.46	14.68	58.66	15.03	23.8	3.23	80.21	3.06
13.75	0.9649	58.98	15.96	31.47	16.32	27.51	3.41	64.29	2.87
15.25	1.0995	28.29	11.31	9.19	11.67	19.1	2.87	45.49	2.07
18.25	1.3804	29.54	13.01	10.79	13.31	18.75	2.83	25.62	2.05
21.25	1.6414	4.47	12.08	-18.55	12.4	23.02	2.78	17.24	1.64
24.25	1.8775	0.78	13.02	-17.92	13.39	18.7	3.14	12.14	1.57

Table 9b: ^{210}Pb chronology of core ALB12A

Depth	Dry mass	Chronology			Sedimentation Rate		
		Date	Age				
cm	g cm^{-2}	AD	yr	±	g cm^{-2} yr^{-1}	cm yr^{-1}	± %
0	0	2006	0				
1	0.0793	2001	5	2	0.0151	0.212	12.6
2	0.1475	1996	10	2	0.011	0.163	11.5
3	0.2116	1990	16	2	0.01	0.163	12
4	0.2698	1983	23	3	0.0085	0.148	13.1
5	0.3265	1977	29	3	0.0081	0.141	15.5
6	0.3831	1970	36	4	0.0083	0.139	18.3
7	0.4473	1962	44	5	0.0078	0.121	22.7
8	0.5138	1954	52	7	0.0083	0.122	27.8
9	0.5804	1946	60	9	0.0092	0.131	32.9
10	0.6553	1937	69	12	0.0087	0.115	40.8
11	0.7332	1927	79	17	0.0074	0.093	56.7
12	0.8109	1916	90	22	0.006	0.074	75
13	0.8977	1900	106	27	0.0052	0.061	89.7

Core Chronology

Due to the non-monotonic variation in unsupported ^{210}Pb activities in the surface of the core, chronology was calculated using the CRS model. The CRS model places the 1963 layer and 1986 layer at c. 7 cm and c. 3.5 cm in the core respectively (Table 9b). The 1963 layer dated by the CRS model is in a good agreement with the date provided by the ^{137}Cs profile, and the 1986 layer is in the peak region of the ^{137}Cs activities derived by the 1986 Chernobyl accident. Sedimentation rates in this core were relatively uniform before the 1980s, but have significantly increased in the last twenty years or so (Fig. 13b).

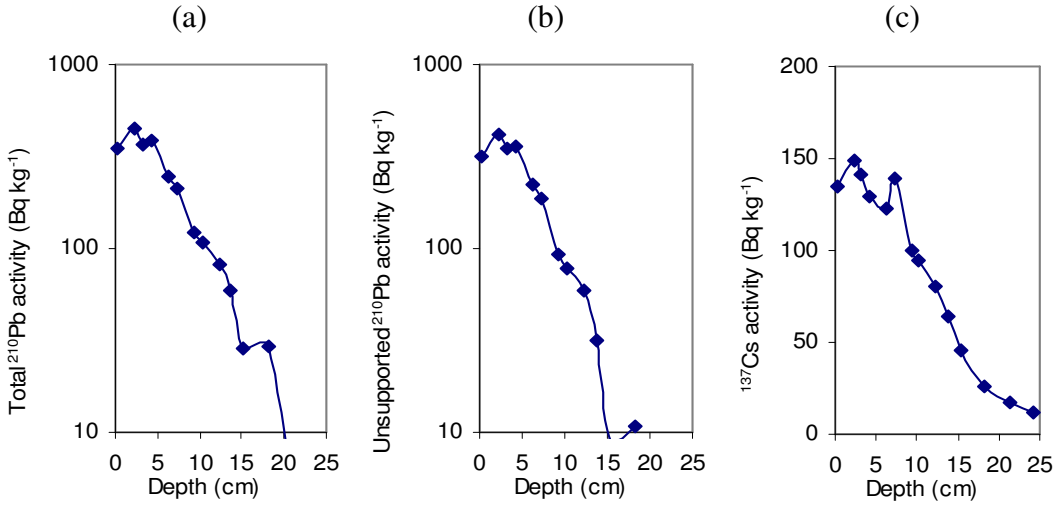

Figure 13a: Fallout radionuclide concentrations in core ALB12A showing (a) total ^{210}Pb, (b) unsupported ^{210}Pb, (c) ^{137}Cs concentrations versus depth.

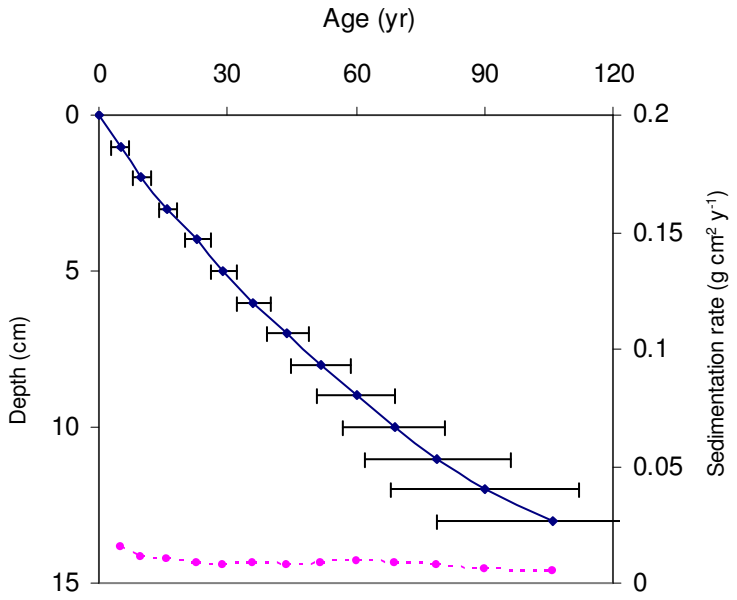

Figure 13b: Radiometric chronology of core ALB12A
(♦ - age ± years; ● – sedimentation rate)

Core ALB15A (lake CM2 / E59 "Rocky Island")

^{210}Pb Activity

Total ^{210}Pb activity may just reach equilibrium with the supporting ^{226}Ra at the bottom of the core (25 cm; Table 10a). Unsupported ^{210}Pb activities, calculated by subtracting ^{226}Ra activity from total ^{210}Pb activity, decline more or less exponentially with depth, suggesting that sedimentation rates in this core are relatively stable (Fig. 14a).

Artificial Fallout Radionuclides

The ^{137}Cs activities versus depths have a relatively well-resolved peak in the core (Table 10a; Fig. 14a). The peak derived from the sample 6 – 6.5 cm almost certainly records the 1963 fallout maximum from the atmospheric testing of nuclear weapons.

Table 10a: Fallout radionuclide concentrations in core ALB15A

Depth	Dry Mass	Pb-210						Cs-137	
		Total		Unsupported		supported			
cm	g cm^{-2}	Bq Kg^{-1}	±	Bq Kg^{-1}	±	Bq Kg^{-1}	±	Bq Kg^{-1}	±
0.25	0.0172	418.48	24.49	375.47	24.86	43.01	4.3	95.13	4.27
3.25	0.2792	340.58	21.24	302.28	21.59	38.3	3.87	120.1	4.42
4.25	0.392	306.86	24.77	272.29	25.21	34.57	4.69	137.21	5.15
5.75	0.5612	222.74	21.51	189.22	21.92	33.52	4.24	149.84	4.99
6.25	0.6176	191.55	21.32	141.63	21.78	49.92	4.46	164.58	5.22
6.75	0.6806	205.93	24.11	169.99	24.58	35.94	4.76	155.98	5.93
7.75	0.8066	166.96	17.99	131.46	18.38	35.5	3.75	136.82	4.38
9.25	0.9956	135.44	18.77	95.97	19.13	39.47	3.71	97.61	3.87
12.25	1.4251	81.44	9.87	41.16	10.09	40.28	2.09	37.26	1.66
15.25	1.9081	47.21	11.19	6.49	11.49	40.72	2.59	16.29	1.52
18.25	2.41	58.56	9.24	20.52	9.45	38.04	1.96	11.46	1.22
21.25	2.9306	46	9.03	2.89	9.27	43.11	2.08	5.19	1.04
24.25	3.5018	40.83	7.57	0.35	7.79	40.48	1.82	1.37	0.83

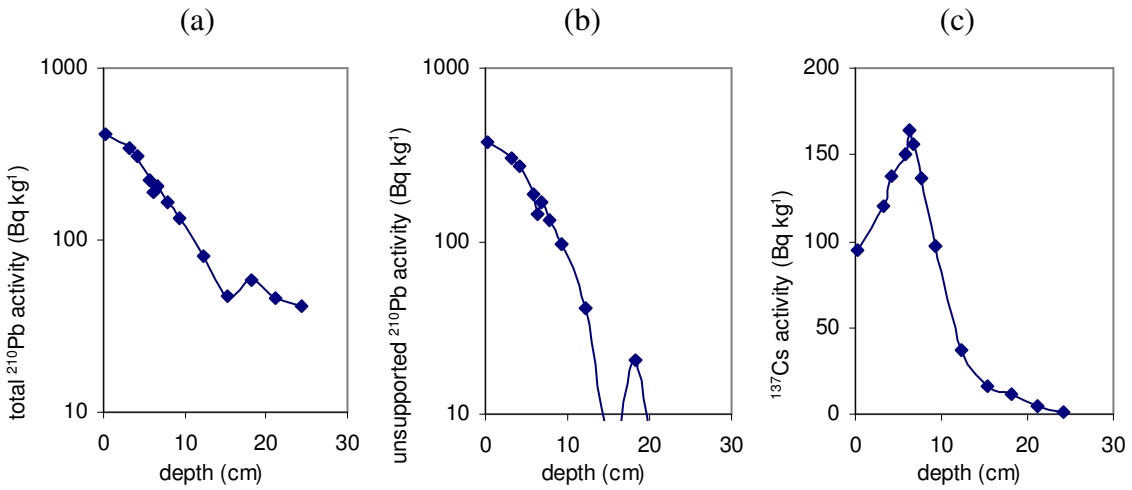

Figure 14a: Fallout radionuclides in core ALB15A showing (a) total ^{210}Pb, (b) unsupported ^{210}Pb, and (c) ^{137}Cs concentrations versus depth.

Core Chronology

Chronological data were calculated using the CRS and the CIC dating models. The raw CRS and CIC models place 1963 at about 7.5 cm and 8 cm, respectively, which are all below the depth suggested by the ^{137}Cs record. The final ^{210}Pb dates were calculated using the CRS model and the 1963 layer in the ^{137}Cs record as a reference point (Fig. 14b; Table 10b). Calculated sedimentation rates based on the revised ^{210}Pb dates suggest that sedimentation rates since the 1870s were relatively stable in a range of 0.013 – 0.029 g cm^{-2} y^{-1} with a mean of 0.0183 g cm^{-2} y^{-1}.

Table 10b: ^{210}Pb chronology of core ALB15A

Depth	Dry mass	Chronology			Sedimentation Rate		
		Date	Age	Std			% Std
cm	g cm^{-2}	AD	yr	±	g cm^{-2} yr^{-1}	cm yr^{-1}	± %
0	0	2006	0				
0.5	0.039	2004	2	2	0.0193	0.224	6.5
1	0.0827	2001	5	2	0.0186	0.213	6.6
1.5	0.1264	1999	7	2	0.0179	0.202	6.7
2	0.17	1996	10	2	0.0172	0.191	6.8
2.5	0.2137	1994	12	2	0.0164	0.18	6.9
3	0.2574	1991	15	2	0.0157	0.169	7
3.5	0.3074	1988	18	2	0.0149	0.152	8.5
4	0.3638	1984	22	2	0.0138	0.13	11.4
4.5	0.4202	1980	26	2	0.0133	0.118	13.5
5	0.4766	1976	30	3	0.0131	0.116	14.7
5.5	0.533	1972	34	3	0.0129	0.115	15.9
6	0.5894	1967	39	3	0.014	0.12	18.3
6.5	0.6491	1963	43	4	0.0175	0.143	20.1
7	0.7121	1960	46	4	0.018	0.143	20.6
7.5	0.7751	1956	50	5	0.01575	0.125	21.7
8	0.8381	1952	54	5	0.01575	0.125	23.5
8.5	0.9011	1948	58	6	0.01575	0.125	26.1
9	0.9641	1944	62	6	0.0163	0.125	28.7
9.5	1.0314	1940	66	7	0.0174	0.125	31.9
10	1.103	1936	70	9	0.0159	0.111	35.5
10.5	1.1746	1931	75	10	0.0143	0.1	39.2
11	1.2461	1926	80	11	0.0159	0.111	42.9
11.5	1.3177	1922	84	12	0.0159	0.111	46.5
12	1.3893	1917	89	14	0.0164	0.111	50.2
12.5	1.4654	1913	93	15	0.0196	0.125	53.8
13	1.5458	1909	97	16	0.023	0.143	57.4
13.5	1.6264	1906	100	17	0.023	0.143	60.9
14	1.7069	1902	104	18	0.0201	0.125	64.5
14.5	1.7873	1898	108	20	0.0201	0.125	68.1
15	1.8679	1894	112	21	0.0232	0.143	71.7
15.5	1.9499	1891	115	22	0.0237	0.143	75.4
16	2.0336	1887	119	23	0.0239	0.143	79.4
16.5	2.1172	1884	122	25	0.0279	0.167	83.3
17	2.2009	1881	125	26	0.0239	0.143	87.2
17.5	2.2845	1877	129	27	0.0239	0.143	91.2
18	2.3682	1874	132	28	0.0239	0.143	95.1

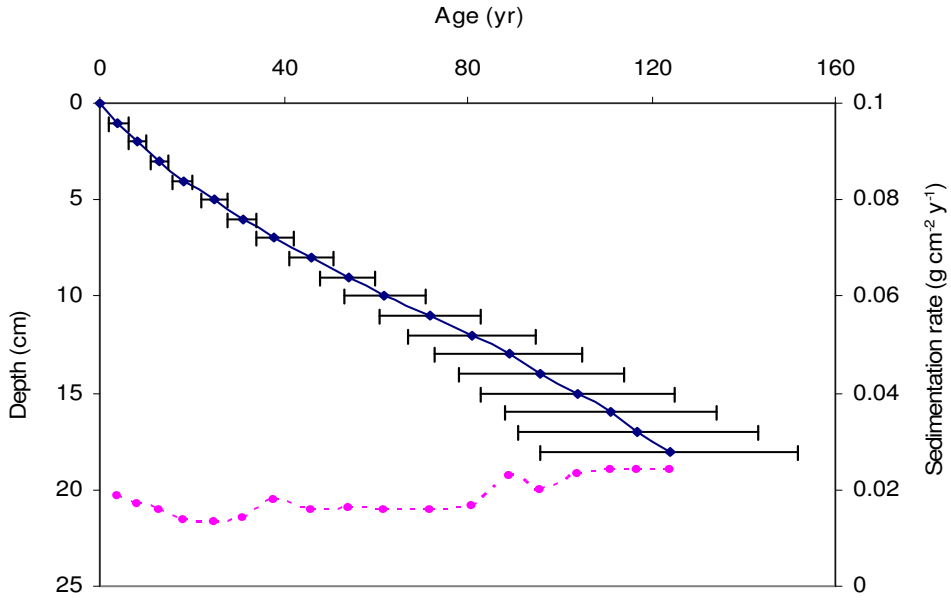

Figure 14b: Radiometric chronology of core ALB15A
(♦ - age ± years; ● – sedimentation rate)

Core ALB16A (lake CM5 / E55)

^{210}Pb Activity

Equilibrium between total ^{210}Pb activity and supporting ^{226}Ra activity occurs at a depth of c. 10 cm (Table 11a). Unsupported ^{210}Pb activity declines irregularly with depth, with maximum activity occurring 2.75 cm below the surface sediments (Fig. 15a), implying an increase in sedimentation in recent years.

Artificial Fallout Radionuclides

The ^{137}Cs activity versus depth profile shows a relatively broad peak between 2 – 3 cm (Fig. 15a). This peak is derived from the 1963/4 fallout maximum from the atmospheric testing of nuclear weapons. There is also a peak at 2.75 cm in the ^{241}Am record, which supports the ^{137}Cs peak indicating the 1963/4 depth.

Core Chronology

Use of the CIC model has been precluded again because of the non- monotonic decline in unsupported ^{210}Pb. Core chronologies were calculated using the CRS dating model. The raw CRS model places the 1963 depth at 4.75 cm, which is below 2.75 cm suggested by the ^{137}Cs and ^{241}Am records. Final dates for the core were calculated using the 1963/4 depth suggested by the ^{137}Cs and ^{241}Am records as a reference point (Table 11b; Fig. 15b). The mean post-1963 unsupported ^{210}Pb flux is calculated to be 41 Bq m^{-2} y^{-1}, compared to 21 Bq m^{-2} y^{-1} before 1963. ^{210}Pb flux in the core is lower than average deposition in the region, suggesting that this core has suffered sediment focussing, i.e. movement of sediment away from the coring location.

Table 11a: ^{210}Pb concentrations in core ALB16A

Depth	Dry Mass	Pb-210						Cs-137	
		Total		Unsupported		Supported			
cm	g cm^{-2}	Bq Kg^{-1}	±	Bq Kg^{-1}	±	Bq Kg^{-1}	±	Bq Kg^{-1}	±
0.25	0.0215	210.65	24.21	187.23	25.08	23.42	6.53	95.01	5.73
2.25	0.1781	297.71	35.91	262.63	37.11	35.08	9.38	253.93	9.47
2.75	0.2172	365.87	39.5	327.49	41.3	38.38	12.05	248.93	10.92
3.25	0.2564	342.16	21.51	322	21.95	20.16	4.38	219.39	5.98
4.25	0.3487	278.82	25.94	215.62	26.82	63.2	6.8	166.97	5.91
4.75	0.3948	188.73	28.91	154.16	29.89	34.57	7.6	133.32	7.24
5.25	0.4409	181.79	24.78	144.4	25.61	37.39	6.47	118.02	5.7
6.25	0.5332	108.29	14.49	76.17	14.99	32.12	3.82	61.7	3.17
7.75	0.7073	92.92	17.82	58.33	18.47	34.59	4.86	29.45	3
9.25	0.8813	46.6	6.36	17.04	6.62	29.56	1.82	17.04	1.12
10.75	1.0733	34.23	16.33	-6.09	17.08	40.32	5	7.99	2.28
12.25	1.2653	34.86	7.15	1.7	7.45	33.16	2.08	6.31	1.08

Table 11b: ^{210}Pb chronology of core ALB16A

Depth	Dry mass	Chronology			Sedimentation Rate		
		Date	Age				
cm	g cm^{-2}	AD	yr	±	g cm^{-2} yr^{-1}	cm yr^{-1}	± %
0	0	2006	0				
0.5	0.0411	2001	5	2	0.0098	0.124	16.2
1	0.0802	1995	11	2	0.008	0.101	17
1.5	0.1194	1988	18	3	0.0062	0.078	17.7
2	0.1585	1982	24	3	0.0044	0.056	18.4
2.5	0.1976	1971	35	4	0.0029	0.037	14.8
3	0.2368	1955	51	5	0.0036	0.045	12.3
3.5	0.2795	1948	58	5	0.0063	0.073	11.9
4	0.3256	1941	65	6	0.0063	0.07	15
4.5	0.3718	1934	72	7	0.0066	0.072	19.9
5	0.4179	1927	79	9	0.0065	0.071	23.3
5.5	0.464	1920	86	10	0.0064	0.066	24.6
6	0.5101	1913	93	10	0.0071	0.069	27.2
6.5	0.5622	1904	102	12	0.0068	0.063	31.3
7	0.6203	1893	113	12	0.0054	0.05	36.9
7.5	0.6783	1882	124	14	0.0041	0.036	42.6
8	0.7363	1864	142	16	0.0031	0.0238	47.5
8.5	0.7943	1840	166	19	0.0024	0.0204	51.8
9	0.8523	1815	191	23	0.0023	0.02	56.1

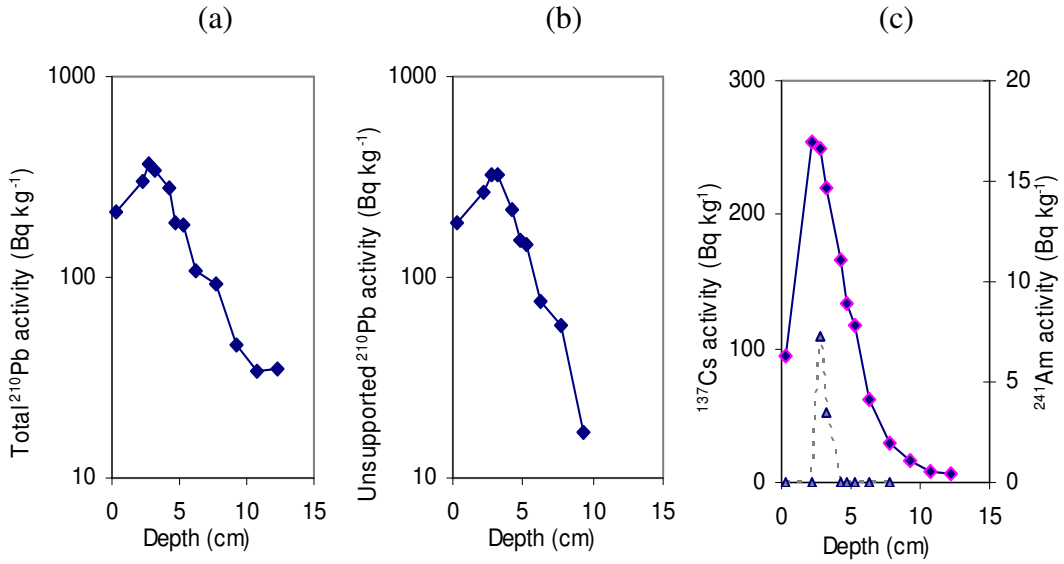

Figure 15a: Fallout radionuclide concentrations in core ALB16A showing (a) total ^{210}Pb, (b) unsupported ^{210}Pb, (c) ^{137}Cs & ^{241}Am concentrations (Δ) vs depth.

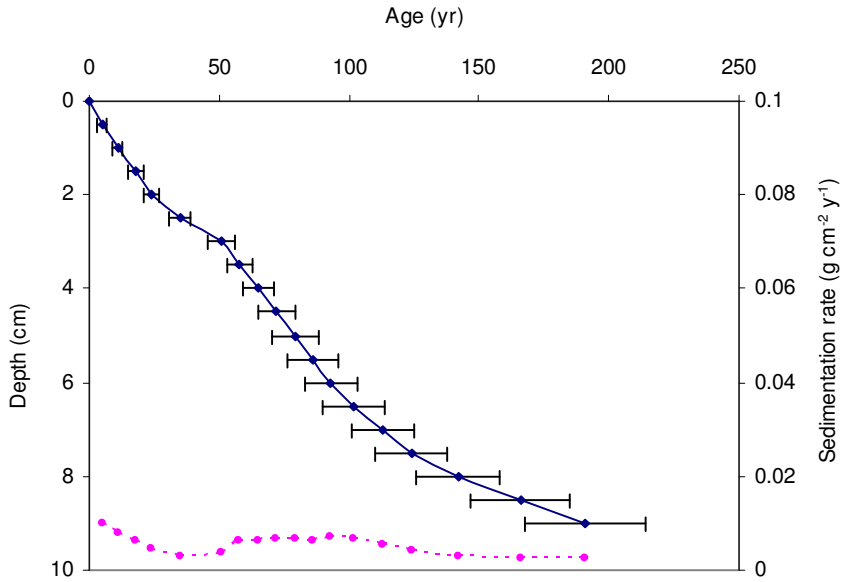

Figure 15b: Radiometric chronology of core ALB16A (♦ - age ± years; ● – sedimentation rate)

Core ALB17A (lake S4 / A301)

^{210}Pb Activity

Equilibrium depth of total ^{210}Pb activity to supporting ^{226}Ra activity is at about 18.5 cm (Table 12a). Unsupported ^{210}Pb activity again declines irregularly with depth (Fig. 16a), with maximum activity occurring at 2.25 cm below the surface, implying a sharp increase in sedimentation in recent years. The exponential curve (Fig. 16b) suggests that sedimentation has gradually increased through this section of the core.

Artificial Fallout Radionuclides

Although the ^{137}Cs activity versus depth profile shows a poorly resolved peak at 6.25

cm, there is little net change in ^{137}Cs activity in 0 – 6.5 cm (Fig. 16a), which raises the possibility of mixing, though the decline in ^{210}Pb between 0-6.5 cm argues against that. The peak at 6.25 cm may be derived from the 1963/4 fallout maximum from the atmospheric testing of nuclear weapons. The ^{241}Am record has a peak at the same depth, which supports the ^{137}Cs peak indicating the 1963/4 depth.

Table 12a: ^{210}Pb concentrations in core ALB17A

Depth	Dry Mass	Pb-210						Cs-137	
		Total		Unsupported		Supported			
cm	g cm^{-2}	Bq Kg^{-1}	±	Bq Kg^{-1}	±	Bq Kg^{-1}	±	Bq Kg^{-1}	±
0.25	0.0185	754.41	41.91	687.1	43.07	67.31	9.91	124.94	7.83
2.25	0.1484	797.64	34.51	733.07	35.29	64.57	7.39	124.99	6.16
3.25	0.2133	675.93	29.03	631.24	29.58	44.69	5.67	132.85	5.81
4.25	0.2793	576.6	29.08	521.66	29.6	54.94	5.52	133	5.8
5.75	0.3783	464.49	26.12	419.87	26.62	44.62	5.16	118.87	5.13
6.25	0.4113	424.68	27.4	377.92	28.1	46.76	6.22	136.24	6.31
6.75	0.4505	393.77	24.75	348.9	25.42	44.87	5.78	114.42	5.27
9.25	0.6467	242.61	24.17	190.32	24.86	52.29	5.8	59.73	4.74
12.25	0.9152	133.02	11.81	89.01	12.26	44.01	3.3	27.12	1.95
14.25	1.133	72.39	11.61	27.87	12.02	44.52	3.13	17.72	1.72
15.25	1.2419	69.44	13.11	22.85	13.67	46.59	3.87	15.66	2.17
16.25	1.3512	58.25	9.63	16.72	10.02	41.53	2.78	10.09	1.41
18.25	1.5698	43.53	10.98	0.47	11.44	43.06	3.21	10.51	1.59

Table 12b: ^{210}Pb chronology of core ALB17A

Depth	Dry mass	Chronology			Sedimentation Rate		
		Date	Age				
cm	g cm^{-2}	AD	yr	±	g cm^{-2} yr^{-1}	cm yr^{-1}	± %
0	0	2006	0				
1	0.0672	2001	5	2	0.0129	0.197	9.9
2	0.1322	1995	11	2	0.0105	0.161	10.5
3	0.1971	1989	17	2	0.0095	0.145	12.1
4	0.2628	1982	24	3	0.0091	0.138	14.8
5	0.3288	1974	32	4	0.0084	0.127	18.6
6	0.3948	1966	40	6	0.0088	0.125	23.2
7	0.4701	1958	48	7	0.0090	0.117	30.4
8	0.5486	1949	57	7	0.0091	0.117	13.7
9	0.6271	1941	65	7	0.0089	0.106	16.1
10	0.7138	1930	76	8	0.0082	0.094	18.7
11	0.8033	1918	88	10	0.0074	0.081	21.4
12	0.8928	1906	100	11	0.0065	0.068	24.1
13	0.9969	1891	115	14	0.0067	0.066	38.7
14	1.1058	1875	131	18	0.0073	0.067	57.2
15	1.2147	1858	148	24	0.0058	0.053	82.3
16	1.3239	1834	172	29	0.0046	0.042	98.9

Core Chronology

Core chronologies were calculated using the CRS dating model. The raw CRS model

places the 1963 depth at 7 cm, which is slightly below 6.25 cm suggested by the ^{137}Cs and ^{241}Am records. Using the 1963/4 depth suggested by the ^{137}Cs and ^{241}Am records as a reference point, chronology dates were given by the CRS model (Table 12b). Sedimentation rates show a slight increase from the 1830s at c. 0.005 g cm^{-2} yr^{-1} to the present time at c. 0.013 g cm^{-2} yr^{-1}. The mean unsupported ^{210}Pb flux is 110 Bq m^{-2} y^{-1}, compared to 21 Bq m^{-2} y^{-1} before 1963. Reduction in ^{210}Pb flux after 1963 may imply missing surface sediment. The ^{210}Pb flux in the core is lower than average deposition in the region, suggesting that this core has suffered sediment focussing, i.e. movement of sediment away from the coring location.

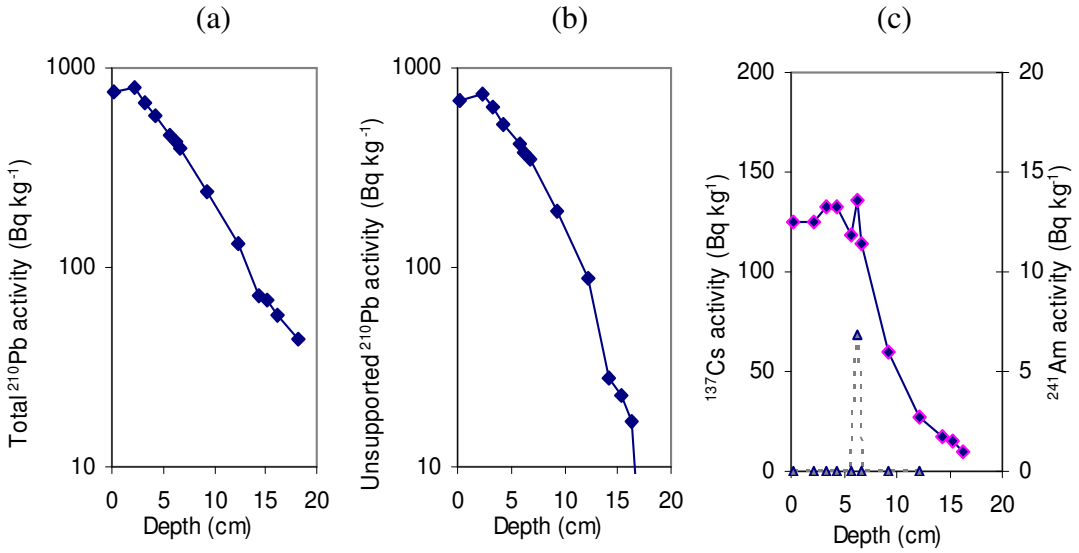

Figure 16a: Fallout radionuclide concentrations in ALB17A showing (a) total ^{210}Pb, (b) unsupported ^{210}Pb, (c) ^{137}Cs & ^{241}Am concentrations (Δ) vs. depth.

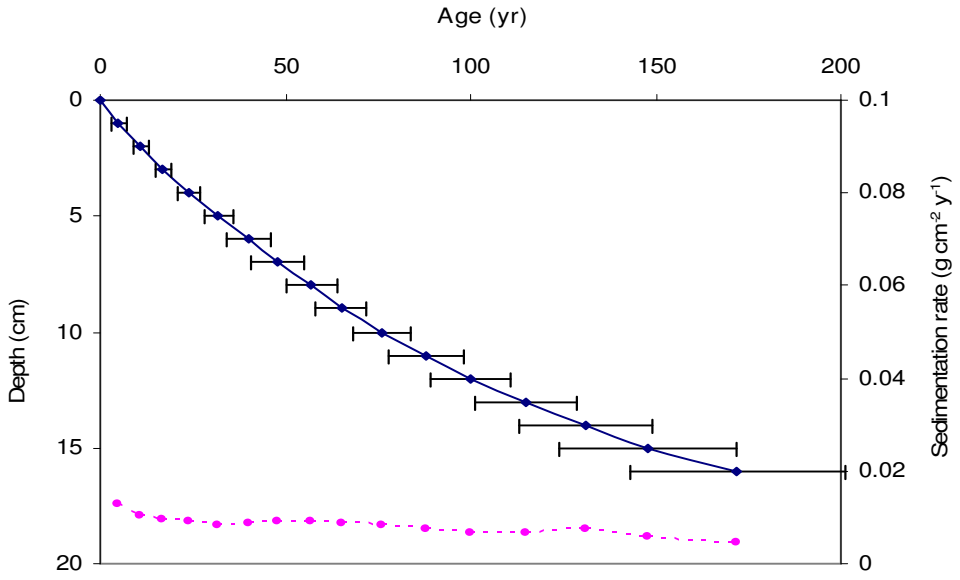

Figure 16b: Radiometric chronology of core ALB17A
(♦ - age ± years; ● – sedimentation rate)

Core ALB18A (lake S3)

^{210}Pb Activity

Equilibrium of total ^{210}Pb activity with supporting ^{226}Ra activity appears to occur at c. 22 cm (Table 13a). Unsupported ^{210}Pb activity again declines irregularly with depth, with maximum activity occurring at 5.25 cm, implying a sharp increase in sedimentation in the surface of the core (Fig. 17a). The relatively small change between 7 – 8.5 cm and the non-monotonic feature at 10.25 cm suggest that these parts of the core suffer increases in sedimentation.

Artificial Fallout Radionuclides

The ^{137}Cs activity versus depth profile shows a well-resolved peak at 6.25 cm (Fig. 17a), which is derived from the 1963/4 fallout maximum from the atmospheric testing of nuclear weapons.

Core Chronology

The CIC dating model was precluded by the non-monotonic feature in unsupported ^{210}Pb. The raw CRS model places the 1963 depth at c. 9 cm, which is below the depth suggested by the ^{137}Cs records. The significant discrepancy between them may be attributed to a decline in the ^{210}Pb flux associated with reduced sedimentation rates in the top part of the core, or surface sediments were missing during coring. Using the 1963/4 depth suggested by the ^{137}Cs record as a reference level, chronology dates were given by the CRS model (Table 13b). Sedimentation rates show a slight increase from the 1850s to the 1940s, with a dip between the 1960s and 1980s, but appear to have increased again during last two decades (Fig. 17b). The mean unsupported ^{210}Pb flux is 167 Bq m^{-2} y^{-1} before 1963, and declines to 126 Bq m^{-2} y^{-1} after 1963.

Table 13a: ^{210}Pb concentrations in core ALB18A

Depth	Dry Mass	Pb-210						Cs-137	
		Total		Unsupported		Supported			
cm	g cm^{-2}	Bq Kg^{-1}	±	Bq Kg^{-1}	±	Bq Kg^{-1}	±	Bq Kg^{-1}	±
0.25	0.0239	428.54	29.77	396.7	30.39	31.84	6.09	64.59	4.59
3.25	0.2939	440.77	26.46	409.74	26.93	31.03	5.02	77.57	4.43
5.25	0.5886	466.3	20.82	432.77	21.14	33.53	3.64	82.46	3.59
6.25	0.7359	349.46	18.26	310.39	18.64	39.07	3.73	90.52	3.42
7.25	0.9614	189.89	15.71	153.03	16.09	36.86	3.49	78.11	3.23
8.25	1.1868	178.74	16.45	150.65	16.81	28.09	3.46	67.57	3.12
9.25	1.4123	147.07	14.2	121.74	14.46	25.33	2.74	44.7	2.43
10.25	1.6623	105.78	14.56	76.32	14.89	29.46	3.12	35.92	2.13
11.25	1.9123	115.38	9.5	83	9.69	32.38	1.9	16.17	1.19
12.25	2.1623	85.63	9.95	61.69	10.17	23.94	2.08	8.45	1.15
15.25	2.8803	69.72	8.66	40.05	8.87	29.67	1.93	6.84	0.98
18.25	3.5862	45.39	7.61	21.78	7.79	23.61	1.68	4.38	0.86
21.25	4.3626	27.28	8.29	1.41	8.49	25.87	1.82	2.08	0.93
24.25	5.1746	26.63	8.33	-6.21	8.57	32.84	2	1.14	0.87

Table 13b: ^{210}Pb chronology of core ALB18A

Depth	Dry mass	Chronology			Sedimentation Rate		
		Date	Age				
cm	g cm^{-2}	AD	yr	±	g cm^{-2} yr^{-1}	cm yr^{-1}	± %
0	0	2006	0				
1	0.0914	2003	3	2	0.0289	0.307	9.9
2	0.1814	1999	7	2	0.0258	0.257	10.1
3	0.2714	1996	10	2	0.0227	0.207	10.2
4	0.4044	1988	18	2	0.0181	0.151	11.6
5	0.5518	1979	27	3	0.014	0.0953	13.4
6	0.6991	1967	39	4	0.0186	0.1053	18.5
7	0.905	1960	46	4	0.0308	0.1429	33
8	1.1304	1953	53	5	0.0322	0.1429	44
9	1.3559	1946	60	5	0.0321	0.1429	15.6
10	1.5998	1939	67	6	0.0389	0.157	21.5
11	1.8498	1932	74	7	0.0331	0.132	20.5
12	2.0998	1924	82	8	0.0314	0.129	23.8
13	2.3418	1915	91	10	0.0291	0.121	29.7
14	2.5811	1906	100	12	0.0255	0.106	35.7
15	2.8205	1897	109	14	0.0219	0.092	41.8
16	3.0568	1883	123	15	0.0178	0.075	46.6
17	3.2921	1866	140	17	0.014	0.057	51
18	3.5274	1850	156	18	0.014	0.06	55.3

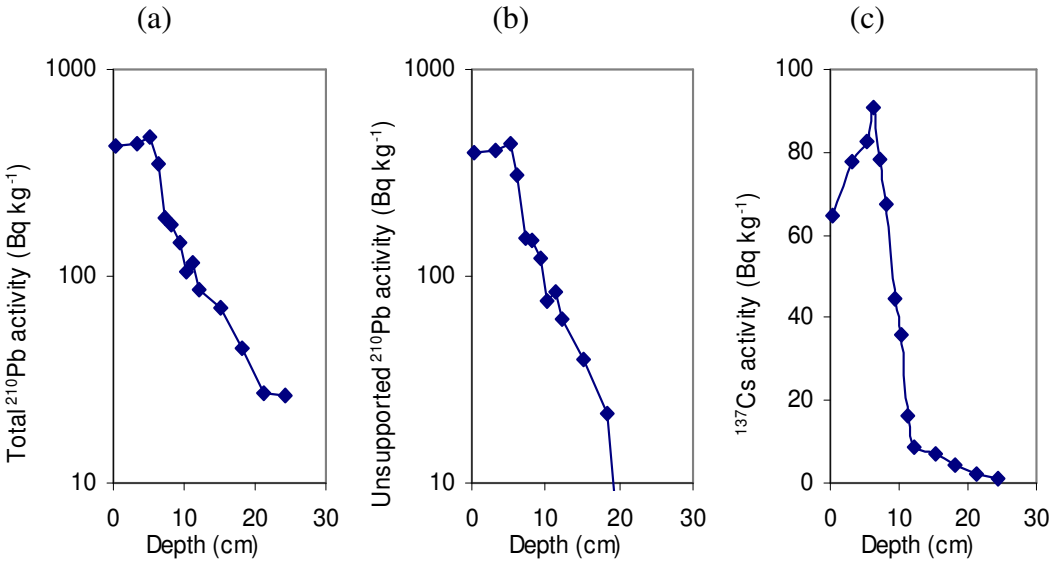

Figure 17a: Fallout radionuclide concentrations in core ALB18A showing (a) total ^{210}Pb, (b) unsupported ^{210}Pb, (c) ^{137}Cs concentrations versus depth.

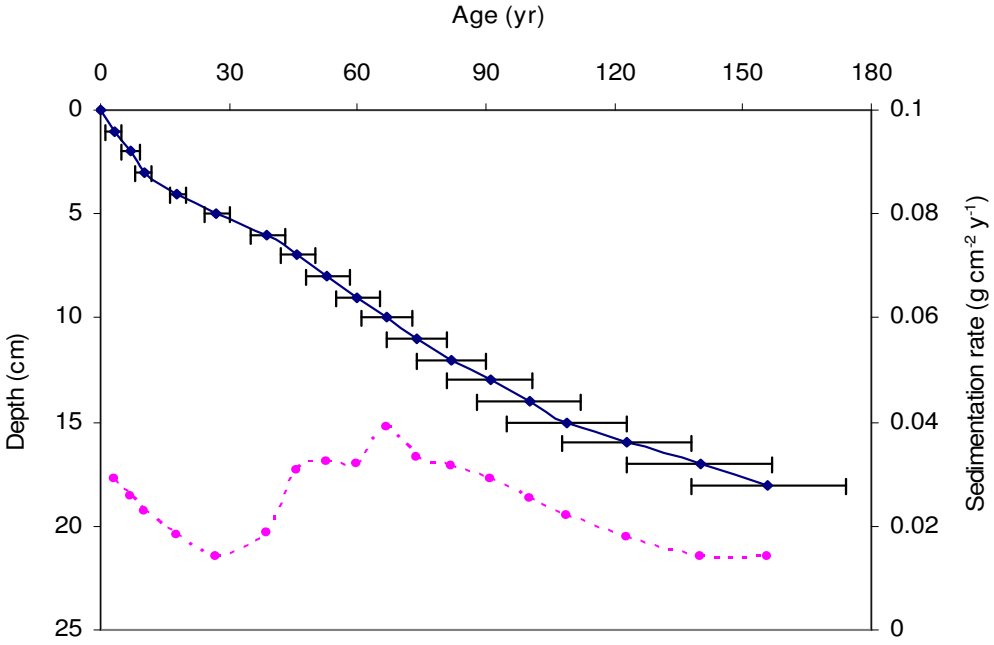

Figure 17b: Radiometric chronology of core ALB18A
(♦ - age ± years; ● – sedimentation rate)

Core ALB21A (lake NE7 / 185)

^{210}Pb Activity

Equilibrium of total ^{210}Pb activity with supporting ^{226}Ra activity appears to occur at c. 14 cm (Table 14a). Unsupported ^{210}Pb activity declines irregularly with depth, with two non-monotonic points at 5.25 and 9.25 cm, suggesting there are changes in sedimentation rate (Fig. 18a).

Artificial Fallout Radionuclides

The ^{137}Cs activity versus depth profile again shows a well-resolved peak at 6.5 cm, which is derived from the 1963/4 fallout maximum from the atmospheric testing of nuclear weapons (Fig. 18a).

Core Chronology

The CIC dating model was not suitable for this core due to the non-monotonic feature in unsupported ^{210}Pb. The raw CRS model places the 1963 depth at c. 7.5 cm, which is again below the depth suggested by the ^{137}Cs records. Chronology of the core was re-calculated by the CRS model using the 1963 depth suggested by the ^{137}Cs record as a reference level (Table 14b). Sedimentation rates increased from 12 cm (the 1880s) to 9 cm (the 1940s) followed by a relatively uniform period to 4 cm (the 1980s), and then increased again to the surface (Fig. 18b).

Table 14a: ^{210}Pb concentrations in core ALB21A

Depth	Dry Mass	Pb-210						Cs-137	
		Total		Unsupported		Supported			
cm	g cm^{-2}	Bq Kg^{-1}	±	Bq Kg^{-1}	±	Bq Kg^{-1}	±	Bq Kg^{-1}	±
0.25	0.0046	393.06	28.15	365.64	29.18	27.42	7.68	137.17	6.12
3.25	0.1068	297.68	32.04	276.67	33.34	21.01	9.23	172.72	8.19
4.25	0.151	301.88	31.72	274.23	32.56	27.65	7.37	191.11	7.78
5.25	0.1951	267.04	41.67	248.97	42.87	18.07	10.06	209.04	9.66
6.25	0.2393	286.01	31.66	259.75	32.76	26.26	8.42	212.92	8.33
6.75	0.2706	225.91	25.87	201.02	26.74	24.89	6.76	213.31	7.37
8.25	0.3644	151.9	15.15	127.02	15.68	24.88	4.03	146.57	4.1
9.25	0.4269	86	13.98	64.38	14.45	21.62	3.67	84.38	3.35
10.25	0.5006	111.79	15.29	80.94	15.86	30.85	4.2	67.02	3.25
11.25	0.5742	87.99	17.52	76.21	18.25	11.78	5.12	54.33	3.5
12.25	0.6479	56.69	13.46	33.04	14.01	23.65	3.87	37.14	2.54
13.75	0.7649	40.59	14.39	18.75	14.93	21.84	3.97	19.71	2.47
15.25	0.8819	13.51	14.65	-7.01	15.2	20.52	4.05	22.98	2.43

Table 14b: ^{210}Pb chronology of core ALB21A

Depth	Dry mass	Chronology			Sedimentation Rate		
		Date	Age				
cm	g cm^{-2}	AD	yr	±	g cm^{-2} yr^{-1}	cm yr^{-1}	± %
0	0	2006	0				
1	0.0302	2002	4	2	0.008	0.24	11.3
2	0.0642	1998	8	2	0.008	0.22	12.8
3	0.0983	1993	13	2	0.007	0.2	14.3
4	0.1399	1987	19	2	0.006	0.15	15.3
5	0.1841	1979	27	3	0.005	0.12	19.5
6	0.2282	1970	36	4	0.006	0.11	20.4
7	0.2862	1961	45	4	0.006	0.1	17.1
8	0.3488	1950	56	5	0.006	0.1	18.9
9	0.4113	1941	65	7	0.008	0.1	26.8
10	0.4822	1930	76	8	0.006	0.08	31.2
11	0.5558	1913	93	13	0.003	0.05	44.1
12	0.6295	1889	117	24	0.003	0.04	81.8

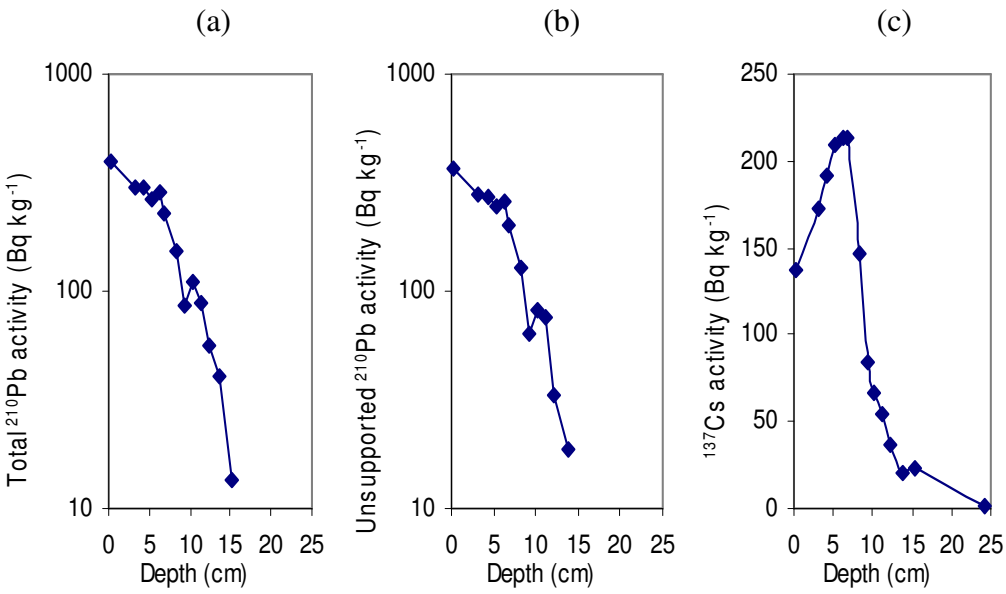

Figure 18a: Fallout radionuclide concentrations in core ALB21A showing (a) total ^{210}Pb, (b) unsupported ^{210}Pb, (c) ^{137}Cs concentrations versus depth.

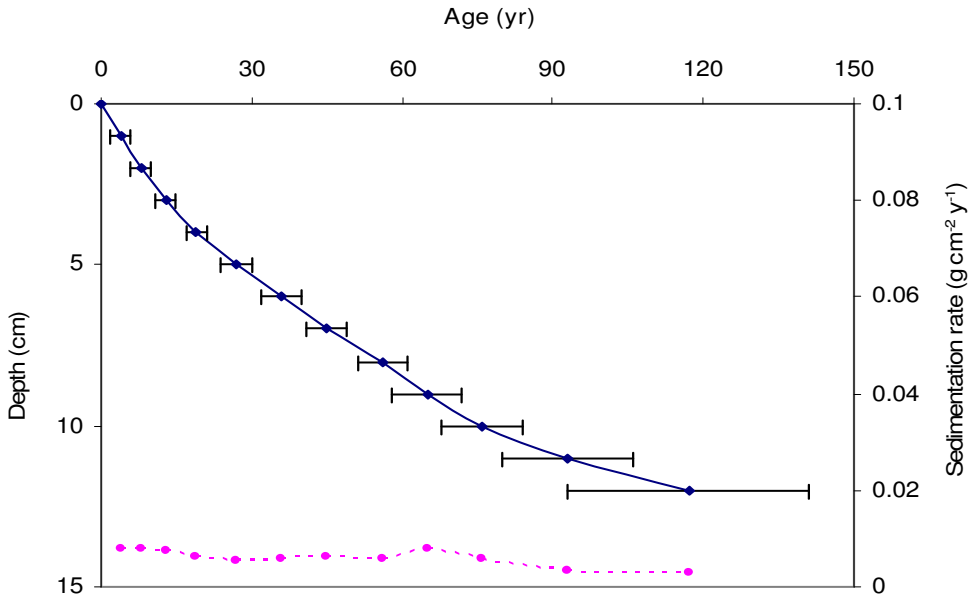

Figure 18b: Radiometric chronology of core ALB21A
(♦ - age ± years; ● – sedimentation rate)

3.5 Stable isotope analysis

Rationale and Methods

C and N isotope measurements on bulk organic matter in sediments provide information on the sources of the organic matter and on biogeochemical processes through time, allowing changes in source material and processes to be identified. This can be achieved because various sources of organic matter have different $\delta^{13}C$ values, for example allowing distinctions between C3 and C4 plants and, when combined with C:N ratio values, between C3 plant and lacustrine algal sources. The latter have more depleted $\delta^{13}C$ values (~ -25 - -30‰) and low C:N ratios (5-8).

N isotopes reflect an array of biogeochemical processes associated with the N cycle and assimilation of nutrients. Of particular relevance are the suggestions that vehicular and industrial sources of N to the atmosphere have low or depleted $\delta^{15}N$ values, and that increased assimilation of inorganic N by aquatic algae can also lead to lower $\delta^{15}N$ values being observed. Both may be the result of increased deposition of N from the atmosphere, the latter by stimulation of growth in algal communities resulting from increased N availability.

Bulk organic matter sub-samples from sediment cores from each lake were air dried at 40 °C or below. These sub-samples were then milled to a fine powder using a Retsch mixer mill. Approximately 0.001g of milled sediment was transferred to pre-weighed tin capsules, which were then sealed. The amount of dried sediment in each capsule was recorded.

The samples were analysed for total N and C, $^{14}N/^{15}N$ and $^{12}C/^{13}C$ at the UC Davis Stable Isotope Facility, California, USA via isotope ratio mass spectrometry on Hydra 20-20 or Anca-GSL isotope ratio mass spectrometers.

The concentration of N and C in the samples is expressed as grams N or C per gram dry weight of sediment. The isotopic ratio of $^{14}N/^{15}N$ and $^{12}C/^{13}C$ is expressed using the delta (δ) notation in parts per thousand (or per mille, ‰), where $\delta^{15}N$ (‰) and $\delta^{13}C$ (‰) = $[(R_{sample} / R_{standard}] - 1] \times 1000$, where R is the $^{14}N/^{15}N$ or $^{12}C/^{13}C$ ratio in the measured sample or the appropriate standard. The standard for nitrogen is the $\delta^{15}N$ of atmospheric nitrogen (commonly referred to as AIR), and for $\delta^{13}C$ the standard is Vienna Pee Dee Belemnite (VPDB). The C/N ratio was calculated from the mass of N and C and converted to atomic ratios by multiplying the mass ratios by 1.167 (the ratio of the atomic weights of N and C).

Results

Carbon Isotopes

The $\delta^{13}C$ and C/N ratio profiles demonstrate the clearest signs of an alteration of i) lake biogeochemistry, ii) sources of organic matter or iii) changes in productivity. Figure 19 shows the measured $\delta^{13}C$ profiles for the studied lakes.

The $\delta^{13}C$ values are all indicative of contributions from lacustrine organic matter (algae) or C3 land plants, with values of -27‰ – -31‰ observed across the set of study lakes.

The observed changes in $\delta^{13}C$ values are small, on the order of <1‰ – 2‰. In all lakes studied, the trend is towards isotopically lighter organic matter in more recent sediments. The changes in ALB17, ALB18, ALB21, ALB09 and ALB03 document the most significant shifts in $\delta^{13}C$ values following relatively stable periods of isotopically heavier material. In these 5 sites, the observed switch to isotopically lighter organic matter occurred around 1930-1945, with the changes in ALBs 17, 18, and 21 all occurring ~1930. The changes in ALBs 03 and 09 occur somewhat later.

Switches to more negative (isotopically lighter) $\delta^{13}C$ values are generally indicative of an increase in or greater abundance of dissolved inorganic carbon (DIC) in the epilimnion, arising from the stronger discrimination in favour of ^{12}C, leading to less negative $\delta^{13}C$ values in algal organic matter.

Nitrogen Isotopes
Figure 20 shows the observed $\delta^{15}N$ profiles for the studied sites. There are few strong, consistent shifts in the $\delta^{15}N$ values, with most lakes having low (~2‰ – 3‰) but highly variable $\delta^{15}N$ values.

There are clear shifts to isotopically heavier organic matter (higher $\delta^{15}N$ values) of ~1‰ in ALBs 16 and 21 and to a lesser extent in ALB12 and ALB03. In ALBs 12, 16 and 21, the trend occurs throughout the retrieved sediment cores and precede the industrialisation in Western countries and the later Oil Sands activities, whereas the increase of ~1‰ in the upper 2-3 cm of ALB03 occurs in the middle of the 20th century.

Trends towards less positive $\delta^{15}N$ values are observed in ALBs 02, 05, 11, 17 and 18, though in all but ALB02 and ALB05, these shifts are small. In ALB02, a decline of ~1‰ occurs from c. 1900 at the base of the core to c. 1965 at 9cm after which the isotope values fluctuate around ~2.2‰. In ALB05, $\delta^{15}N$ values decline from an initial value of ~2.75‰ in the 1800s to ~1.5‰ by the middle of the 20th century (c. 14 cm.). $\delta^{15}N$ values remain relatively stable at ~1.75‰.

The observed trends and shifts in the $\delta^{15}N$ values do not indicate any changes in N biogeochemistry that are concomitant with the increased industrialisation in the region associated with Oil Sands activities.

C/N Ratios
Figure 21 shows the C/N ratios of the sediment material expressed as atomic ratios. The trends in C/N ratio largely exhibit the same patterns as those described for C isotopes above. Exceptions are ALB11 and ALB15. In the latter an outlier sample at ~4.5 cm, with low N content relative to sediments either side of this level, dominates the profile.

C/N ratios are generally low, ranging from 7-18. These values are within the range expected for lacustrine algae (c. 5-8) and C3 land plants (c. 16 +), but outside the range of values expected for C4 land plants (c. 35+). The observed values can be interpreted as mixtures therefore of lacustrine algae and C3 land plant sources, with lower C/N ratios reflecting a greater proportional input from aquatic algae.

In the majority of sites there are decreases in the C/N ratio suggesting increased contributions from aquatic sources of organic matter. This impression is further highlighted when C/N ratios are plotted against $\delta^{13}C$ values (Fig. 22). The highlighted region represents observed C/N ratios and $\delta^{13}C$ values for lacustrine algae. Recall that in many sites a trend towards more negative $\delta^{13}C$ values was observed in the sediment samples. The overwhelming impression from Figure 22 is that the source of organic matter to the lakes has originated, progressively, from greater contributions of aquatic algae. This could be interpreted as a productivity response and is in agreement with observations from the diatom analysis in several of the sites, though there are no signs of increased productivity in either the $\delta^{13}C$ or the $\delta^{15}N$ values.

Conclusions

Overall, the isotope and C/N ratio profiles for the study sites do not show any systematic changes in the biogeochemistry of the lakes that can be attributed to recent Oil Sands activities related to the extraction of oil. Whilst many of the cores show changes in the $\delta^{13}C$ values and C/N ratios in particular, the timing of these changes pre-dates the 19th and early 20th century when emissions of N compounds to the atmosphere were on the increase in the Northern Hemisphere. The C/N ratios of the sediment cores suggest a greater contribution to organic matter from lacustrine algal sources has taken place in the mid 20th century that may be indicative of increased productivity in these systems. This observation does not tally with the $\delta^{13}C$ values, which would be expected to move towards less-negative values as increased productivity drew down the DIC pool of the lakes.

The $\delta^{13}C$ values do not preclude an increase in productivity if increases in the contributions of inorganic carbon to the lakes occurred that were sufficient to offset the draw down of the DIC pool that would have taken place as productivity increased. Further work will be required to determine whether this is a plausible scenario however.

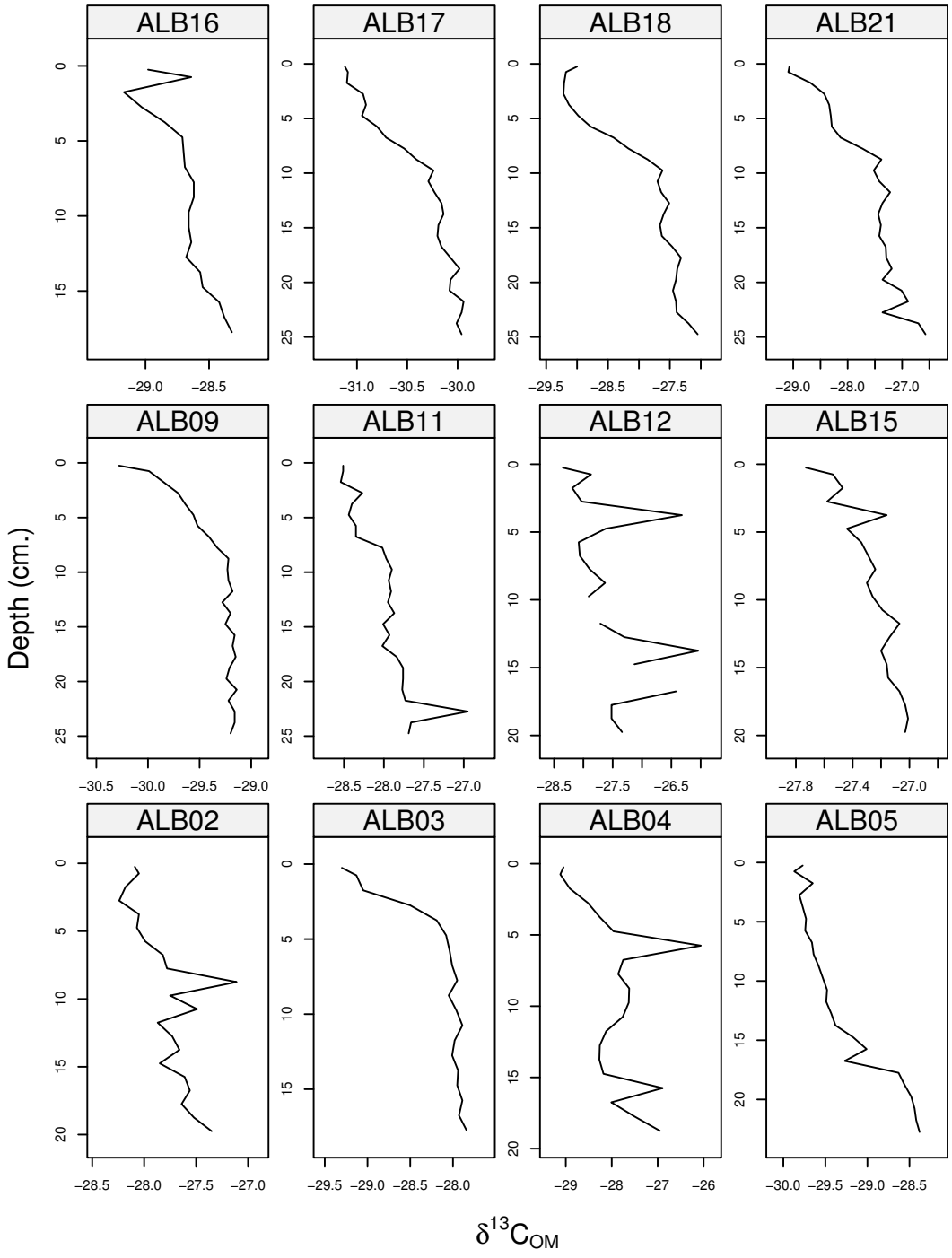

Figure 19: $\delta^{13}C$ profiles of lake sediment core bulk organic matter

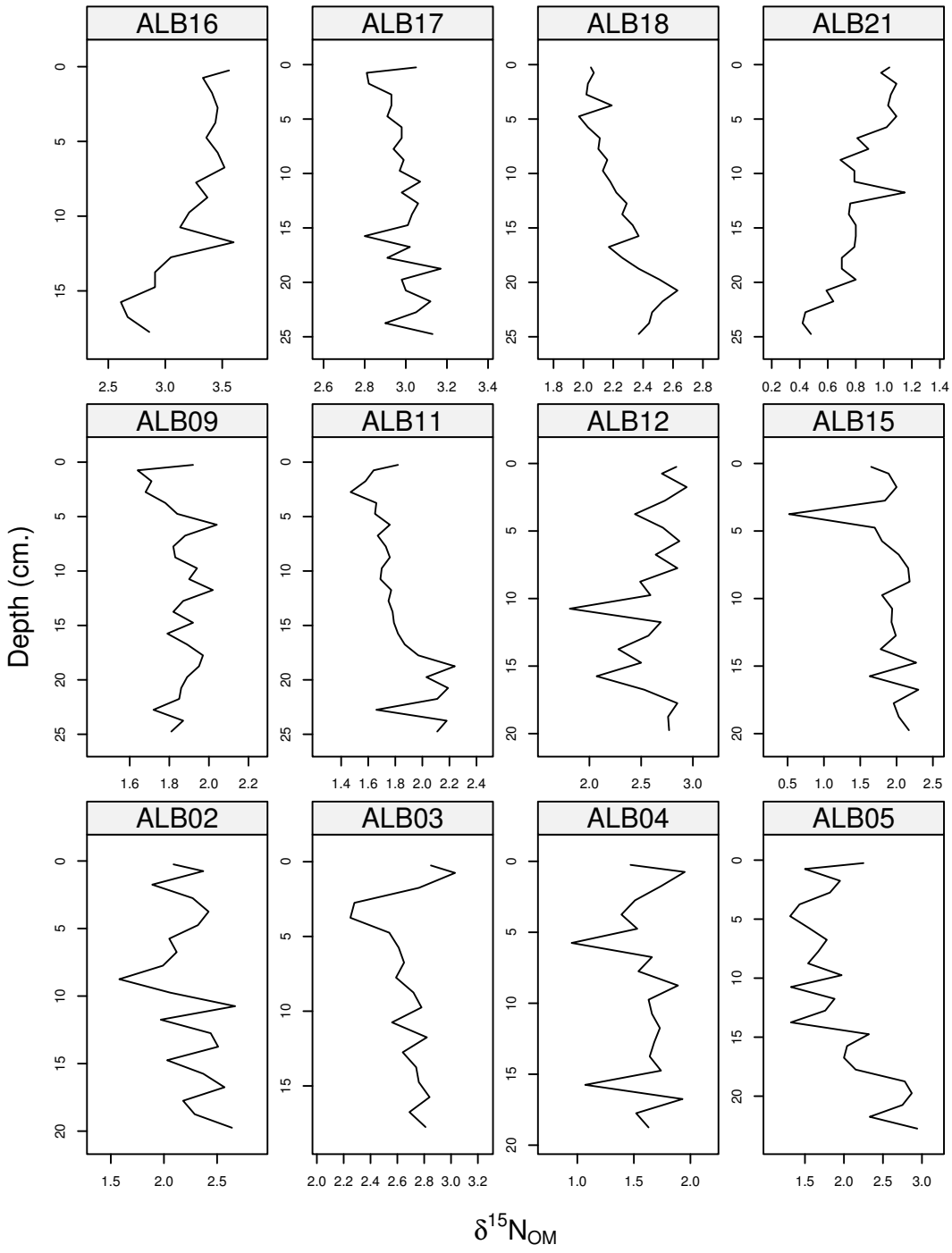

Figure 20: $\delta^{15}N$ profiles of lake sediment core bulk organic matter

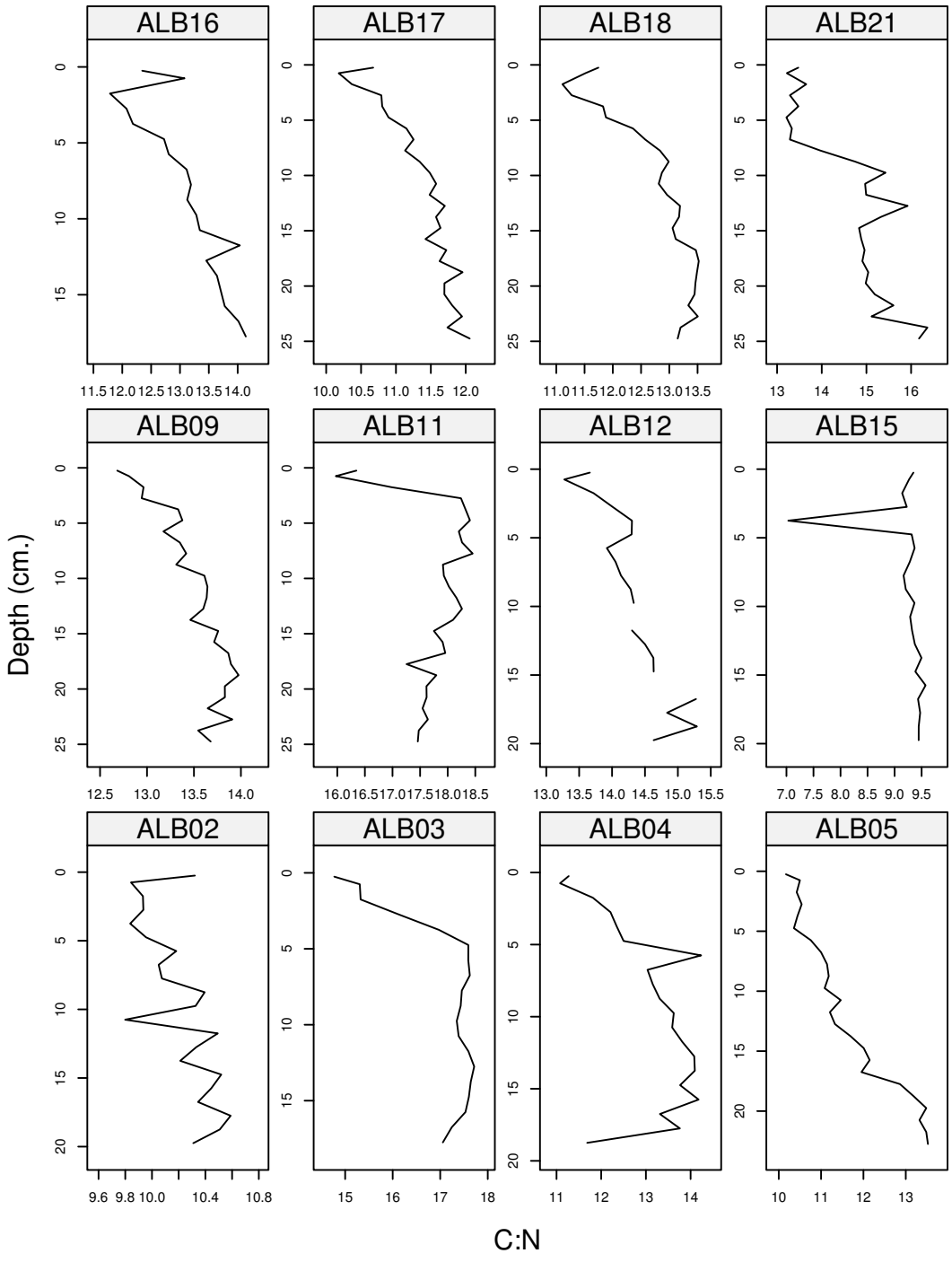

Figure 21: C: N profiles of lake sediment core bulk organic matter

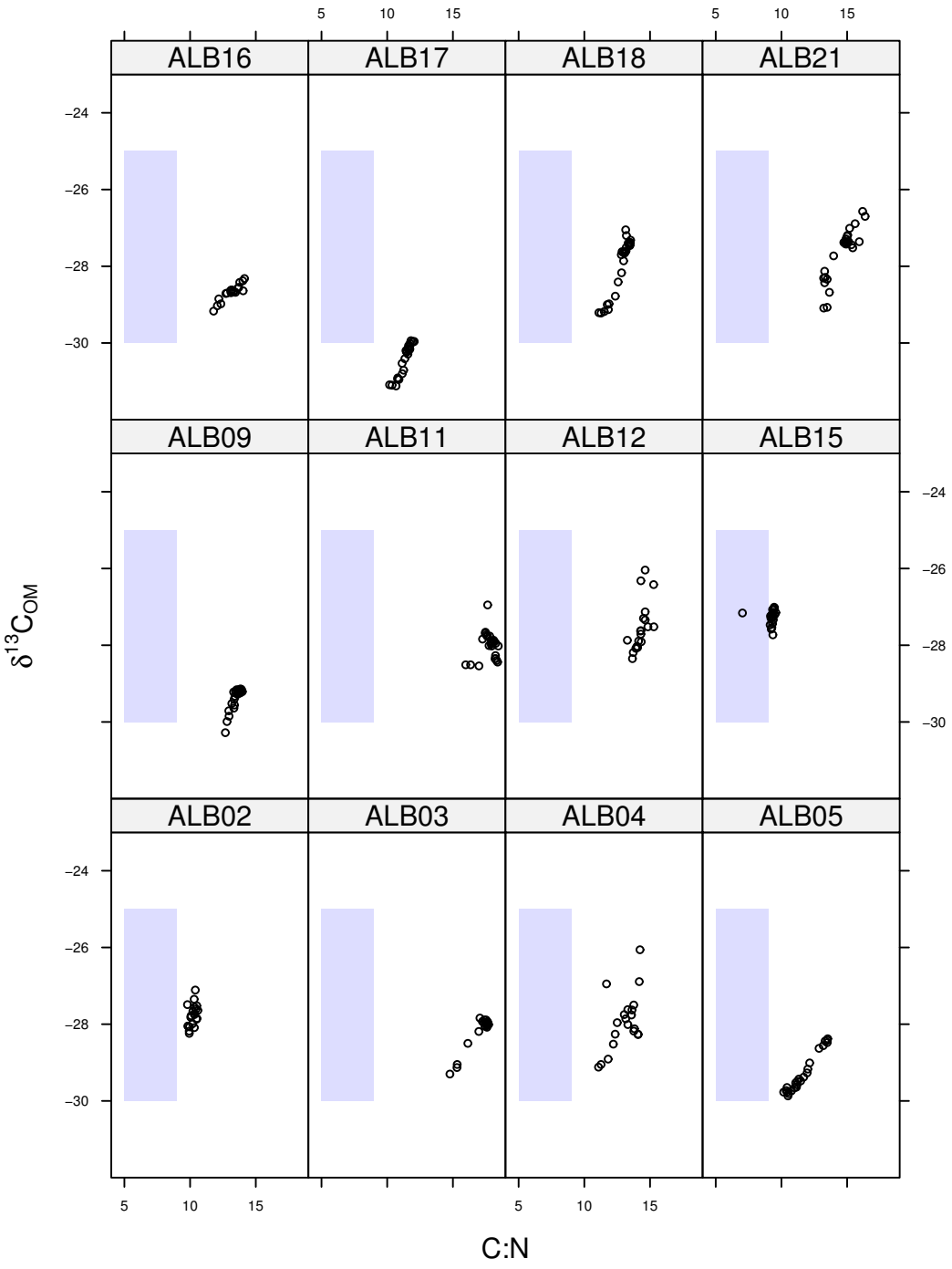

Figure 22: Relationship between $\delta^{13}C$ and C:N ratio in lake sediment core bulk organic matter

3.6 X-ray fluorescence spectrometry (XRF)

Analysis of sediment core geochemistry was undertaken by X-ray fluorescence (XRF) using a Spectro XLAB 2000 in the Department of Geography, University College London. The same freeze dried and milled sediments prepared for non-destructive ^{210}Pb dating were used for XRF analysis.

Results

Selected XRF results are presented in Figs. 23-30 below. Major elements are presented as % by mass while trace metals are presented in μg g^{-1}.

There are few strong trends in the XRF data which could indicate recent anthropogenic pollution related to the Oil Sands extraction activities. Some sites show weak apparent trends, in particular ALB03 (SM6) and ALB04 (SM8) which appear to show minor increases in several elements in the last 10-30 years (P, Si, Pb, V, Al), while ALB02 (BM3) shows strong increases in Fe and P but apparent decreases in Si, Pb and Al, and to a lesser degree S, Zn and V. The only other coherent trends are (mostly) minor increases in both P and Fe in many sites.

While there are no apparent trends in pollutants associated with fossil fuel combustion (e.g. Pb) the widespread increases in P and Fe, in conjunction with diatom data suggesting nutrient enrichment in many sites (see below), suggests that further work in this area would be merited to determine whether Oil Sands activities (i.e. NOx emissions) are affecting the nutrient status of some lakes. Such work would have to take into account possible diagenetic effects in lake sediments, i.e. chemical transformations occurring in situ during the decomposition of lake sediments.

Additional work - Mercury

Additional, unfunded analyses for mercury were performed on surface sediments from cored lakes and then down the core profile for the lake with the greatest surface sediment concentration using freeze dried, milled samples on a Milestone DMA-80 Direct Mercury analyser. Concentration data were converted to fluxes using sediment accumulation rates calculated from ^{210}Pb dates (Table 14b).

Mercury concentrations in lake surface sediments are presented in Fig. 31 and the highest value occurs in the acidified lake NE7 (core ALB21; see below). The regional variation in Hg concentrations observed in the surface sediments needs to be viewed cautiously as many environmental factors will have contributed to the measured values. The data suggests however there may be some comparability in lakes from the same area, e.g. from the Caribou Mountains (~110 ng g^{-1}) and the Stony Mountain sites (~92-93 ng g^{-1}).

Figure 23: XRF Results for Iron (%)

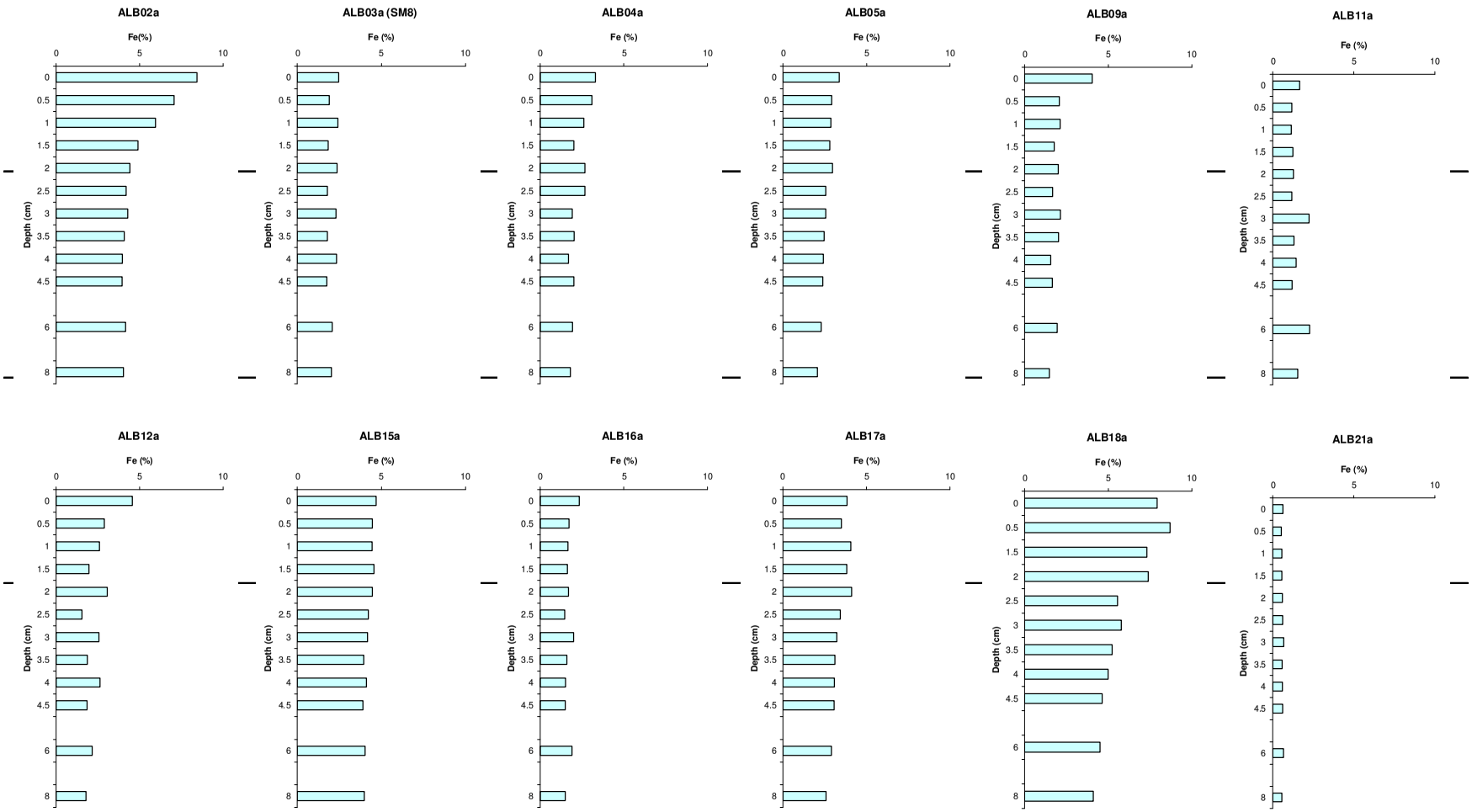

Figure 24: XRF Results for Sulphur (%)

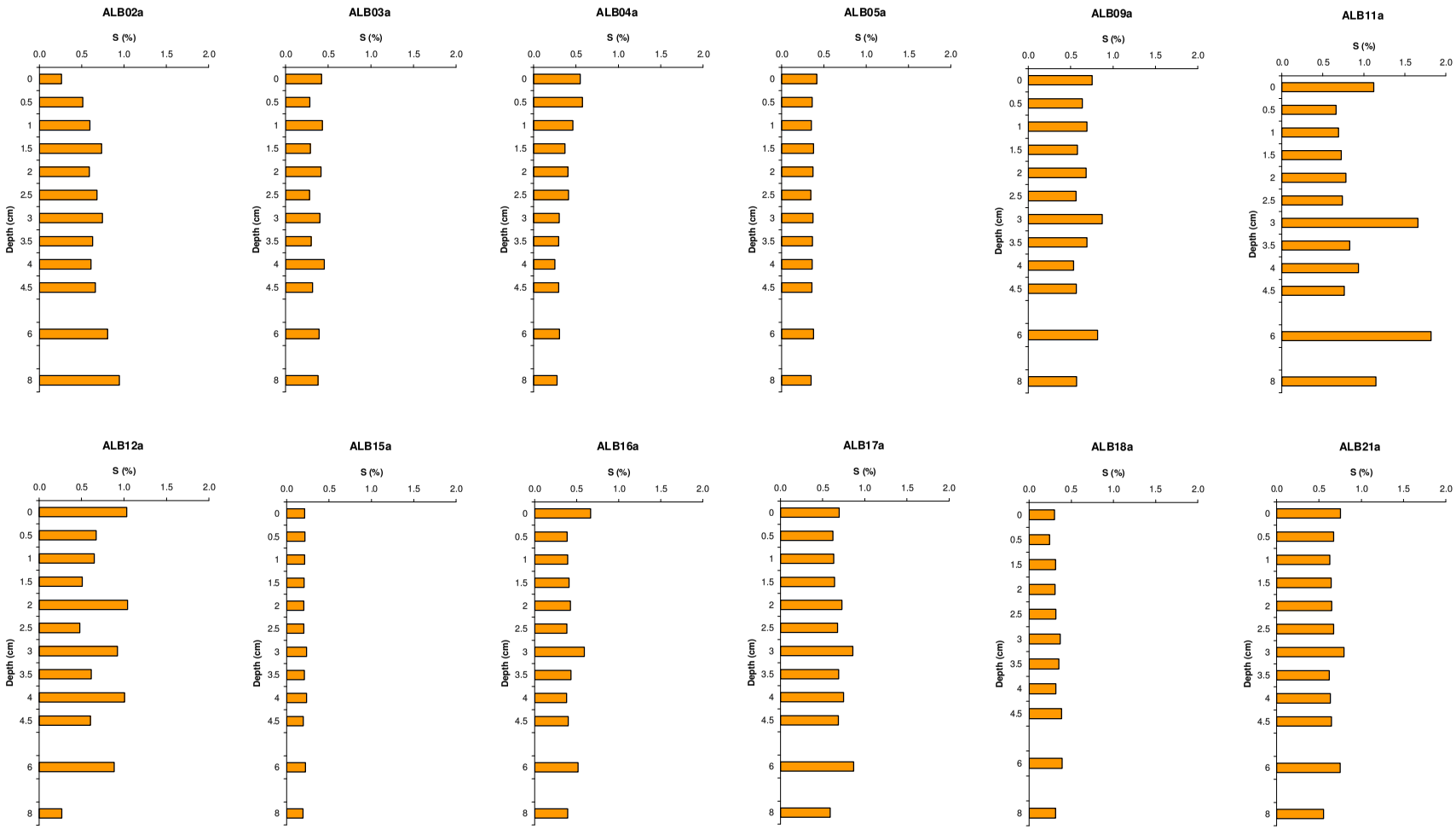

Figure 25: XRF Results for Phosphorus (%)

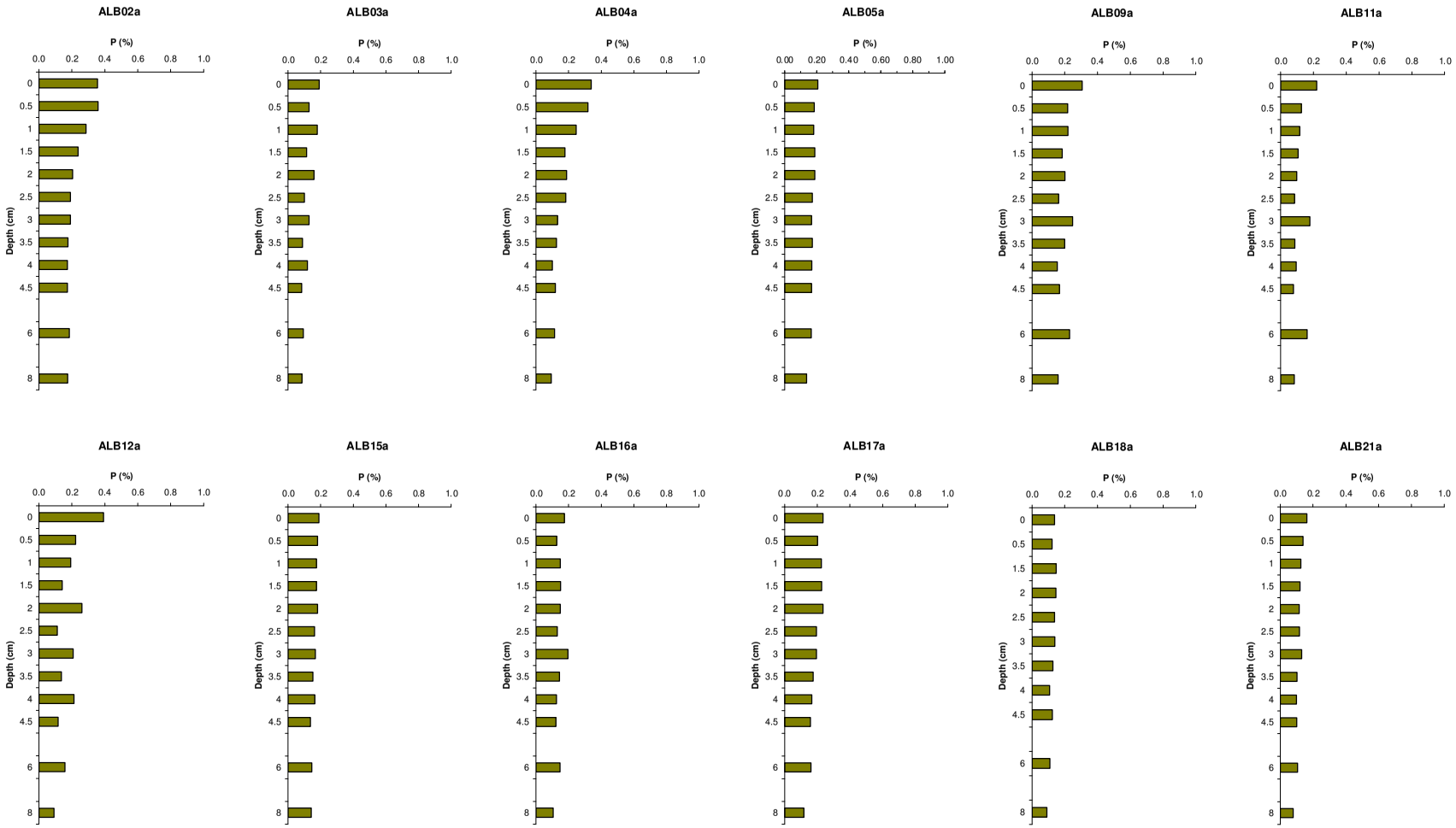

Figure 26: XRF Results for Silicon (%)

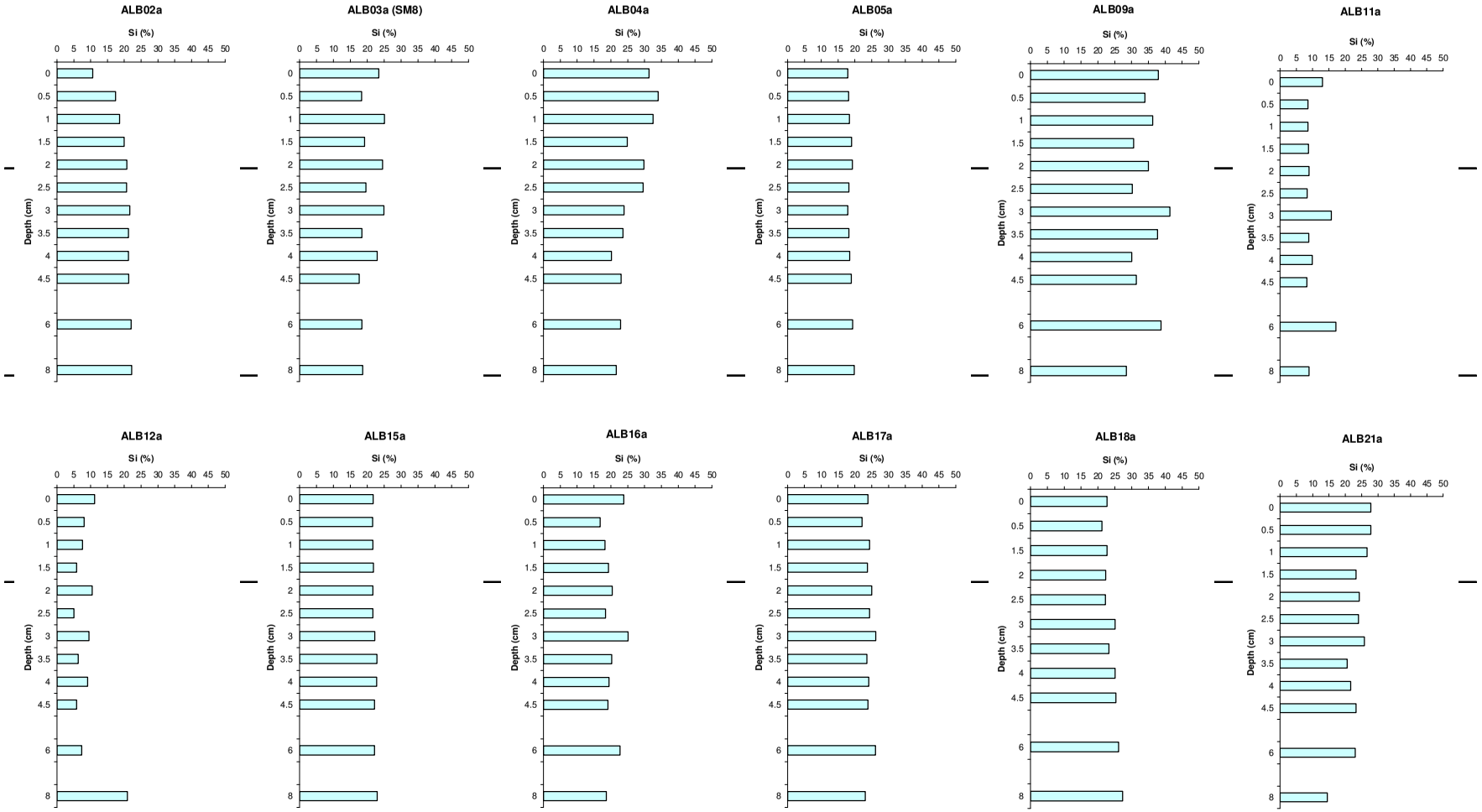

Figure 27: XRF Results for Lead (μg g^{-1})

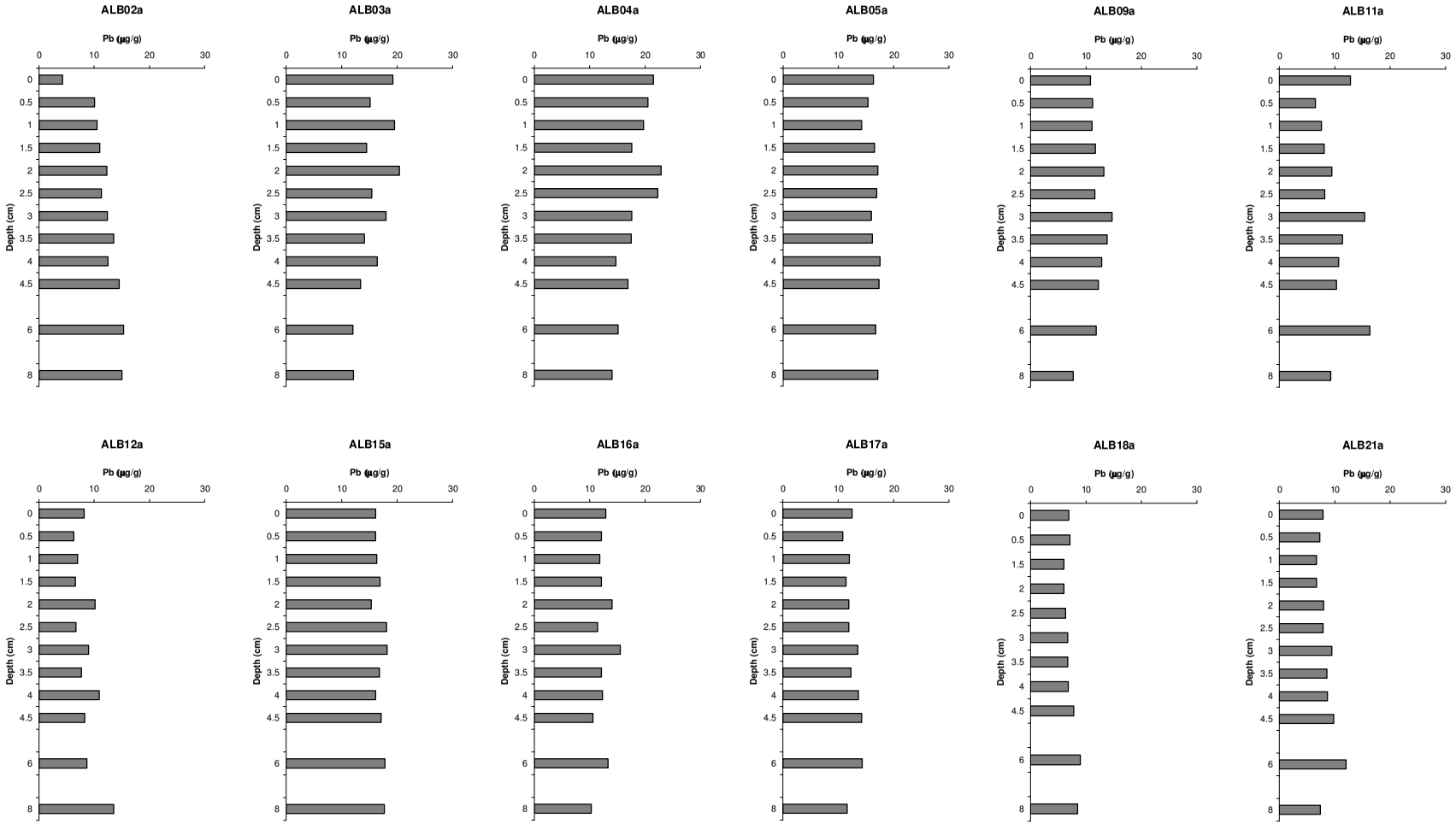

Figure 28: XRF Results for Zinc (µg g^{-1})

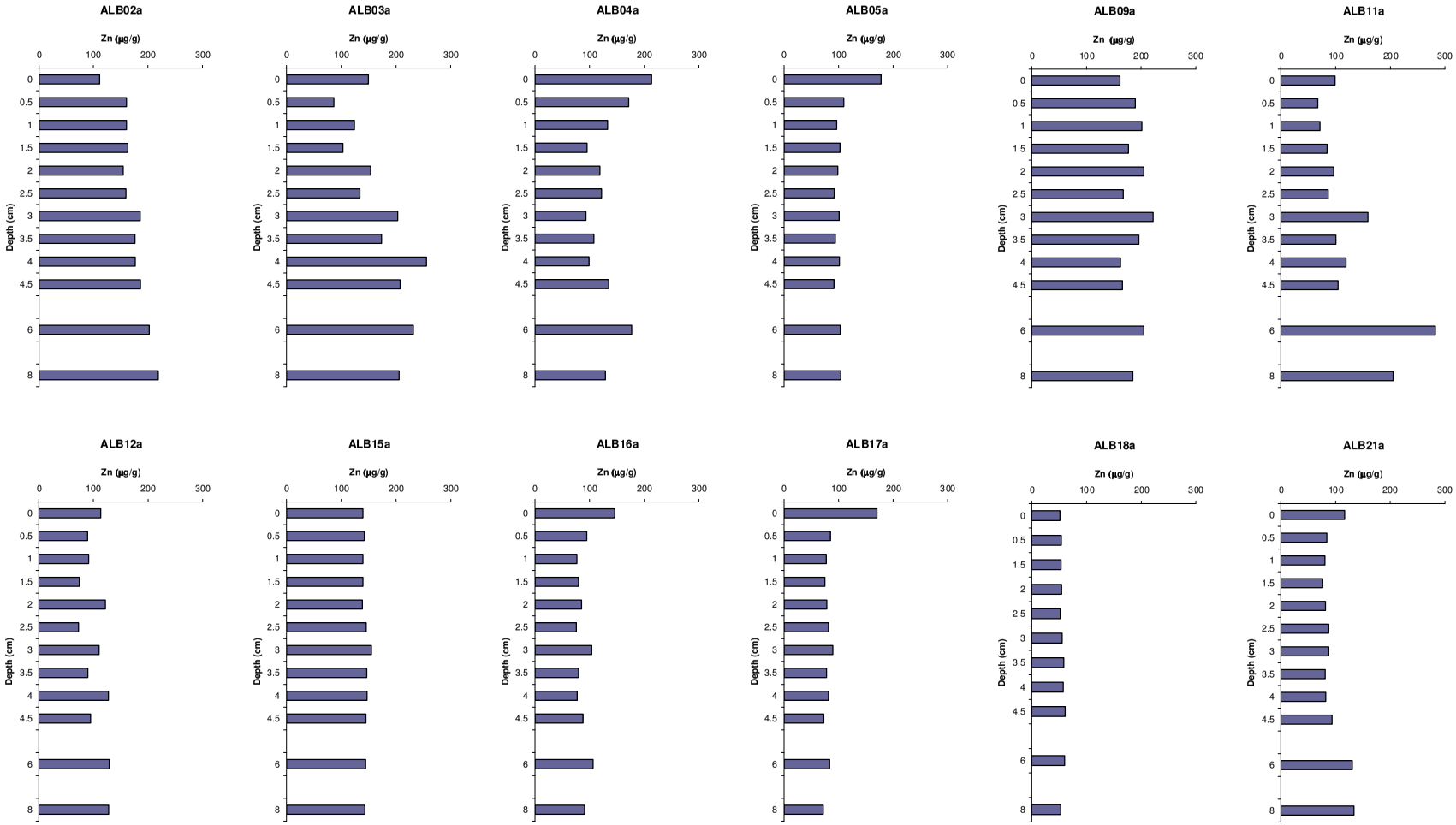

Figure 29: XRF Results for Vanadium (%)

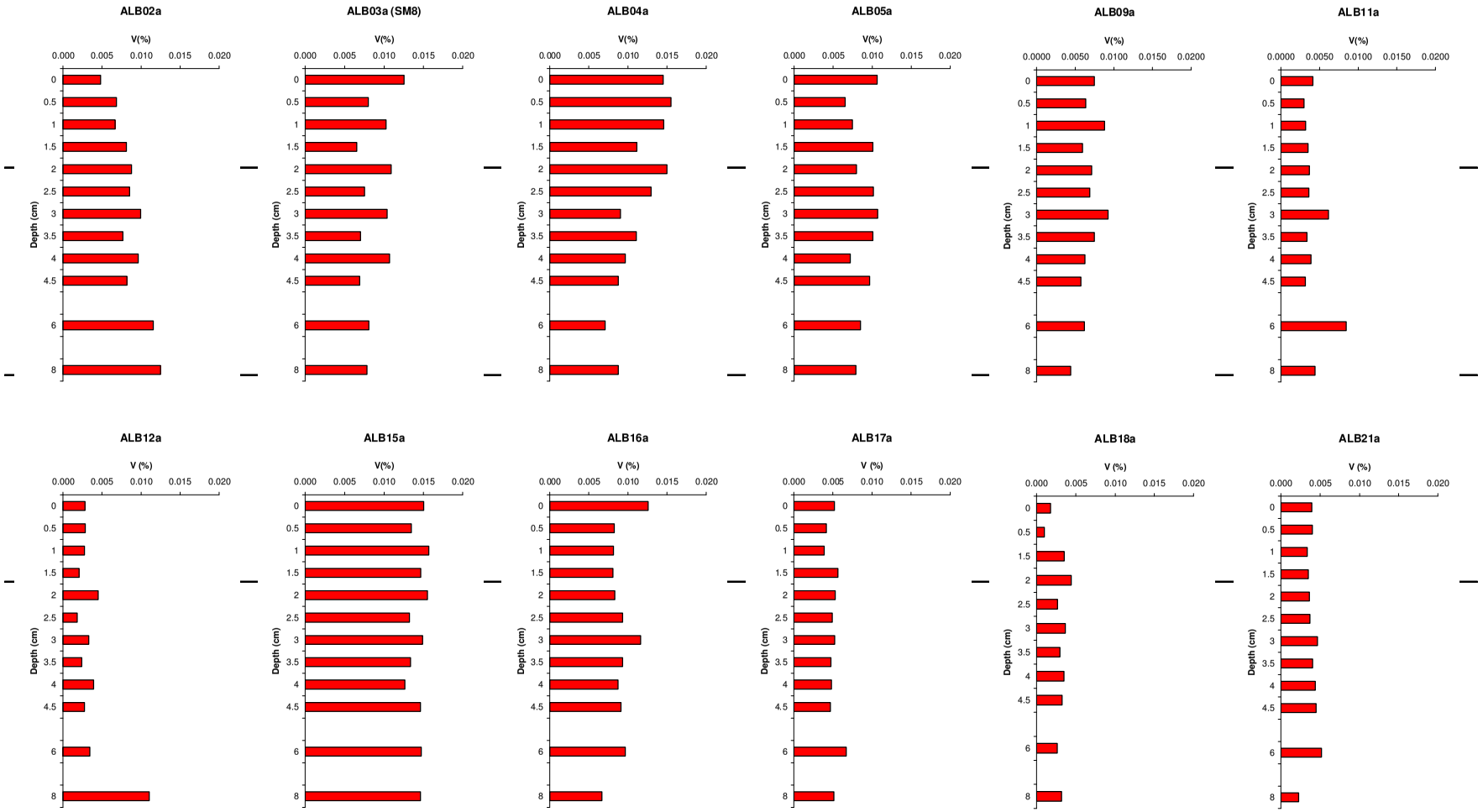

Figure 30: XRF Results for Aluminium (%)

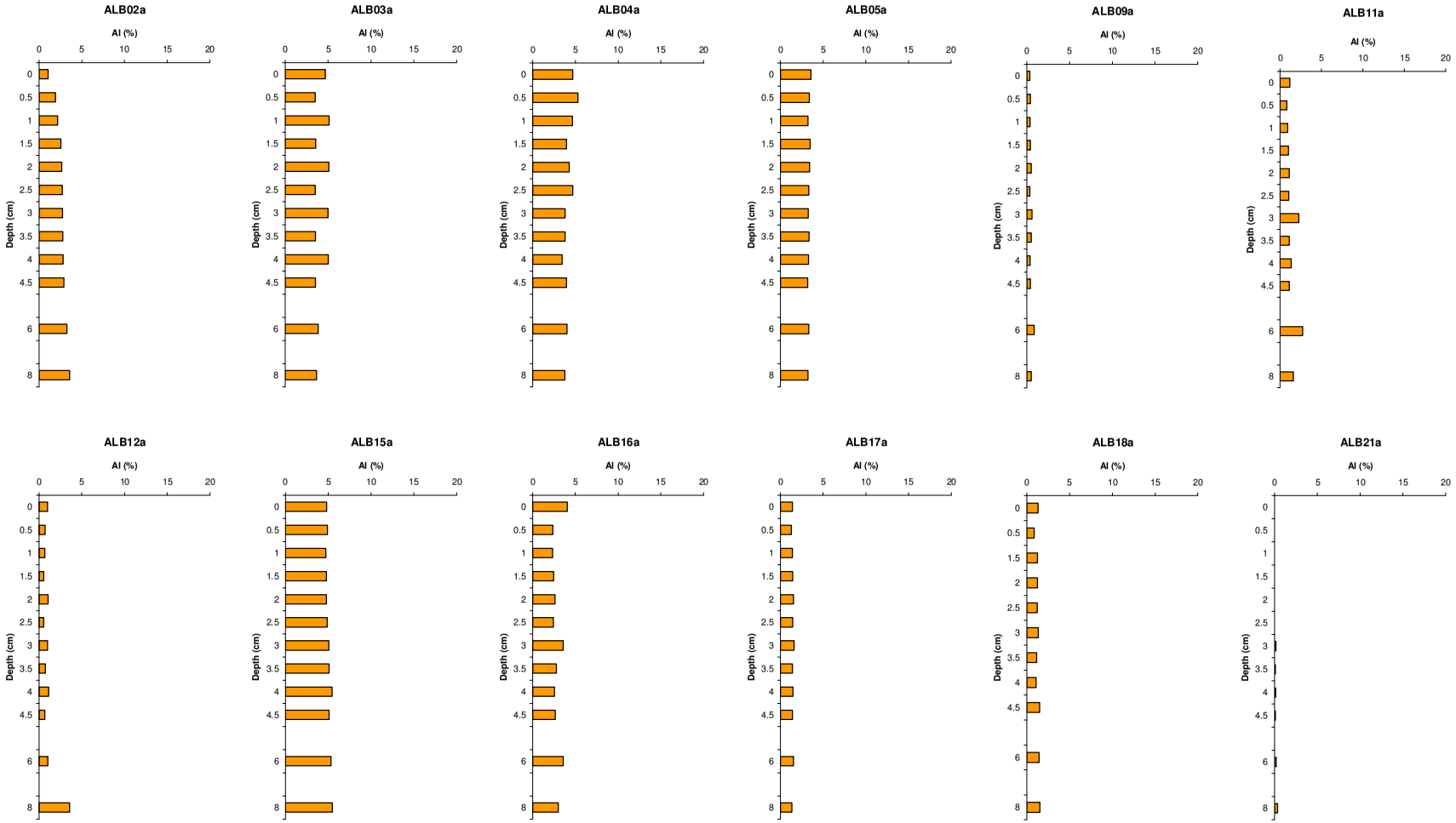

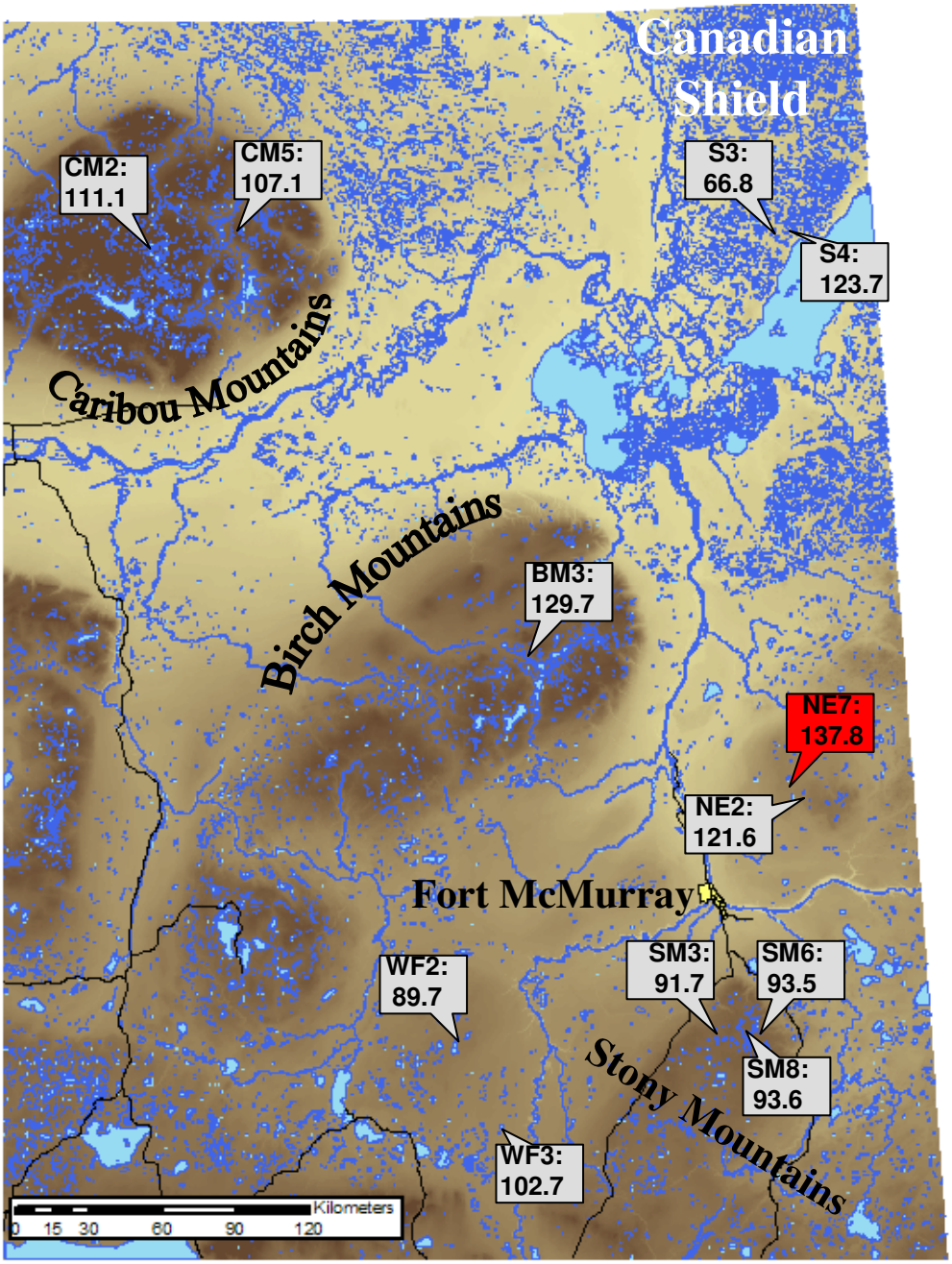

Figure 31: Surface sediment mercury concentrations (ng g^{-1})

The Hg concentration profile from NE7 (Fig. 32a) may indicate that the input of Hg into lakes in the area has increased during the historical past. The onset of increase in Hg concentration started before the mid-19th century, with a rapid increase at a time that coincides with the beginning of the industrial revolution, followed by a slow increase to the 1980s. As for the fluxes (Fig. 32b), the profile also shows a general increase from the 1880s upwards and it is likely that the increase in Hg fluxes in the last c. 20 years is not due to global anthropogenic emission, but local input and increase in sedimentation. The Hg fluxes reported here are comparable to those

reported for Lochnagar in north-east Scotland (Tipping *et al.*, 2007), a lake which is known to be impacted by anthropogenic pollution from industrial processes and fossil fuel combustion.

Further downcore measurements of Hg would improve our understanding of Hg deposition in the area and allow contemporary measurements to be compared with past trends and 'natural' background levels.

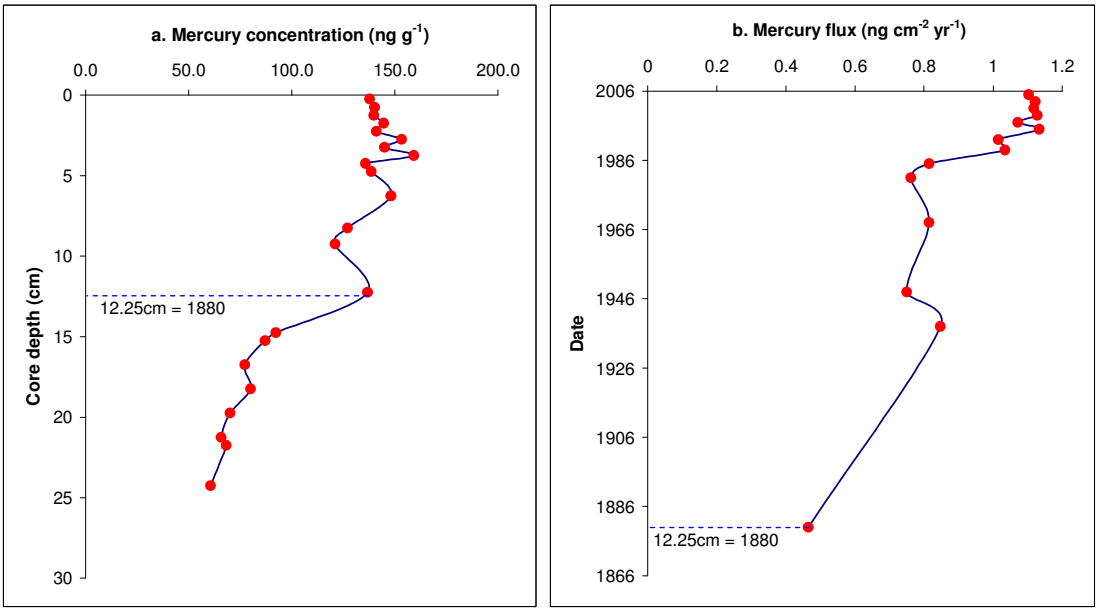

Figure 32: a) Mercury concentration and b) mercury flux to lake sediment core ALB21 from lake NE7

3.7 Diatom analysis

Methods – diatom analysis

Diatoms analysis was undertaken using a Leitz Labrolux light microscope equipped with a phase contrast oil immersion 1.3 NA 100x objective. Approximately 300 valves were counted in each level (except for those sediment sections where diatom preservation was poor).

Diatom slides were prepared according to Battarbee *et al.* (2001) and identifications followed the published literature (see Flower, 2005). Diatom taxonomy was improved by collaboration between the two diatom analysts (Flower and Pla) involved with both phases of this palaeolimnological investigation of Northern Alberta lakes.

Environmental and physico-chemical data were obtained from the University of Alberta. Standard multivariate statistical methods were applied (e.g. Lotter et al., 1998; Pla & Anderson, 2005) using CANOCO (ter Braak, 1992) and C2 (Juggins, 2003).

Methods – statistical analysis

The Weighted Averaging – Partial Least Squares regression (WA-PLS) methodology (ter Braak *et al.*, 1993) previously employed to derive a diatom-pH transfer function from 47 sediment core top samples (Pla and Curtis, 2006) was used here after taxonomic harmonization of diatom counts between the two contracts and combination of the two core top datasets. All diatom taxa and all surface sediments were used to build the new model and all counts from the sediment record were used for pH reconstruction. No taxa were omitted to avoid poor correlation between sediment core taxa and training set taxa, in order to produce the most correct reconstruction despite the potential loss of predictive power from the model. Validation was performed using bootstrapping procedures.

Model performance was assessed using between one and five components in the WA-PLS model (Table 15). The simplest one component model (C1) performed almost as well as the two component model (C2) with a deterioration in RMSEP thereafter as further components were added (Table 15). Hence the one-component model (WA-PLS C1) was used here to determine diatom-inferred pH for down-core reconstruction.

Table 15: Diatom-pH transfer function (WA-PLS) models using 1-5 components (C1 – C5)

Name	RMSE	R^2	Av. Bias	Max. Bias	Boot. R^2	Boot. Av. Bias	Boot. Max. Bias	RMSE s1	RMSE s2	RMSEP
C1	0.3055	0.8528	0.0000	0.7323	0.6876	-0.0315	0.8704	0.1298	0.4588	0.4768
C2	0.1672	0.9559	0.0000	0.2617	0.6902	-0.0588	0.8433	0.1522	0.4490	0.4741
C3	0.1073	0.9818	0.0000	0.1736	0.6921	-0.0568	0.8360	0.1729	0.4471	0.4794
C4	0.0718	0.9919	0.0000	0.1121	0.6867	-0.0589	0.8749	0.1822	0.4511	0.4865
C5	0.0480	0.9964	0.0000	0.0399	0.6815	-0.0608	0.9092	0.1925	0.4547	0.4938

Results – diatom stratigraphies

Stratigraphic diatom frequency diagrams are presented for each sediment core in Figs. 33-44 below (where taxa with frequency abundances of <3% are omitted).

Core ALB02 (lake BM3)

The diatom assemblages in this core were diverse with 138 taxa being recorded. Over the 0-21 cm section of the sediment core the diatom biostratigraphy showed strong increases in the planktonic diatoms *Aulacoseira ambigua* and *A. subarctica;* these two diatoms dominated the assemblages throughout (Fig. 33). Also of significance were the increases of the distinctive planktonic diatom *Stephanodiscus niagarae*, and of *Cyclostephanos tholioformis,* both from above about 11 cm sediment depth (c. 1948) in the core. The planktonic form of *Tabellaria flocculosa* also showed a small abundance increase from above c. 15 cm sediment depth (c. 1900). Several of the semi-benthic fragilarioid taxa (*Staurosira elliptica* and *St. construens* v. *venter* and *Staurosirella pinnata*) displayed a declining trend in abundances towards the core top. The frequencies of several diatom species fluctuated in the upper 2 cm of sediment (i.e. from c. 1999) and benthic *Opephora martyi* showed a small increase in the surface sediment. Overall, the diatoms in this core show a clear trend in increasing abundances of species that indicate more nutrient rich conditions. The decline in semi-benthic fragilarioid taxa perhaps indicates increased development of the phytoplankton crops. There is no diatom evidence of recent acidification in this lake; diatom-inferred pH shows little change except for possibly a very minor increase over recent decades. The perturbation in some diatom frequencies at the core top (upper 3 cm) suggests a very recent disturbance has occurred in the lake. The diatom taxa involved seem unrelated to water quality changes and possibly indicate a lake level fluctuation.

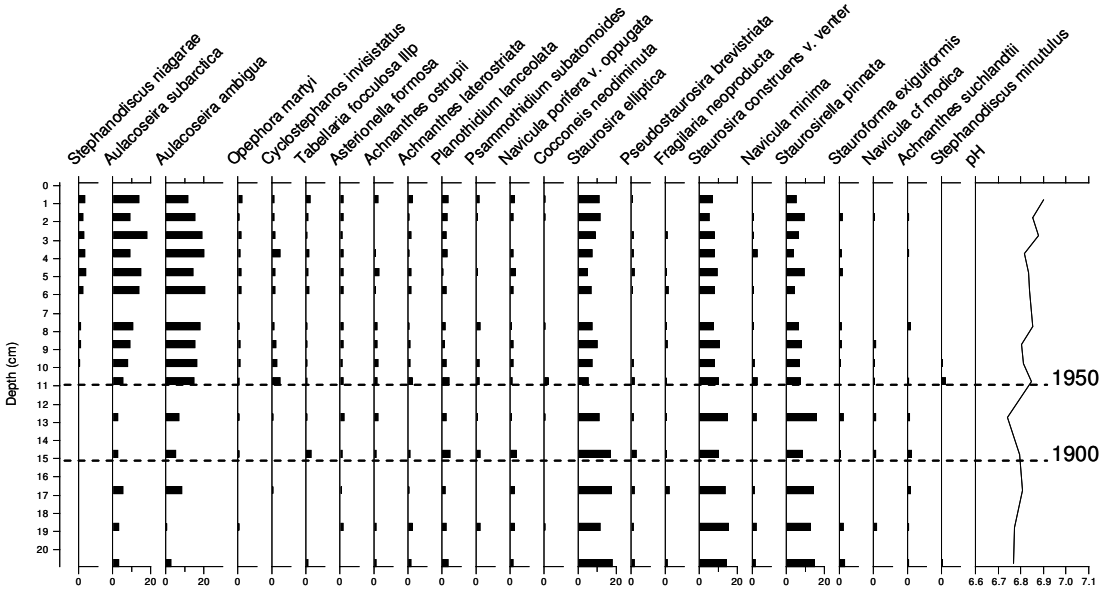

Figure 33: ALB02 Diatom inferred pH change

Core ALB03 (lake SM8)

The diatom assemblages in this core were species poor with only 88 taxa being recognized. Over the top 17 cm of sediment, the diatom biostratigraphy showed modest changes in diatom frequency abundances. The semi-benthic fragilarioid species *Staurosira construens* v. *venter* dominated the sediment core assemblages but showed a declining trend from above c. 7 cm sediment depth (Fig. 34). *Stauroforma exiguiformis* showed a similar trend but this species declined from c. 10 cm depth. A small increase in the planktonic diatom *Asterionella formosa* was recorded in the upper 3 cm of the core (from c. 1950) as it replaced the more acid indicating *A. ralfsii*. Although never common, a number of small naviculoid species showed increasing abundance trends in the core, notably with *Navicula subrotunda*, *N. difficultissima* and *N. minima*. Other benthic species such as *Stauroneis anceps* and some *Pinnularia* species showed marked abundance declines above c. 10 cm depth in the core. At 17 cm sediment depth diatom preservation was a problem but this depth corresponds to several centuries before present. Overall, this core indicates the persistence of moderately stable conditions with regard to water quality, although the appearance of *A. formosa* in the upper sediment does indicate that a small degree of nutrient enrichment of the lake has occurred since c. 1950. Diatom-inferred pH shows an increasing trend from around 9 cm which is undated but is well before 1900 according to the dating profile. The rather unusual increases of some of the small naviculoid diatoms in this core could well indicate that lake water level has declined. These diatoms were occasionally observed adhering to small fragments of macrophyte remains within the core and hence an increase in the abundance of aquatic macrophytes in the lake could explain abundances of these small diatoms by providing additional habitat. Similarly this change may be responsible (by shading) for the decline in abundances of the larger surface mud dwelling (epipelic) diatoms such as *St. anceps*. Furthermore, the ^{210}Pb profile for this core suggested that surface sediment material may be missing which could be related to changes in water level.

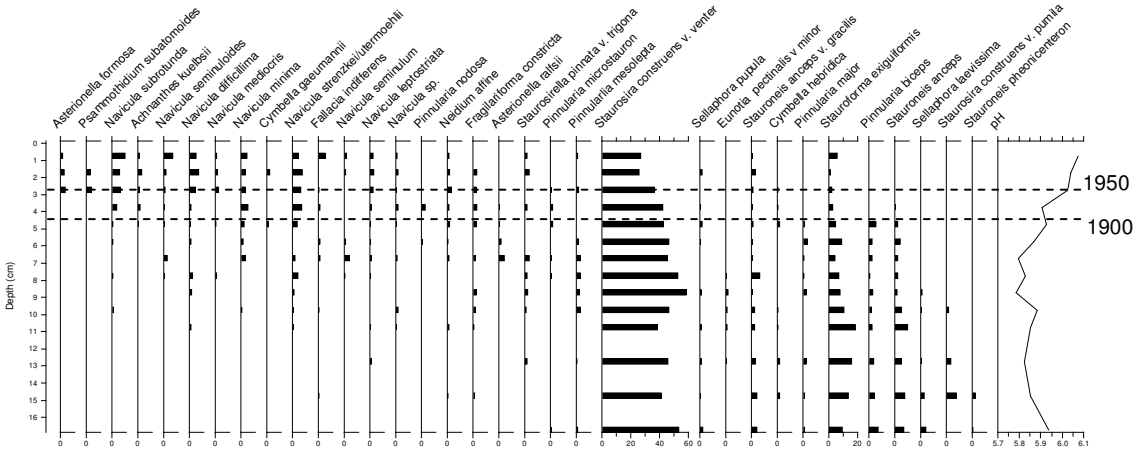

Figure 34: ALB03 Diatom inferred pH change

Core ALB04 (lake SM6)

The diatom assemblages in this core were rather species poor with 99 taxa being recognized. Over the top 19 cm of sediment, the diatom biostratigraphy showed relatively modest changes in species composition. The semi-benthic fragilarioid species *Staurosira elliptica* dominated all the sedimentary assemblages and achieved abundances of over 50% (Fig. 35). However, the abundances of this taxon showed a small declining trend from above 7 cm depth in the core, corresponding to the late 19th century. The rather unusual tri-radiate diatom, *Staurosirella pinnata* v. *trigona* showed an increasing trend from above 15 cm depth. Although never abundant, this trend was paralleled by that of the planktonic diatom *Asterionella formosa,* which showed a clear increase above 7 cm depth. Several naviculoid taxa showed similar increased abundance changes. *Staurosira construens* v. *venter* showed a gradually declining abundance trend from the core base. Of the larger benthic taxa, *Stauroneis anceps* and several species of *Pinnularia* showed abundance declines within the core. Overall, the diatoms in this core indicate a small increase in nutrients, at least from the point *A. formosa* increases towards the end of the 19th century (7 cm). Diatom-inferred pH shows very little variation within at least the last 100 years. The decline in large benthic taxa could indicate that water colour has increased in the lake since phytoplanktonic diatom abundances in the core seem to be low.

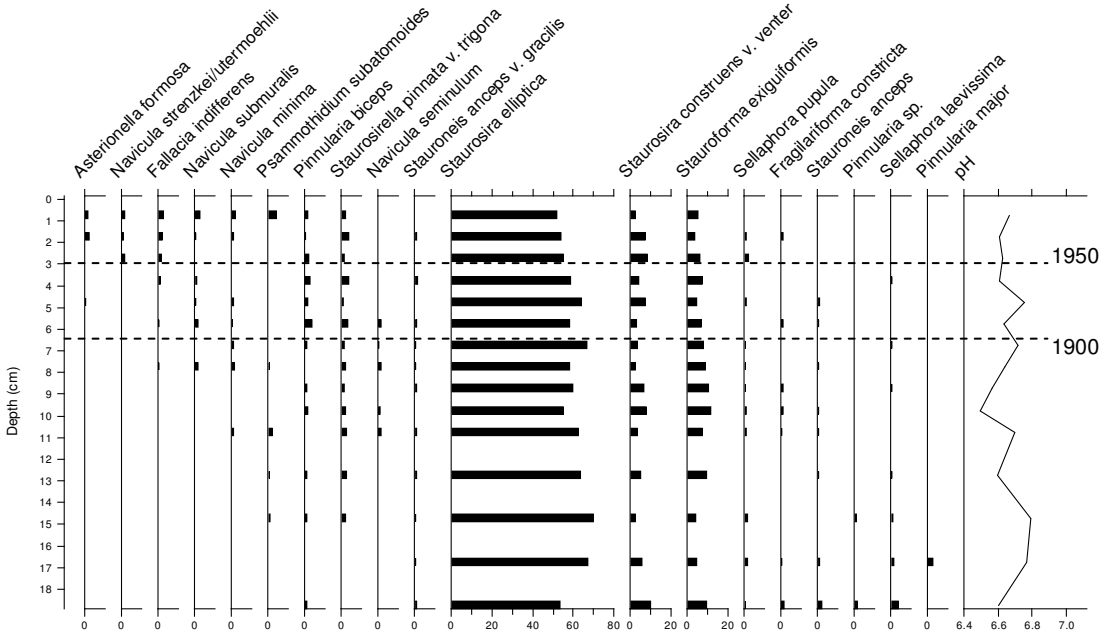

Figure 35: ALB04 Diatom inferred pH change

Core ALB05 (lake SM3)

The diatom assemblages in this core were very species poor with only 62 taxa being recognized. Over the top 21 cm of sediment, the diatom biostratigraphy showed only small changes in diatom frequency abundances and virtually no planktonic diatoms were recorded. The most common diatom *Staurosira construens* v. *venter* was present at over 50% abundance throughout the whole core (Fig. 36). Recorded changes were small with *Fallacia indifferens* and *Psammothidium rossi* showing small increases

while several other low abundance naviculoids declined in abundance. Overall, this low diatom diversity core showed remarkably little change indicating that water quality in this lake has been relatively stable over past decades. A few valves of acidophilous *Asterionella ralfsii* occurred in the upper 2 cm of the core but frequencies were insufficient to markedly affect the reconstructed pH values. Slight acidification may be indicated but no convincing trend in diatom-inferred pH since 1900 is demonstrated.

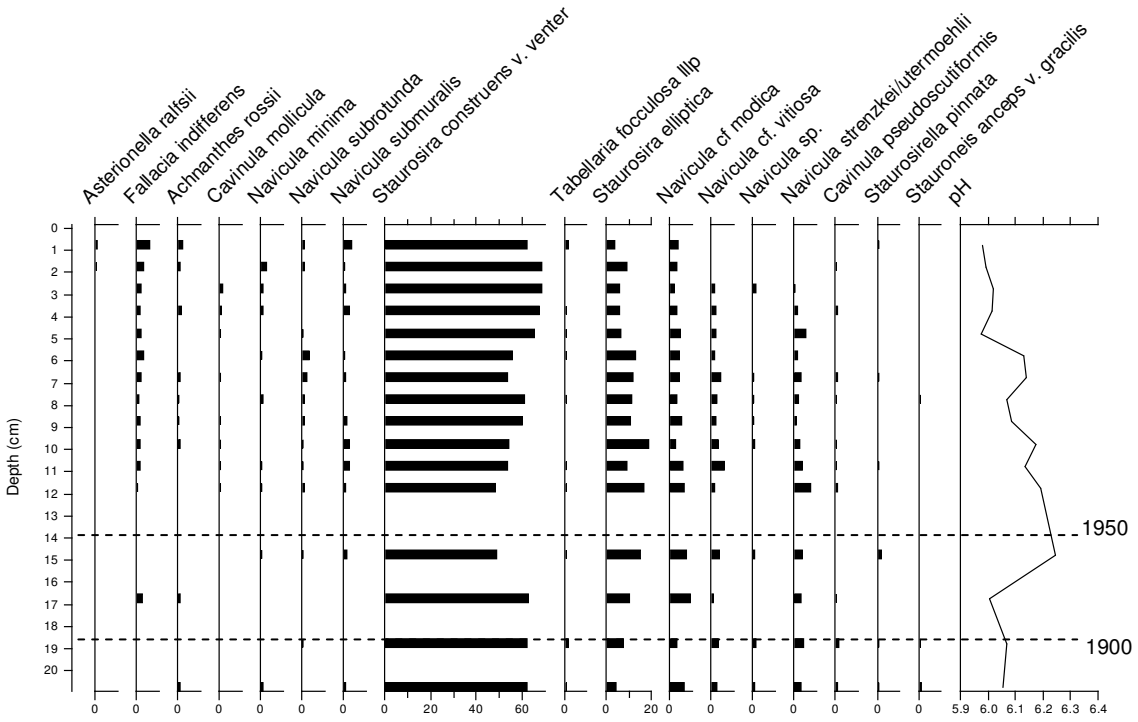

Figure 36: ALB05 Diatom inferred pH change

Core ALB09 (lake NE2)

The diatom assemblages in this core were moderately diverse with 124 taxa being recognized. Over the top 21 cm of sediment, the diatom biostratigraphy showed relatively small changes in species composition. The semi-benthic fragilarioid species *Staurosira construens* v. *venter* was the most common species in the sediment core but its abundance fluctuated around 20% and showed no clear change trend (Fig. 37). Several diatoms showed a small trend towards higher abundances from the core base to around 7-5 cm sediment depth (c. 1960-1976) before declining. One of these species *Aulacoseira ambigua* is an indicator of higher nutrient conditions. Only two species showed an increasing abundance trend above about 6 cm depth (1969), *Asterionella ralfsii* and *Staurosira elliptica*. The former species is planktonic in habit and, although present at only low abundances, its presence is characteristic of acid water. Overall, the diatoms in this core indicate fairly stable conditions but the small increase in *A. ambigua* could indicate that slightly more nutrient rich conditions persisted around 5 cm depth in the core (c. 1976) but the later decline suggests that this change was not sustained. Above 5 cm sediment depth the presence of a few percent of *A. ralfsii* could indicate very slightly more acid conditions have affected

the lake in the recent past (see ALB05 above), but this effect is not detectable in the diatom-inferred pH which shows no convincing trend.

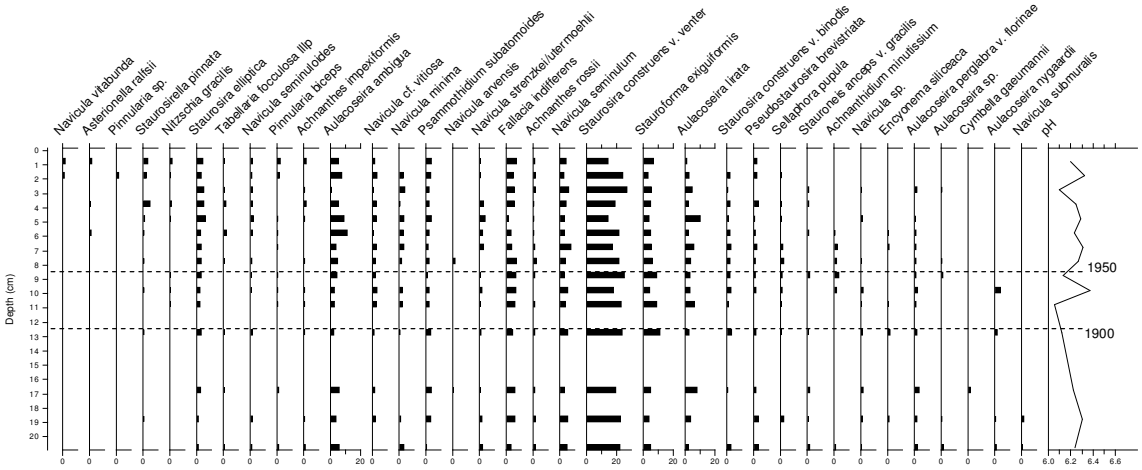

Figure 37: ALB09 Diatom inferred pH change

Core ALB11 (lake WF3)

The diatom assemblages in this core were rather species poor with only 92 taxa being recognized. Over the top 21 cm of sediment, the diatom biostratigraphy showed a strong abundance increase in the planktonic diatom *Asterionella formosa* and indicates a considerable amount of nutrient enrichment (Fig. 38). This taxon was unrecorded below 12 cm depth and showed a major abundance increase from above 7 cm depth (c. 1936) to reach almost 50% of the total diatom assemblage in surface sediment. Another planktonic diatom, *Aulacoseira ambigua,* indicative of nutrient enrichment, also showed increasing frequency abundances, from the core base to the most recent sediment. Less common but also indicating increased nutrients, *Nitzschia gracilis* increased in the more recent sediment. Commensurate with the increasing abundances of these taxa indicating higher nutrient status, several fragilarioids declined in the core with both *Staurosira elliptica* and *St. construens* v. *venter* showing strong declines and only *Fragilariforma constricta* showing a small increase. These taxa are primarily benthic but are easily resuspended into the water column. Similarly some of the more uncommon but larger benthic *Pinnularia* species have also diminished in abundance. Possibly, these changes could reflect diminished under-water light availability as a result of the development of the planktonic diatoms and doubtless other phytoplankton; alternatively, nutrient optima of the benthic species may have been exceeded. Overall, the diatom stratigraphy of this core shows a large increase in planktonic diatom species that indicates strong nutrient enrichment of the lake has occurred. There is a corresponding increase in diatom-inferred pH from pre-1900 to the present day, although higher pH values were also found in the bottom of the core. The ^{210}Pb profile suggests some possible disturbance to the upper levels of the sediment core or loss of material but the nutrient enrichment trend remains very convincing.

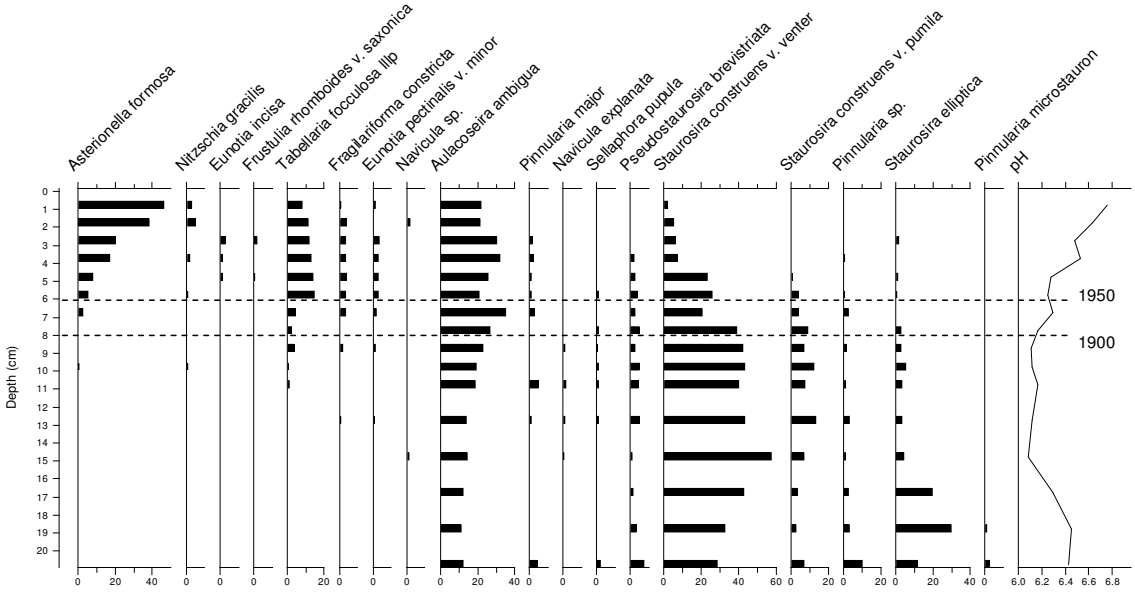

Figure 38: ALB11 Diatom inferred pH change

Core ALB12 (lake WF2)

The diatom assemblages in this core were rather species poor with only 96 taxa being recognized. Over the top 21 cm of sediment, the diatom biostratigraphy showed modest changes in diatom frequency abundances. The semi-benthic fragilarioid species dominated the sediment assemblages and *Staurosira elliptica* and *Staurosirella pinnata* showed increasing abundance trends in the core (Fig. 39). *St. construens* v. *venter* also generally increased but declined sharply in the upper 2 cm (c. 1996) while *Pseudostaurosira brevistriata* generally declined in abundance. The planktonic diatom *Aulacoseira ambigua,* a species indicative of nutrient enrichment, showed a modest increase in frequency abundance from the core base to the most recent sediment. Small abundance changes were also recorded for several small naviculoid species which generally display an increasing trend. The diatoms below 15 cm depth (pre-1900) in this sediment core displayed increasingly poor preservation with many diatom valves being at least partly dissolved. Diatoms were very scarce at c. 20 cm depth but the presence of remains of a green planktonic alga (*Pediastrum*) substantiated the former existence of standing water at the time corresponding to the core base. Overall, the increasing abundance of diatom phytoplankton indicates that some nutrient enrichment of this lake has occurred but diatom dissolution problems in the lower section of the cores makes interpretation of abundance changes in this section difficult. There is very little discernible change in diatom-inferred pH except for a minor increase in the top 3 cm (post 1990) that possibly corresponds to a small nutrient enrichment effect.

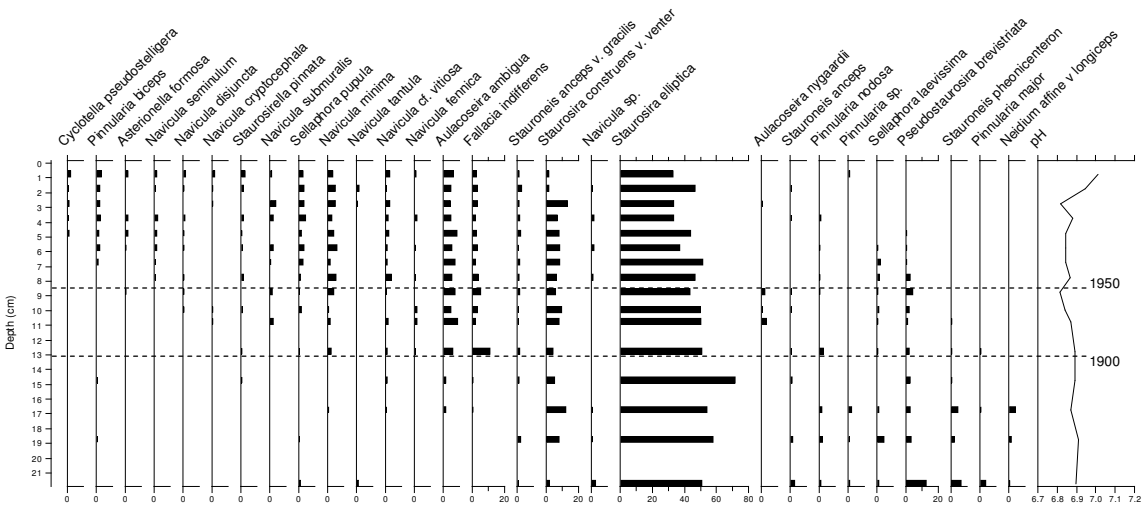

Figure 39: ALB12 Diatom inferred pH change

Core ALB15 (lake CM2)

The diatom assemblages in this core were moderately diverse with 132 taxa being recognized. Over the top 20 cm of sediment the diatom biostratigraphy showed a strong increase in the planktonic diatom *Asterionella formosa*, most notably from about 14 cm depth in the core (c. 1902; Fig. 40). Another distinctive planktonic diatom, *Stephanodiscus niagarae*, also showed increasing abundance but less marked than for *A. formosa*. Both these diatoms offer strong evidence of increasing nutrient enrichment of the lake. Other diatoms, including *Aulacoseira ambigua* (planktonic) and several tychoplanktonic (semi-benthic) forms, *Fragilaria capucina* var. *mesolepta* and *F. crotonensis* also showed an increasing frequency trend within the core and confirm a nutrient enrichment impact on the diatom flora. Other species, most notably *Aulacoseira subarctica* and *Staurosira elliptica* showed an initial frequency increase within the sediment core but then declined in the uppermost sediment. A few species declined in abundance towards the core top, e.g. *Gyrosigma acuminatum* and *Staurosira construens* var. *venter*. The decline in the benthic dwelling epipelic diatom *G. acuminatum* could indicate a decline in light availability in the lake, either as a result of increased phytoplankton turbidity or of increased water colour. Overall, the diatom stratigraphy of this core provides clear evidence of recent increasing nutrient enrichment of the lake, but diatom-inferred pH changes very little throughout the depth of the core.

Core ALB16 (lake CM5)

The diatom assemblages in this core were species poor with only 84 taxa being recognized. Over the top 18 cm of sediment, the diatom biostratigraphy showed modest changes in diatom frequency abundances. The semi-benthic fragilarioid species dominated the sediment assemblages and both *Staurosira elliptica* and *St. construens v. venter* showed increasing abundance trends in the core (Fig. 41). *Staurosirella pinnata* was most common around 10 cm depth in the core. The planktonic diatom *Aulacoseira ambigua,* a species indicative of nutrient enrichment, also showed a modest increase in frequency abundance from around 12 cm to the most recent sediment. Minor abundance changes were also recorded for several small

naviculoid species which generally showed an increasing abundance trend. The acid indicating species *Eunotia exigua* was also present in the core but above c. 12 cm depth abundances showed no apparent trend. The diatoms below 15 cm depth in the sediment of this core displayed increasingly poor preservation (cf. ALB12) with most diatom valves being at least partly dissolved. Hence, inferences about relative frequency changes in this part of the core are insecure, although this section represents a period prior to 1800. Nevertheless, the overall diatom stratigraphy of the core shows that the diatom plankton has clearly increased and this probably indicates moderate nutrient enrichment of the lake. There is no trend in diatom-inferred pH apart from a small increase in the top 2 cm of the core, i.e. since the early 1980s. However, the ^{210}Pb profile suggests that there may be sediment focussing problems at this site.

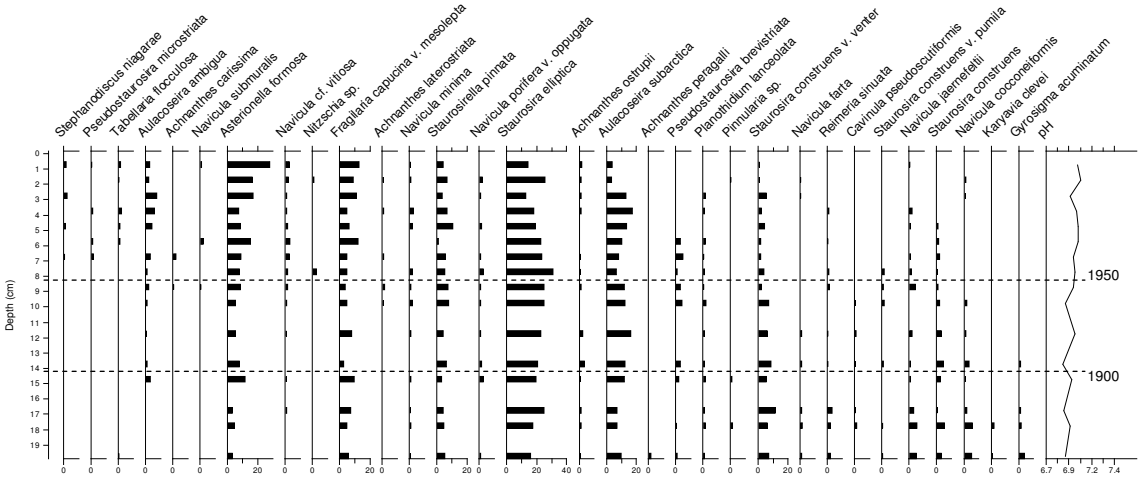

Figure 40: ALB15 Diatom inferred pH change

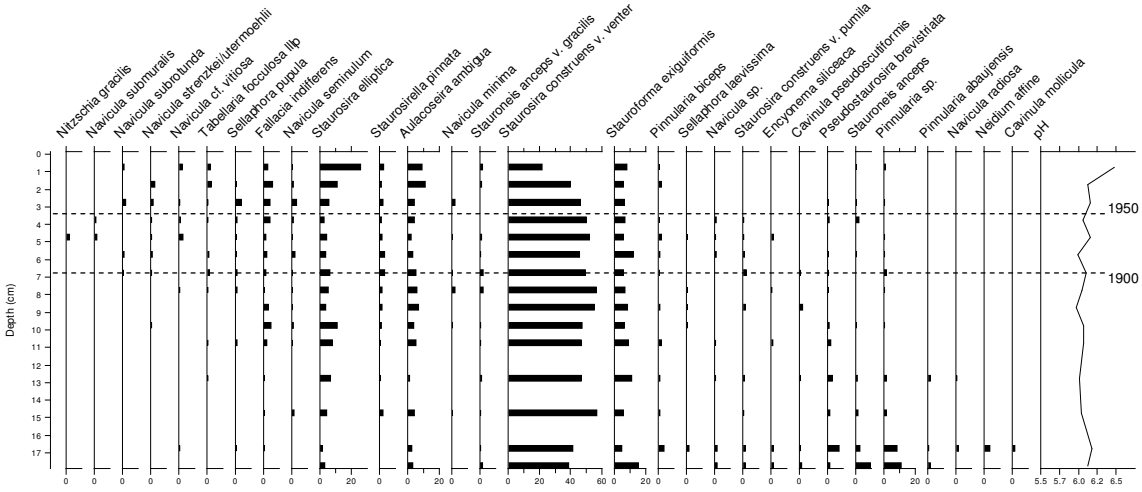

Figure 41: ALB16 Diatom inferred pH change

Core ALB17 (lake S4)

The diatom assemblages in this core were moderately diverse with 137 taxa being recorded. Over the 0-19 cm section of the sediment core the diatom biostratigraphy showed only very moderate changes in species abundances. The planktonic diatoms *Aulacoseira ambigua* and *A. subarctica* were common throughout most of the core and their abundances showed an increasing trend from near the core base (Fig. 42). At 8 cm depth (c. 1949) *A. ambigua* reached a peak abundance of about 30% but above this depth numbers declined, while frequencies of *A. subarctica* showed no such decline. The planktonic form of *Tabellaria flocculosa* showed a similarly increasing trend. The semi-benthic fragilarioid taxa showed little consistent change but two taxa, *Pseudostaurosira brevistriata* and *Staurosirella pinnata*, displayed a small declining trend. Overall, the diatoms in this core indicate an increase in nutrients since about 17 cm depth in the core, i.e. the early 1800s. There is no discernible trend in diatom-inferred pH and no indication of lake acidification. The ^{210}Pb profile suggests that there may be missing surface sediments or sediment focussing problems at this site.

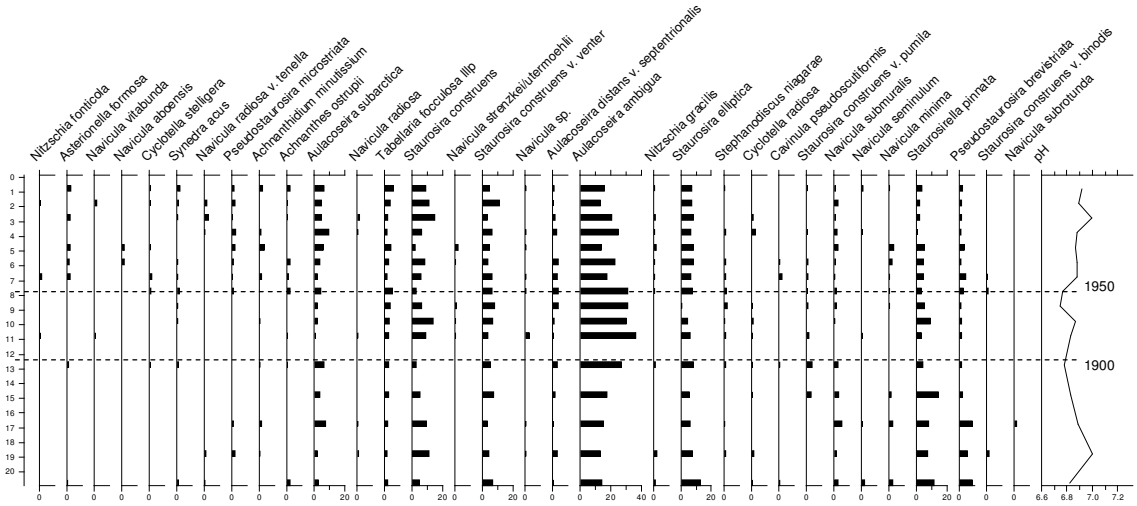

Figure 42: ALB17 Diatom inferred pH change

Core ALB18 (lake S3)

The diatom assemblages in this core were very diverse with 212 taxa being recognized. Over the top 23 cm of sediment, the diatom biostratigraphy showed a moderate abundance increase in the planktonic diatom *Aulacoseira ambigua*, most notably from about 10 cm depth in the core (c. 1940) and indicates a small amount of nutrient enrichment (Fig. 43). Another planktonic diatom, *A. distans* v. *tenella,* also showed a small abundance increase, though less marked than for *A. ambigua*. Several achnanthoid species also showed small abundances increases towards the core top. Other diatoms, including *Diatoma tenue* and the tychoplanktonic *Staurosira construens* var. *venter* showed a decreasing abundance trend towards the core top. Several less common benthic taxa, e.g. *Nitzschia perminuta*, *Cymbella cesatii* and *Achnanthes flexella* v. *alpestris* all showed small but distinctive increases in abundances in the surface sediment indicating the lake has experienced some further disturbance within the past five years. The ^{210}Pb profile does suggest the possibility of missing surface sediment in this core. Overall, the diatom stratigraphy of this core

displayed only relatively small changes but enough to indicate that some recent nutrient enrichment of the lake has occurred. There is no convincing evidence of a trend in diatom-inferred pH in the core.

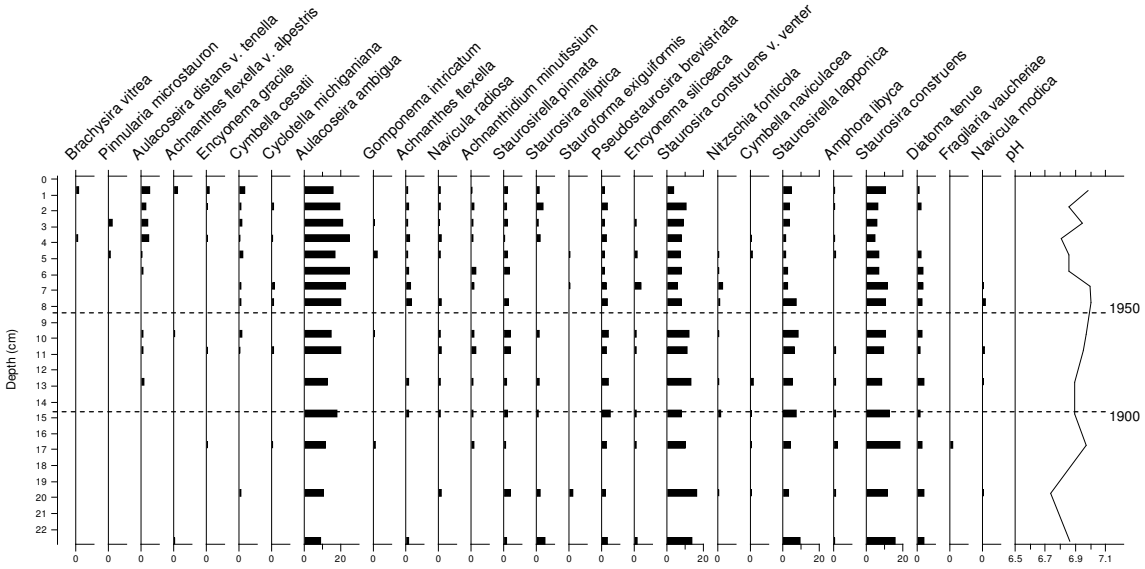

Figure 43: ALB18 Diatom inferred pH change

Core ALB21 (lake NE7)

The diatom assemblages in this core were moderately diverse with 123 taxa being recognized. Over the top 21 cm of sediment, the diatom biostratigraphy showed significant changes and, although circum-neutral species such as tychoplanktonic *Staurosira construens* v. *pumila* dominated the diatom assemblages, a rather unusual acidophilous diatom, *Actinella punctata* (pH optimum in the European SWAP data set is pH 5.2) appears towards the core top (Fig. 44). *Actinella punctata* showed increased abundances from above about 10 cm depth (c. 1930) followed by a sharper increase in the upper 3 cm of sediment in this core (i.e. from the early 1990s). Other acid indicating species such as the planktonic *Asterionella ralfsii* and tychoplanktonic *Fragilariforma polygonata* also showed sharp increases within the upper 3 cm of sediment. Other acidophilous species such as *Frustulia rhomboides* var *saxonica* and several *Cymbella* taxa showed peak abundances in the sub-surface section of the core, around 5 cm depth (c. 1980). Some circum-neutral and tychoplantonic taxa such as *Staurosira elliptica,* some *Aulacoseira* spp. and several (benthic) naviculoids showed abundance declines towards the core top. Overall, this core provides strong evidence that the lake has been recently acidified and pH reconstruction shows a lake water pH decline from about pH 6.2 to pH 5.7 starting around 1970 (Fig. 44). No species typical of nutrient enrichment were observed in this core. Whether the acidity change is caused by acid deposition or by increased release of organic acidity from peaty deposits in or around the lake is so far unknown.

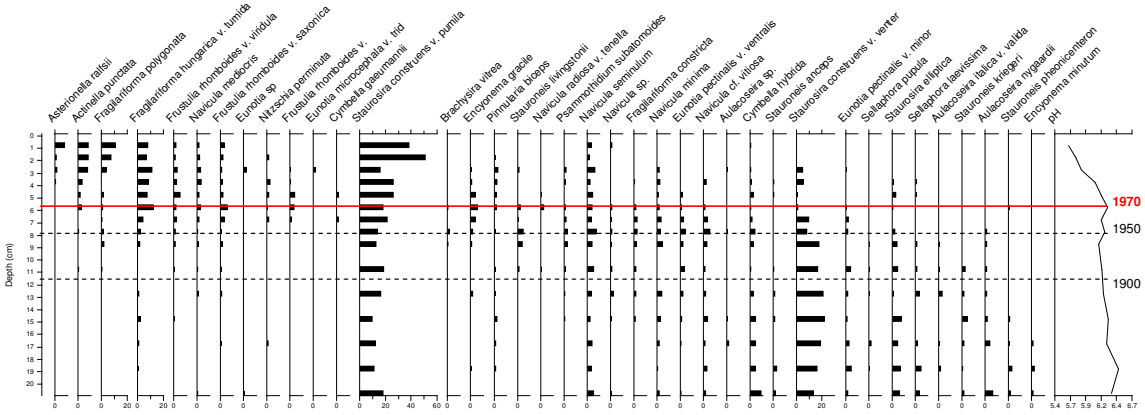

Figure 44: ALB21 Diatom inferred pH change

Conclusions

The sedimentary diatom assemblages examined in these twelve cores display a wide diversity of species that are closely linked to regional water quality variations as well as to specific local site factors. Many of the species are cosmopolitan but North American species (e.g. *Stephanodiscus niagarae, Cyclotella michiganiana*) often contribute significantly to the diatom phytoplankton component. Regionally endemic benthic taxa tend to be less significant but occurrences of such taxa as *Carpartogramma* and some larger fragilarioids were noted. To refine the performance of diatom based environmental change reconstruction models further taxonomic-ecological work is warranted, especially on the taxonomy of the small naviculoids and fragilarioid taxa in the region. Nevertheless, diatom analysis of these twelve cores provides clear convincing evidence of environmental change trends in the majority of sites.

Analysis of the diatom assemblages in the twelve lake sediment cores indicates that only one of the sites (NE7, core ALB21) has recently acidified. No other sites displayed a convincing, recent declining trend in pH. In two lake cores (ALB04 and ALB09), small recent increases in acidophilous *Asterionella ralfsii* were recorded but these were insufficient to cause significant changes in the overall diatom-inferred pH values. Several sites showed increases in diatom-inferred pH (alkalinisation) and many of the sites appear to have experienced nutrient enrichment in the recent past. This is typically demonstrated by the increasing abundance of planktonic diatoms commonly associated with more nutrient rich conditions. Also in several lakes the sedimentary diatoms indicate that water has shallowed and/or aquatic plants have increased in abundance in the recent past. Diatom trends are usually clear but ^{210}Pb profiles suggest disturbance or missing surface sediments in some sites, though not in the acidified site NE7. Deteriorating diatom preservation was observed towards the core base in several lakes but on the basis of ^{210}Pb dates, poor preservation is only associated with sediments from the 19th century and older so does not affect interpretation of recent change during the 20th century.

The acidified site, NE7, is the smallest lake studied and one of the shallowest. It is nevertheless chemically comparable to other cored sites which do not show acidification (Fig. 1b), e.g. SM6 (core ALB04), SM8 (core ALB03) and WF3 (core ALB11). Instead, these three sites which, like NE7, have pH < 6 and alkalinity < 50

µeq l^{-1} show nutrient enrichment according to the diatoms and indeed have much higher measured values of TP and TDP (TP >60 µg l^{-1}, cf. 18.5 µg l^{-1} for NE7 according to RAMP data to 2006).

The widespread increases in pH/alkalinity and nutrient status suggested by the diatoms confirm earlier observations made by Hazewinkel *et al.* (2008), i.e. that the most widespread changes in the region's lakes are linked to in-lake alkalinity production and nutrient enrichment. Possible sources of these nutrients are from industrial atmospheric pollution, forest burning or release from soils in the lake catchments. If the latter is shown to be case then it may be that climate warming is having a greater effect on these wilderness lakes than is industrial activity in the region, but the relative importance of climatic change and anthropogenic pollution is not yet known.

The overall changes in these twelve cores are summarized in Table 16.

Table 16: A summary of the principal overall changes in diatom frequency abundances in the twelve Alberta sediment cores selected for diatom analysis.

Core / Lake	Acidified	Nutrient enriched	High diatom plankton	Species diversity
ALB02 / BM3	No – slight pH increase	yes	yes	high
ALB03 / SM8	No – pH increasing since pre-1900	slightly	no	low
ALB04 / SM6	No – no pH change	yes	no	moderate
ALB05 / SM3	No – slight pH decline	no	no	low
ALB09 / NE2	No – no pH change	no	no	moderate
ALB11 / WF3	No – pH increasing since pre-1900	yes	yes	moderate
ALB12 / WF2	No – pH increasing since c.1990	yes	no	moderate
ALB15 / CM2	No – pH increasing since pre-1900	yes	yes	moderate
ALB16 / CM5	No – pH increasing since 1980s	yes	no	poor
ALB17 / S4	No – no pH change	yes	yes	high
ALB18 / S3	No – no pH change	yes	no	moderate
ALB21 / NE7	Yes – pH decline	no	no	moderate

4. SUMMARY AND POTENTIAL FUTURE WORK

The various palaeolimnological analyses described here indicate that acidification does not appear to be a widespread problem in northern Alberta, although we do show the first evidence for one site with a significant, recent acidification (NE7). As one of the smallest and shallowest of the sites studied with a peaty catchment, it is possible that lakes of a similar type are the most vulnerable to the potentially acidifying impacts of deposition arising from the Oil Sands extraction activities. Any future work to determine whether there are other similarly acidified sites in the region should focus on these shallow, smaller lakes, especially in the region north-east of Fort McMurray. UCL does currently hold a further four archived pairs of sediment cores from this region which were obtained at the same time as the two analysed here. Having cored 22 lakes in the region we have unstudied cores from a total of ten new lakes in the region already, although a new focussed coring programme could be justified. Furthermore, evidence of mercury contamination in the acidified site

suggests there could be merit in exploring the extent of Hg pollution at sites closest to the Oil Sands extraction activities. Comparison of long lake cores with a number of new short cores would indicate the relative importance of longer-term global drivers of Hg increases compared to local, industrial sources. New short cores could indicate the spatial extent of Hg pollution and provide information on possible sources, while biological sampling (e.g. fish) would indicate potential impacts on biota and possible implications for human health.

In addition to identifying the first clearly acidified lake in the region, a key finding from this work concerns the evidence for widespread nutrient enrichment in the region's lakes. While some changes in the sedimentary diatom records are indicative of nutrient enrichment that began in the early 19th century, suggesting longer-term drivers such as climate, stronger enrichment signals were recorded for the last 20-30 years. Diatom analysis of the twelve cores clearly indicates that the majority of lakes investigated are far from stable and are currently undergoing ecological changes. There is clearly scope for establishing a diatom monitoring programme that augments ongoing water quality monitoring so that these changes can be tracked into the future.

The causes of lake ecosystem instability in the region are currently unclear. Climate change and nutrient enrichment are probably involved as well as air pollution. Given the relatively high phosphorus concentrations in some of the regions lakes, it remains a possibility that NOx emissions and N deposition could also be resulting in changes to lake nutrient status which merit further study. A study of the nutrient limitation characteristics of the region's lakes, especially in terms of phytoplankton productivity and diatom species changes, could provide vital information on lake vulnerability to eutrophication caused by N deposition.

5. ACKNOWLEDGMENTS

Ewan Shilland provided assistance with data formatting and C2 plots for stratigraphic analysis and figures. Rod Hazewinkel and Preston McEachern provided advice on selection of study sites for coring, site data and logistical assistance with fieldwork in the region.

6. REFERENCES

Appleby, P. G. (2001) Chronostratigraphic techniques in recent sediments. In W.M. Last and J.P. Smol (eds.) *Tracking Environmental Change Using Lake Sediments. Vol. 1: Basin Analysis, Coring, and Chronological Techniques.* Kluwer Academic Publishers, Dordrecht, pp171-203.

Battarbee, R.W., Jones, V.J., Flower, R.J., Cameron, N.G., Bennion, H., Carvalho, L. & Juggins, S. (2001). Diatoms. In Smol, J.P., Birks, H.J.B. & Last, W.M. (ed.) *Tracking Environmental Change Using Lake Sediments. Volume 3: Terrestrial, Algal, and Siliceous Indicators*. pp. 155-202. Kluwer Academic Publishers, Dordrecht.

Flower, R.J. (2005). A taxonomic and ecological study of diatoms from freshwater habitats in the Falkland Islands. *Diatom Research* 20(1), 23-96.

Hazewinkel, R.R.O., Wolfe, A.P., Pla, S., Curtis, C. and Hadley, K. (2008) Have atmospheric emissions from the Athabasca Oil Sands acidified lakes in northeastern Alberta, Canada? *Canadian Journal of Fisheries and Aquatic Science* **65**, 1554-1567.

Juggins, S. (2003) http://www.campus.ncl.ac.uk/staff/Stephen.Juggins/

Lotter, A. F., Birks, H. J. B., Hofmann, W. and Marchetto, A. (1998) Modern diatom, cladocera, chironomid and chrysophyte cyst assemblages as quantitative indicators for the reconstruction of past environmental conditions in the Alps. II. Nutrients. *Journal of Paleolimnology* **19**:443-463.

Pla, S. and Anderson, N. J. (2005) Environmental factors correlated with chrysophyte cyst assemblages in low arctic lakes of south-west Greenland. *Journal of Phycology* **41**:957-974.

Pla, S. and Curtis, C. (2006) *Lake sediment core top analysis.* Report prepared for the CEMA NOx SOx Management Working Group under Contract Number 2005-0038. Ensis, London, 9pp.

Pla, S., Curtis, C. and Simpson, G. (2006) *Lake sediment core bottom sample analysis and assessment of diatom change.* Report prepared for the CEMA NOx SOx Management Working Group under Contract Number 2006-0020. Ensis, London, 11pp.

Rose, N.L. (1994). A note on further refinements to a procedure for the extraction of carbonaceous fly-ash particles from sediments. J. Paleolim. 11: 201-204.

Rose, N. (2001) Fly-ash particles. In W.M Last & J.P. Smol (Eds.), *Tracking Environmental Change using Lake Sediments. Volume 2: Physical & Geochemical Methods.* Kluwer Academic Publishers, Dordrecht, The Netherlands, pp. 319-349.

Rose, N.L. (2008). Quality control in the analysis of lake sediments for spheroidal carbonaceous particles. Submitted to Limnology and Oceanography: Methods. 6: 172 – 179.

ter Braak, C. J. F. (1992) *CANOCO - a fortram program for Canonical Community Ordination.* Microcomputer Power, Ithaca, New York.

ter Braak, C.J.F., Juggins, S., Birks, H.J.B. and van der Voet, H. (1993) Weighted averaging partial least squares regression (WA-PLS): Definition and comparison with other methods for species-environment calibration. *Multivariate Environmental Statistics* (Patil, G.P. and C.R. Rao), pp. 525-560. Elsevier.

Tipping, E., Yang, H., Lawlor, A., Rose, N.L. and Shotbolt, L. (2007) Trace metals in the catchment, loch and sediments of Lochnagar: measurements and modeling. In N.L. Rose (Ed.), *Lochnagar: The Natural History of a Mountain Lake.* Developments in Palaeoenvironmental Research Vol. 12, Springer, pp. 345-373.